THERMODYNAMICS OF HYDROGEN IN ELECTROSLAG REMELTING

by

Subrata Chattopadhyay
B.E., R.E. College, Durgapur, INDIA, 1978
M.Tech., Indian Institute of Technology, Kanpur, 1980

A THESIS SUBMITTED IN PARTIAL FULFILMENT OF
THE REQUIREMENTS FOR THE DEGREE OF
DOCTOR OF PHILOSOPHY

in

THE FACULTY OF GRADUATE STUDIES
Department of Metallurgical Engineering

We accept this thesis as conforming
to the required standard

THE UNIVERSITY OF BRITISH COLUMBIA
March, 1986

In presenting this thesis in partial fulfilment of the requirements for an advanced degree at the University of British Columbia, I agree that the Library shall make it freely available for reference and study. I further agree that permission for extensive copying of this thesis for scholarly purposes may be granted by the head of my department or by his or her representatives. It is understood that copying or publication of this thesis for financial gain shall not be allowed without my written permission.

Department of Metallurgical Engineering

The University of British Columbia
1956 Main Mall
Vancouver, Canada
V6T 1Y3

Date April 1, 1986

ABSTRACT

Oxide ion activities in binary CaF_2 - CaO and ternary, CaF_2 - CaO - Al_2O_3 and CaF_2 - CaO -SiO_2, slags were determined by CO_2-slag equilibrium experiments at 1400°C. The carbonate capacity of these slags was computed and compared with the sulfide capacity data available in the literature. The similarity in their trends suggests the possibility of characterizing carbonate capacity as an alternative basicity index for fluoride-based slags. The optical basicity of these slags is difficult to define, and with the assumption of CaF_2 as an inert diluent, this parameter did not show any distinct relationship with carbonate capacity. Slag-D_2O equilibrium experiments were performed at 1400°C with binary (CaF_2 - CaO) and ternary (CaF_2 - CaO - Al_2O_3 and CaF_2 - CaO -SiO_2) slags to determine water solubility at two different partial pressures of D_2O. A new technique of slag sampling was employed using a quartz tube. A new and reliable method of water analysis in ESR slags was developed. The new water solubility data were higher than the previous data by an order of magnitude, however, the solubility data showed a linear relationship with the square root of water vapour partial pressure. Also, the solubility was at a maximum in binary slags and a minimum in ternary slags containing SiO_2 with $N_{CaO}/N_{SiO_2} \leq 2$.

These experimental findings were used along with literature data to generate a new equilibrium ratio for hydrogen distributed between the slag and the metal during an ESR process. This information was further

extended to compute the maximum permissible water content in an initial ESR slag for the production of an ESR ingot with an acceptable level of hydrogen.

Table of Contents

List of Tables

Table Page

List of Figures

Figure Page

List of Symbols

A	: Al_2O_3
a	: Inter-ionic distance
B_{carb}	: Basicity on the basis of carbonate capacity
C	: CaO
$C_{CO_3^{2-}}$	: Carbonate capacity of a slag
$C^*_{CO_3^{2-}}$	: Carbonate capacity of a reference slag
C_S	: Sulfide capacity
e	: Interaction parameter
Fl	: CaF_2
ΔG°	: Standard free energy change
hyd	: Hydroxyl ion
I	: Ion-oxygen interaction
K	: Equilibrium reaction constant
L	: Avogadro's number
L_H	: Distribution coefficient of hydrogen between slag and metal
$\bar{M}$	: Average molecular weight
N	: Mole fraction
No	: Mole fraction of oxygen atoms in a melt
OB	: Optical Basicity
p	: Partial pressure
R	: Gas constant, 1.987 calories/degree.mole
S	: SiO_2

T	: Temperature
X	: Mole fraction
x	: Pauling electronegativity
Z_1	: valency of anion
Z_2	: valency of cation
a	: Activity
γ	: Activity coefficient
ρ	: Density
ϕ	: Diameter
( )	: slag phase
[ ]	: metal phase
{ }	: gas phase

ACKNOWLEDGEMENTS

I would like to express my sincere gratitude to Professor A. Mitchell for his guidance through out the course of this work. Helpful discussions with other faculty members and fellow graduate students also contributed to the success of this study. I am indebted to Professor R. Butters and Mr. Rudy Cardeno for all the technical assistance at different stages of the experimental work.

I wish to gratefully acknowledge the financial assistance of NSERC, Canada and the Consarc Corp.

CHAPTER 1

INTRODUCTION

The Electroslag Remelting (ESR) process has been widely used as a secondary refining step for structural constructional steels, stainless steels and various other alloys such as Inconels and Hastelloys. A schematic of the process is shown in figure 1.1, where a consumable electrode is remelted in a water-cooled crucible through a molten pool of basic slag. The thermal energy of this process is supplied by the resistance heating of the slag pool for which the electrical connections from a transformer are made between the electrode and the water-cooled base-plate. The final remelted products, so obtained, are not only chemically refined by the slag-metal reactions, but they also possess reproducible isotropic mechanical properties and good surface finish. Moreover, the process offers the advantage of precise alloy additions and control over the final ingot structure. However, comparing the features of other secondary refining processes, such as Vacuum Arc Remelting (VAR) and Electron Beam Melting (EBM), the ESR process stands well over others in its potential to produce ingots of bigger sizes.

This advantage would lose its merit, if the problem of hydrogen, as observed in the form of hairline cracks around the ingot basal mid-radius region, is not avoided (figure 1.2). The problem with hydrogen is more noticeable in ESR ingots with diameters exceeding about 500mm. The smaller ingots have a favourable thermal history to permit adequate diffusion before crack formation problems develop.

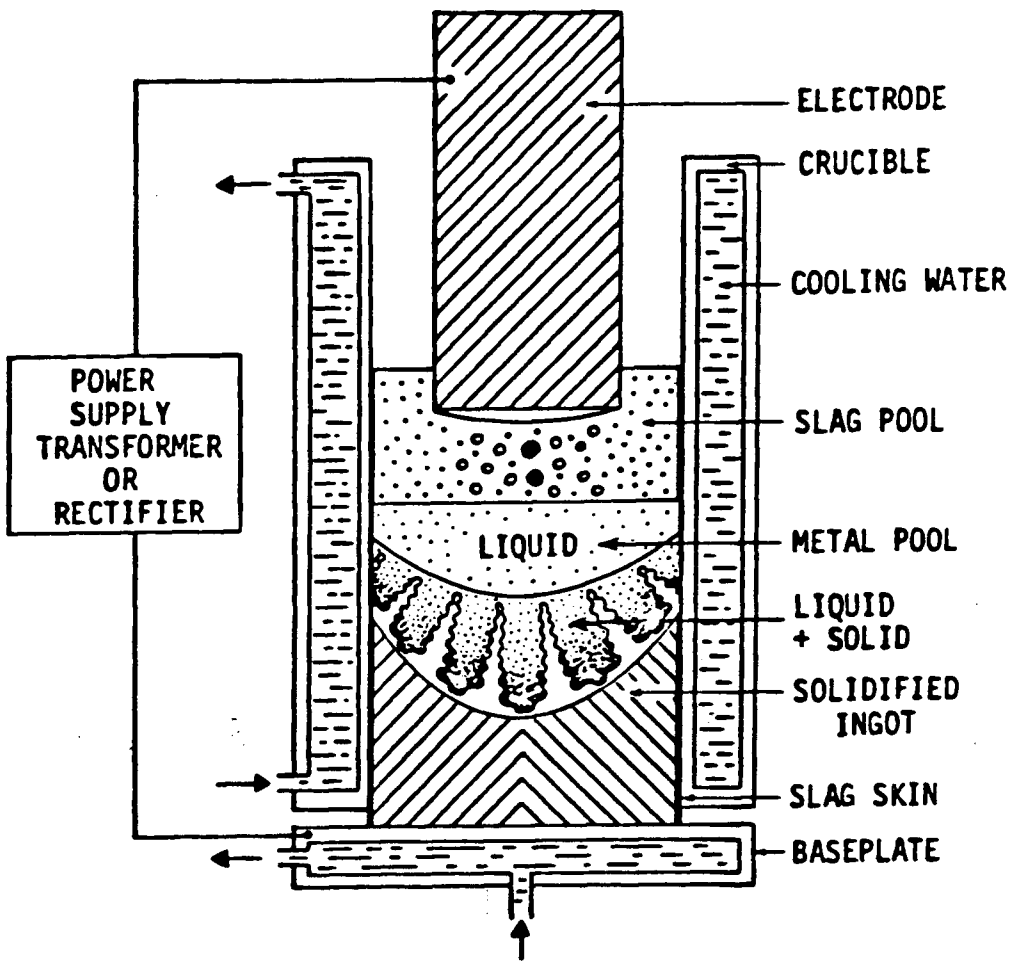

Fig. 1.1 Schematic diagram of Electroslag Remelting Process

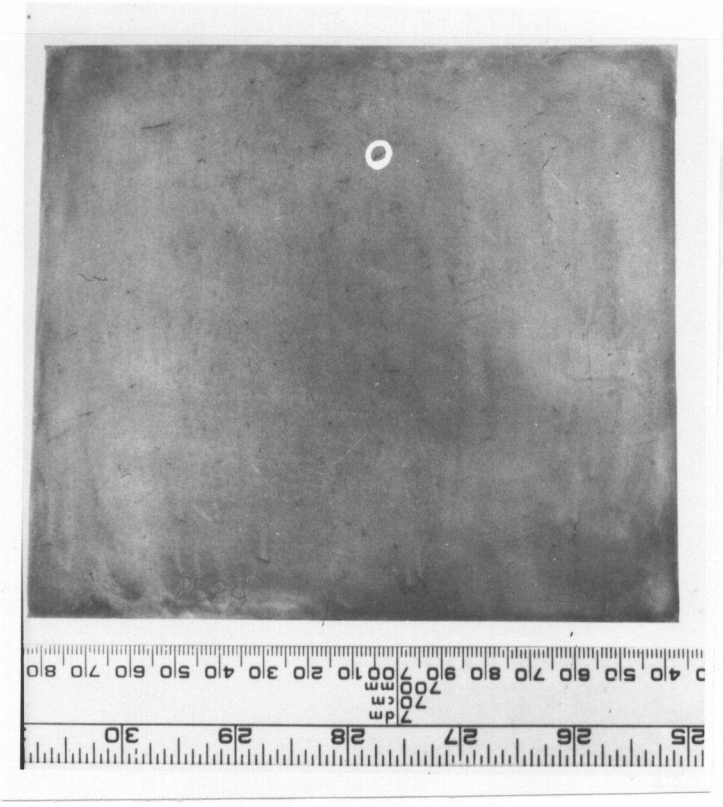

Fig. 1.2 Hydrogen flaking in an ESR ingot of AISI 4340 steel, 700mm dia., Transverse section, as cast, nital etch. The circled area shows a typical hydrogen flake.

The tolerable level of hydrogen in steels is only around 2ppm. An increase beyond this level not only gives rise to hairline cracks, but also reduces the fatigue strength and fracture toughness of steels. These hairline cracks, also known as flakes, are generally very visible on a fracture or metallographic surface and are in almost all cases readily detectable in as-cast and heavy section forged steels. Moreover, these defects are also often detected by ultrasonic testing of forgings from ESR ingots as reflections are produced from the discontinuties.

Before the cracks develop the only way to salvage a costly ESR ingot with a high level of hydrogen is to transfer the ingot quickly to an annealing furnace and soak the ingot for a sufficient length of time (depending on the cross-section of the ingot). The extra facilities and the time involved in this operation would make the ESR process financially less viable.

The solution to this problem lies in the operation of the process itself where the hydrogen level in the ingot should be monitored as the remelting progresses. Unfortunately, there is no safe method of sampling the liquid steel, which is below a pool of liquid slag, without endangering the quality of the ingot. While sampling with a quartz tube, any broken piece of the tube, if it remains in the liquid steel, will ruin the whole ingot. On the other hand, sampling the slag and monitoring its composition are relatively easy and are safer operations. In addition, previous studies[1,2,3] indicate that there is an equilibrium partition of hydrogen between the slag and the metal. Thus, the monitoring of slag composition would give an indirect measurement of hydrogen in the ESR ingot.

There are three major sources of hydrogen during an ESR process: the consumable electrode, the atmosphere on top of the slag and the slag itself. The hydrogen level in the electrode is normally low (≃2ppm) and in the ideal case, the hydrogen content in an ESR ingot should not be more than that of the electrode. Most ESR slags contain a considerable amount of CaO which is very hygroscopic in nature. Consequently, any slag, not dried and stored properly before it is used, would inherently contain a substantial amount of hydrogen. In addition, the moisture in the atmosphere, which is in direct contact with the slag during remelting, influences the hydrogen level in the slag.

The hydrogen transfer mechanism during an ESR process involving highly basic slag can be depicted as in figure 1.3. The free oxide ions in the molten slag react with water vapour present in the atmosphere and stablilize hydroxyl ion in the slag:

$$\{H_2O\} + (O^{2-}) = 2(OH^-) \qquad 1.1$$

The final transfer of hydrogen from the slag to the ingot takes place according to the following reaction:

$$2(OH^-) = 2[H] + (O^{2-}) + [O] \qquad 1.2$$

Considering the above reactions and the need to monitor slag composition, the importance of the reaction(1.1) is clearly evident in controlling the hydrogen in the slag and subsequently in the ingot. Therefore, the present work is directed principally toward the investigation of oxide ion activity and the hydroxyl ion capacity of ESR slags.

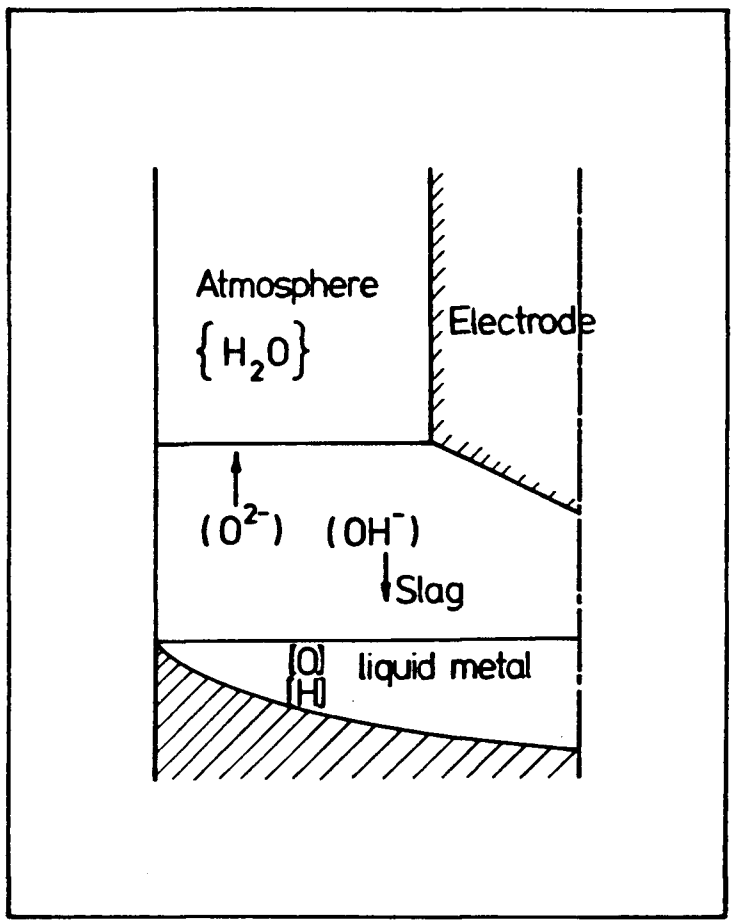

Fig. 1.3 Schematic diagram of hydrogen movement in ESR

CHAPTER 2

LITERATURE REVIEW

2.1. HYDROGEN IN ESR SLAGS

In the Electroslag Remelting process, the slag plays an unique role, being at the same time, the source of thermal requirements and also of chemical reactions to produce a chemically refined and physically sound ingot. As far as the movement of hydrogen is concerned, the critical role of ESR slags has been studied by many authors.[1-7] The data reported here are obtained from laboratory experiments except in the cases of Jaeger et al.[4] and Chuiko et al.[8] who investigated the hydrogen problem in industrial ESR units.

2.1.1 FORM OF HYDROGEN PRESENT IN ESR SLAGS

Hydrogen can be present in ESR slags as dissolved gas, in the form of proton H^+ and hydroxyl ion, OH^-. To date there are no literature reports of the existence of hydrogen dissolved in its molecular form. Moreover, the Sievert's law relationship as observed in most studies, showing the squareroot dependency of the partial pressure of water vapour on the solubility of hydrogen in slags, does not support any molecular dissolution of hydrogen. Nevertheless, it is, in principle, possible to have a minute quantity of hydrogen dissolved in slags, but probably because of the difficulties in the determination technique, sufficient precision is not available to detect it.

The presence of hydrogen as proton (H^+) in steel making slags is suggested by Walsh et al.[9] because of the proton's small ionic size. In blast furnace slag ($40SiO_2$–40 CaO –20 Al_2O_3) the direct evidence of D^+ (in a isotope tracer study) is reported by Kobayashi et al..[10] Similar consideration is made by Forno et al.[11] in ESR slags because of the electrochemical nature of reactions occurring during this process.

$$[H] = H^+ + e \qquad 2.1$$

The above anodic reaction is possible in an acidic slag, but in the ESR system, most slags are highly basic in nature and thus doubt is raised as to the feasibility of that reaction. Holzgruber et al.[6] suggested that for slags with high O^{2-} anion concentration, hydrogen is transported in the slag by the jumping of cation H^+ from one anion to another even though some hydrogen may be present as OH^- ion. The reactions occur as follows.

$$\{H_2O\} + (O^{2-}) = 2(OH^-) \qquad 2.2$$

$$(OH^-) + (O^{2-}) = (O^{2-}) + (H^+) + (O^{2-}) \qquad 2.3$$

A more feasible proposal is made by Medovar et al.[12] regarding the form of existence of hydrogen in slags. They proposed that the presence of both forms of ions, such as OH^- and H^+, and their proportion would depend on the composition of the slag. The increase of hydroxide formers such as oxides and salts of Ca, Mg, K and Na in the slag would result in the predominance of hydroxyl ion (OH^-). The presence of hydroxyl anions in basic ESR slags is also justifiable on the basis of the existence of sulfide[13], fluoride and cyanide[14] ions which also have similar negative charges and ionic sizes. Other authors[7,15] have mainly considered the presence of hydroxyl ions in their respective studies concerning hydrogen in

ESR slags.

2.1.2 SOLUBILITY OF HYDROGEN IN ESR SLAGS

Whatever the form of hydrogen may be, there are reports available on its solubility in fluoride slags, as tabulated in table 2.1. Other data are not complete in nature: also discrepancies can arise through the differences in sampling and determination techniques employed. Because of the doubt associated with the form of hydrogen present in ESR slag, some authors[6,16] preferred reporting the equivalent water solubility whereas others[1,3,4,12,17] reported it as the hydrogen content dissolved in the slag. The latter method seems more popular since it allows a direct comparison with hydrogen level in an ingot whereas the water solubility data gives correlation with the moisture level in the atmosphere, in contact with the slag. The hydrogen solubility data can be converted to equivalent water solubility by multiplying the former by a factor of 9, without any noticeable error.[18]

Jaeger et al.[4] studied mainly $CaO-Al_2O_3-CaF_2$ types of slag where the hydrogen concentration was found to be 30 to 60 ppm (figure 2.1). Due to the hygroscopic nature of these slags, proper storage and handling systems are required to keep the hydrogen level under control. The increase of lime in the slag increases the diffusibility of hydrogen. The hydrogen also increases with the decreasing grain size of the slag as a result of increasing the specific surface area.

The hydrogen distribution coefficient (L_H) between slag and metal becomes almost constant after remelting for more than an hour. For a slag with 30–40% CaO and the humidity of the atmosphere of 14 to 16

Table 2.1 Reported data on water solubility in ESR slags
(refererences in brackets)

Slag	Composition(wt.%)					p_{H_2O}	Temp.	(H_2O)
No.	CaF_2	CaO	Al_2O_3	SiO_2	MgO	torr	°C.	ppm
1	77.1	21.6	0.1	0.4(2)		1.0		166.5
						8.0		432
						17.0		558
2	67.2	3.3	28.1	0.8(2)		1.0		51.3
						8.0		144
						17.0		198
3	40	30	30(1)			6.97	1780	216
4	60	20	20(1)			0.98	1730	315
5	50	25	25(3)			6		252
6	75		25(3)			6		49.4
7	43.5	30.2	1.5	21.2	0.9(3)	6		41.7
8	20	40	40(5)			16		418
9	60	15	25(5)			15.6		330
						18		110
10	51	24.5	19.5(17)			150	1600	225

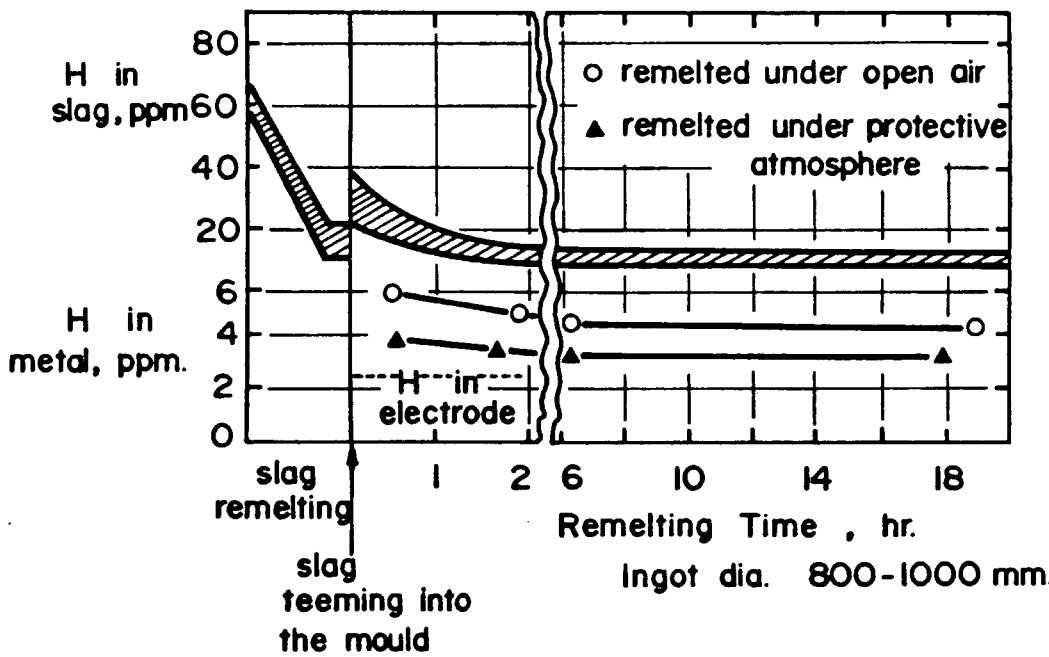

Fig. 2.1 Hydrogen contents in ESR slag and metal under different conditions[4]

gm/Nm^3, the distribution constant attained a value between 3.5 and 4.5 which is in close agreement with the values of Shurmann et al.[1] (figure 2.2). The hydrogen level is further reduced while remelting under a protective hood containing a dry atmosphere, a finding which is also reported by other authors.[8,12]

A detailed investigation involving fluoride slags of compositions CaF_2 -25% Al_2O_3 , CaF_2-25%CaO, CaF_2-25%CaO-25% Al_2O_3 , CaF_2-30%CaO-20%SiO_2 and CaF_2-30%CaO-10%SiO_2 -10%Al_2O_3 is carried out by Nakamura et al..[3] The distribution ratio of hydrogen (L_H) is indicated to vary from 1.9 to 10.5, the maximum being in a binary slag containing CaO and the minimum in the quarternary slag having both SiO_2 and Al_2O_3 . This ratio is not dependent on the hydrogen level of the electrode and the water vapour pressure on top of the slag. However, the hydrogen content of the slag can be expressed as a linear function of the hydrogen content of electrode and the square root of water vapour pressure (figure 2.3).

Many Soviet investigations[2,8,19-21] involve the slag designated as ANF-6 (67.2%CaF_2-3.3%CaO-28.1% Al_2O_3 -0.8%SiO_2). Nikilskii et al.[19] observed that the hydrogen distribution coefficient reached an equilibrium value of 6 whereas according to Latash et al.[2], it was 3.8 and independent of water vapour pressure. No specific temperature is given in either of these reports. On the other hand, Rebrov et al.[21] indicated that a maximum hydrogen distribution ratio of 3 is attained after approximately 30 minutes of remelting operation, and subsequently the distribution ratio showed a gradual decreasing trend with time.

It is also suspected that CaF_2 has an effect in decreasing the solubility of water in slag, but no proper reason is cited to support this

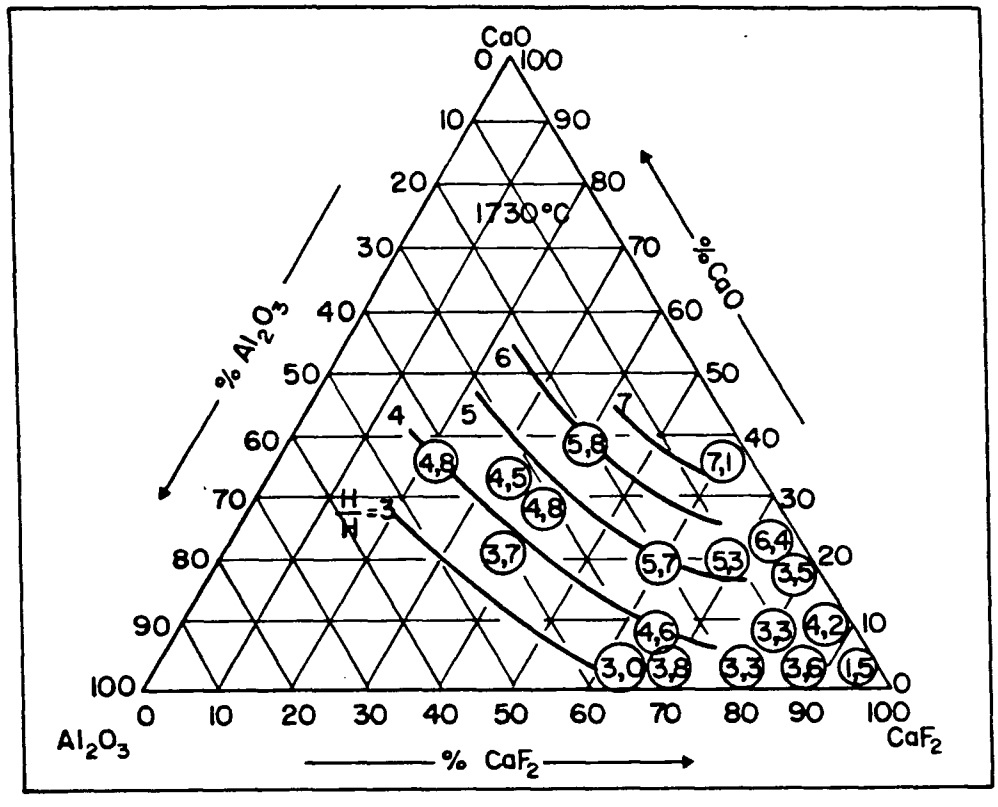

Fig. 2.2 Distribution coefficient of hydrogen between slag and metal during ESR as a function of slag basicity

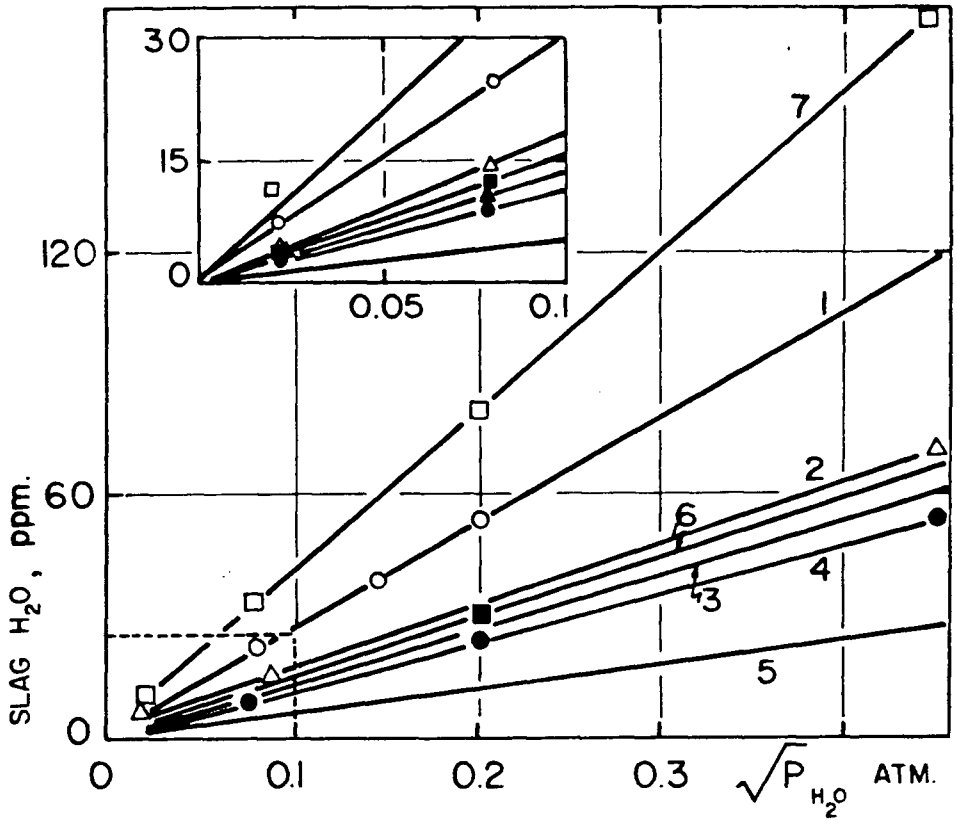

Fig. 2.3 Variation of water solubility in slags with water vapour partial pressure at 1650°C[24].

influence of CaF_2. There is some uncertainty regarding the potential influence of iron, manganese and chromium oxide on the solubility of water in ESR slag. The assumption of CaF_2 as an inert diluent and the observation on the effect of addition of FeO and TiO_2 on water solubility in non-fluoride slag[22] support this trend. The addition of CaO-clinker (containing some Fe_2O_3 and a trace amount of TiO_2) in CaF_2-based slag reduces the hydrogen content by a factor of ten.[23] Evidently, further fundamental studies are needed to establish this aspect of fluoride slags.

The effect of adding Y and rare earth (specially Ce and La) oxides and fluorides is quite favourable as far as the reduction of hydrogen in slag is concerned.[20] Adding only rare earth oxides result in a 30% reduction of hydrogen in remelted metal whereas the replacement by rare earth fluorides is not found to be as effective.

The hydrogen content of ANF-6 slag is 40-115 $cm^3/100gm$ before any preheating.[19] It can be reduced to 20-80 $cm^3/100gm$ depending on the heating/storing practice. Chuiko et al.[8] measured a much lower level of hydrogen (17-19 $cm^3/100gm$) after treating the ANF-6 flux at 400°C for 4 hours. The process of melting the flux with a graphite electrode further reduces the hydrogrn to 10-15 $cm^3/100gm$. In a remelting process, a maximum level of hydrogen, around $30cm^3/100gm$, is reported by other authors[7,21].

Very little information is available on hydrogen solubility in binary fluoride slags. Mainly CaF_2-CaO[3,24] and CaF_2-Al_2O_3[3,5] systems have been investigated revealing that slags containing CaO have a greater water capacity than those containing Al_2O_3. In the CaF_2-CaO system at 1600°C water solubility increases from 71 ppm to 414 ppm as the lime

concentration changes from 1.6% to 21.6%[24], whereas in 30% Al_2O_3 binary fluoride slag it is only 79.2 ppm at 1780°C. The higher solubility of water in lime slag is explained by the presence of free oxide ions and the water vapour-slag reactions as given in equation 2.2.

In the case of Al_2O_3 binary slags, the corresponding water solubility reaction is not as clear. Rather the binary slag may transform into a ternary melt (CaF_2 - Al_2O_3 - CaO) as a result of the following reaction at high temperature:

$$3\ CaF_2 + Al_2O_3 = 2AlF_3 + 3\ CaO \qquad 2.4$$

In such a case, the final water solubility would be dictated by the ternary composition. There is no information available on the water solubility in CaF_2 -SiO_2 binary. As far as the operation of ESR is concerned the properties of this binary are not at all favourable. Moreover, studying this system as a 'strict binary' is impossible because of the occurrence of the following reaction at high temperature:

$$2\ CaF_2 + SiO_2 = 2\ CaO + SiF_4(g) \qquad 2.5$$

The available water solubility data on ternary systems are presented in table 2.1 where it is evident that under similar situations, CaF_2 - CaO - Al_2O_3 would have a higher concentration of hydrogen than the CaF_2 - CaO -SiO_2 system. In most cases, the water content does not increase beyond 0.1%. However, some reports indicate a much higher value, such as in CaO - Al_2O_3 - CaF_2 slags which contain water of the order of 0.2% to 0.5%[6] and a slag of composition CaF_2-25%CaO-25%Al_2O_3 with 1600

ppm of hydrogen at 1550°C and 188 torr water vapour pressure[3].

2.1.3 FACTORS AFFECTING SOLUBILITY OF HYDROGEN IN FLUORIDE SLAGS

Hydrogen is mainly transferred from the moisture in the atmosphere to the slag even though there are some other sources such as hydrogen in the electrode and the initial hydrogen level of the slag itself (whatever pretreatment is done to ESR slag, there is always some residual hydrogen in the starting slag). All the authors[1-5,12,24,25] reported the square root of water vapour pressure dependency on the solubility of hydrogen in slag (Sievert's law). Consequently, operating the process in a dry atmosphere[2,4] or blowing argon through the slag[12] should reduce the level of hydrogen significantly.

Different pretreatments of slag such as calcining it under a neutral atmosphere[12] having a minimum content water vapour and other hydrogenous compounds (CH_4, C_2H_2 etc.), or premelting the slag[6,8] with a graphite electrode are recommended to obtain a low hydrogen slag.

The importance of the gas-slag water reaction, as already been mentioned, and the location of the reaction, i.e. the gas/slag interface, become further evident when we consider the production of bigger diameter ESR ingots. In this situation, the larger gas/slag interface area[25] would enable more hydrogen transfer reaction in a shorter time. Therefore, the remelting rate[5] will limit the hydrogen concentration in the slag.

Due to the electrochemical nature of ESR reactions, it is suggested that the hydrogen is removed from the slag by electrolysis.[4] Using the non-consumable electrode and superimposed DC supply, hydrogen

can be reduced from the slag (figure 2.4), but the problem of corrosion of the electrode by the fluoride slag is reported to be the real hindrance against this idea.[95]

Finally, the slag composition[20-25] which dictates the activity of oxide ion is a very important factor in controlling the hydrogen level in the slag. Any reduction in free oxide-ion concentration would result in a lower hydrogen level in the slag, but in industrial practice, the change in the slag composition has to be balanced with decreasing desulfurizing power of the slag. Probably, the SiO_2/Si and Al_2O_3 /Al reactions are more important, because the most critical steels are also very rigidly controlled for [Si] and [Al]. A slag made acidic by high SiO_2 and Al_2O_3 leads to excessive pick-up of [Si] and [Al]. Moreover, composition changes alter the physical properties of slag, such as permeability and viscosity, which can also influence the hydrogen transfer to the slag.[24] The most direct influence, however, is of composition on the furnace slag operating temperature.

2.2. HYDROGEN IN NON-ESR SLAGS

Extensive studies have been carried out on the solubility of water in petrological materials such as magmas and granite involving a very high pressure of water vapour (>>1atm).[26] In recent years, interest has also been shown in water solubility in glasses and metallurgical slags where the partial pressure of moisture is below atmospheric pressure. In the present context the latter case is of particular interest to the present

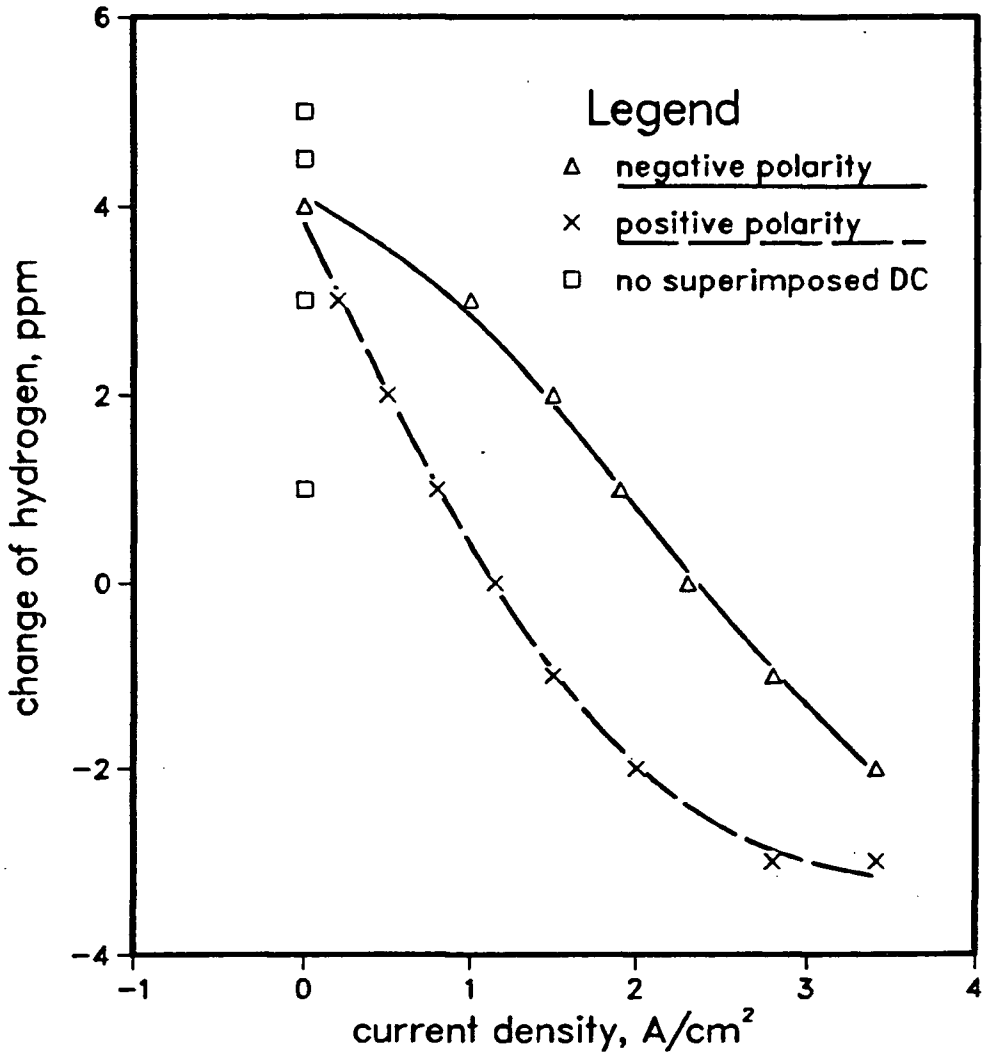

Fig. 2.4 Effect of superimposed DC on the hydrogen level in ESR process[4]

work.

2.2.1 WATER SOLUBILITY IN GLASS

There are reports[27-31] available on water solubilities mainly in binary silicate glasses containing oxides such as, Li_2O, ZnO, Na_2O etc. The parameters which are found to be of prime interest in controlling the solubility are composition, temperature and partial pressure of water vapour. The exact nature of the influences is difficult to confirm because of the experimental problems arising out of high melting point, high viscosity and loss of volatile constituents.[31]

2.2.1.1 WATER SOLUBILITY IN BINARY GLASS SYSTEMS

Most reports, except the work of Tomlinson[29], show a linear relationship of the water solubility with the square root of water vapour pressure. $Na_2O.2SiO_2$ system is studied by this author and it is concluded that possibly there are two reasons for the apparent deviation from linearity at higher partial pressures of water vapour. First, the accuracy of the analysis is comparatively poor ($\pm$ 15%); and secondly, the gas flow rate employed during equilibration experiments is substantially high (1 lpm), which may result in an unsaturated water vapour in the gas stream. In $Na_2O-P_2O_5$ and $Na_2O-2B_2O_3$ melts[27], the integral extinction function of OH bands (a measure of water in quenched slag) also shows linearity with the water vapour partial pressure.

In Na_2O-SiO_2 melts, water solubility increases with decreasing temperature.[28-30] Even though the same trend is noted in all three reports, the amount of dissolved water is found to be considerably lower in the report of Tomlinson[29] (300 ppm as opposed to 800 ppm around 1200°C

according to the other two reports). The similar affect of temperature is recorded in K_2O–SiO_2, Cs_2O–SiO_2 melts,[28,30] whereas the opposite trend is observed in Li_2O–SiO_2, SrO–SiO_2, BaO–SiO_2 systems[28] (figure 2.5). Uys and King[31] did not see any noticeable effect of temperature in ZnO–SiO_2 systems (figure 2.6) .

A probable reason for these conflicting reports may be that the analytical technique differed in the various studies. Russel and Kurkjian[28,30] purged 'dry' oxygen (assumed dry with respect to water solubility) through the melts to evolve the dissolved water. This method, as Russel[28] points out, does not give the total dissolved water in the melt, but the amount of water removed by 'dry' oxygen. Tomlinson[29] analyzed water in the glass by evolving it in a vacuum at 1200°C and measuring the partial pressure manometrically. Surprisingly, the evolution takes a considerable time (10hrs) at this temperature. In the vacuum fusion technique, as reported by Uys and King,[31] the evolved water is reduced to hydrogen by an aluminium foil and subsequently this gas is analyzed in a thermal conductivity cell. The major problem of this vacuum technique is that the alkali oxides are also vaporized during the evolution of water and condensed around the cold zone of the apparatus, where the condensate would absorb part of the evolved water.

The effect of composition on water solubility is also not very consistent according to different authors.[30-32] For the Na_2O–SiO_2system Kurkjian and Russel[30] observed a minimum water solubility around 25 mole percent Na_2O, (figure 2.7), while Scholze et al.[32] reported a decreasing water solubility with the decrease of base in the glass. Similar conflicting trends are also evident in a Li_2O–SiO_2 melt, which is also studied by Uys and

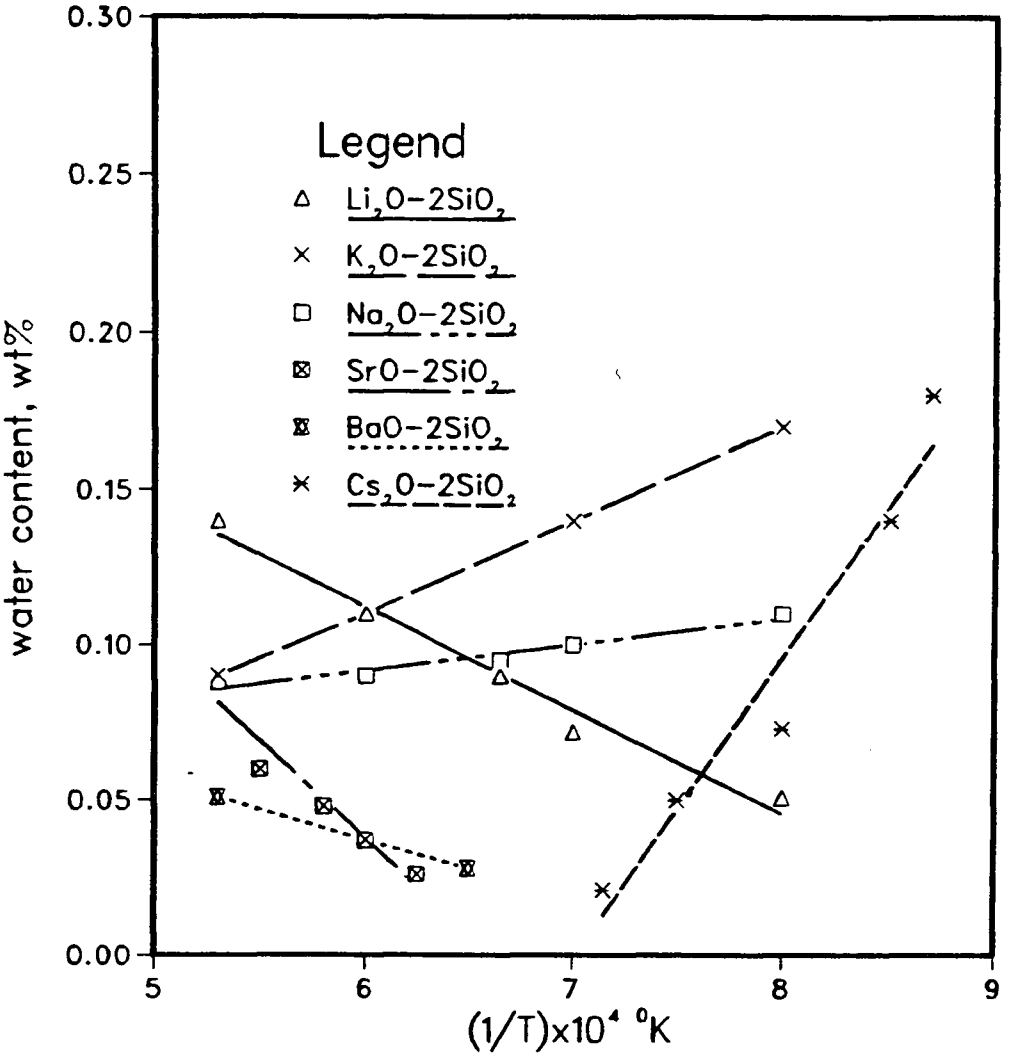

Fig. 2.5 Effect of temperature on water solubility in alkali and alkaline earth disilicate glasses[28]

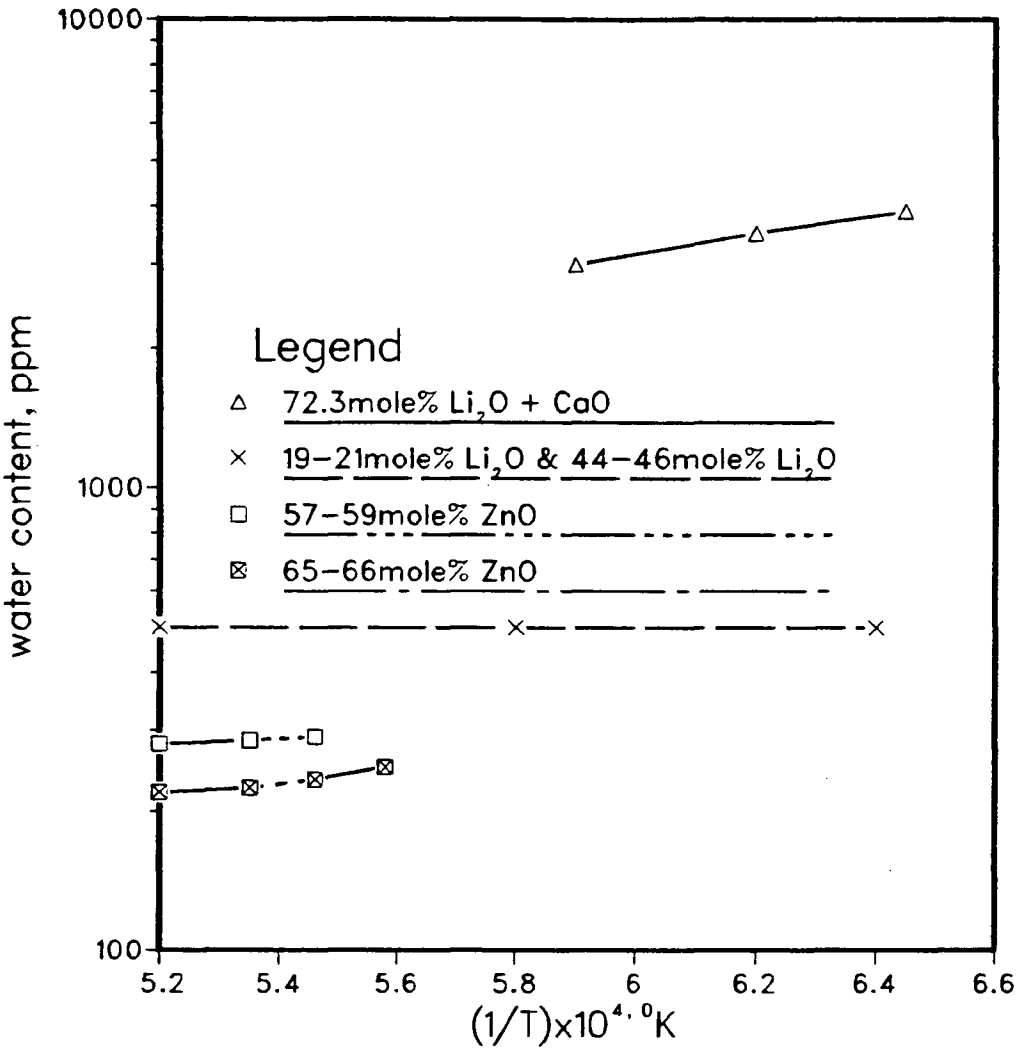

Fig. 2.6 Effect of temperature on water solubility in silicate slags obtained at p_{H_2O} = 146torr[31]

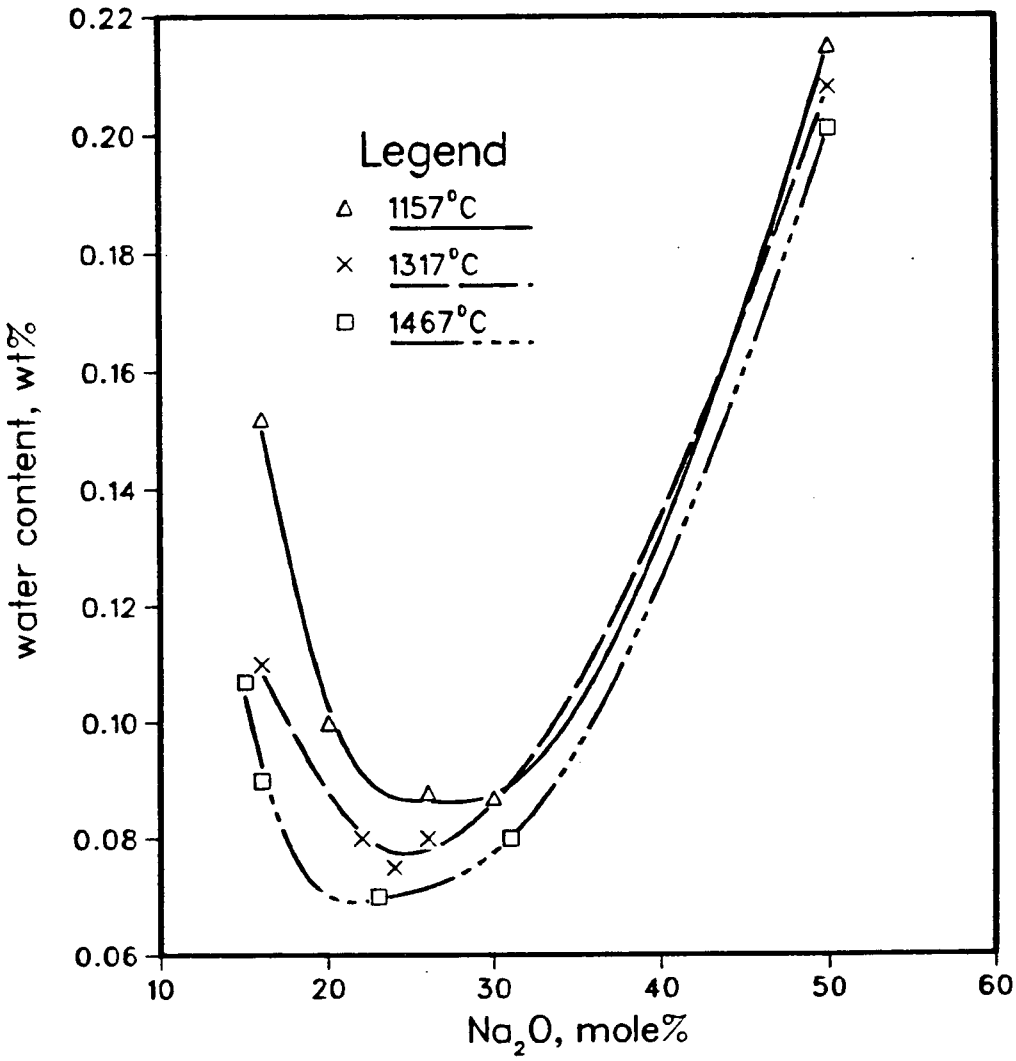

Fig. 2.7 Water solubility as a function of Na_2O content in Na_2O–SiO_2 system[30]

King[31] (figure 2.8 and 2.9). A decreasing trend of solubility is observed, but the trend is changed around 50 mole percent base. Within the small range of composition in $ZnO-SiO_2$ and $CaO-SiO_2$, the effect of composition is reversed.

2.2.1.2 WATER SOLUBILITY IN TERNARY GLASS SYSTEMS

In SiO_2- CaO - acid oxide melts[33], at a constant molar ratio of CaO/SiO_2, the addition of acid oxides, such as P_2O_5,B_2O_3 and GeO_2, increases the water solubility, the effect being a maximum with P_2O_5 and a minimum with GeO_2 (figure 2.10). The addition of amphoteric oxides such as Al_2O_3 and TiO_2 shows a minimum solubility behavior at around 20% amphoteric oxide, and this composition possibly demarcates the transition from basic to acid behavior (figure 2.11).

Iguchi et al.[34] studied the effect of additions of alkali metal oxides and alkaline-earth metal oxides on the solubility of water in liquid silicate melts (figure 2.12 and 2.13). In all cases, a minimum solubility is observed around the metasilicate composition. However, the addition of an alkali-metal oxide such as Li_2O, Na_2O and K_2O increases the solubility of water, the effect of K_2O being the strongest and that of Li_2O being the weakest. On the other hand, the addition of an alkaline-earth-metal oxide such as BaO and SrO decreases the water solubility except for MgO additions where the effect is reversed. The effect of BaO is larger than that of SrO. All these ternary melts show little effect of temperature on

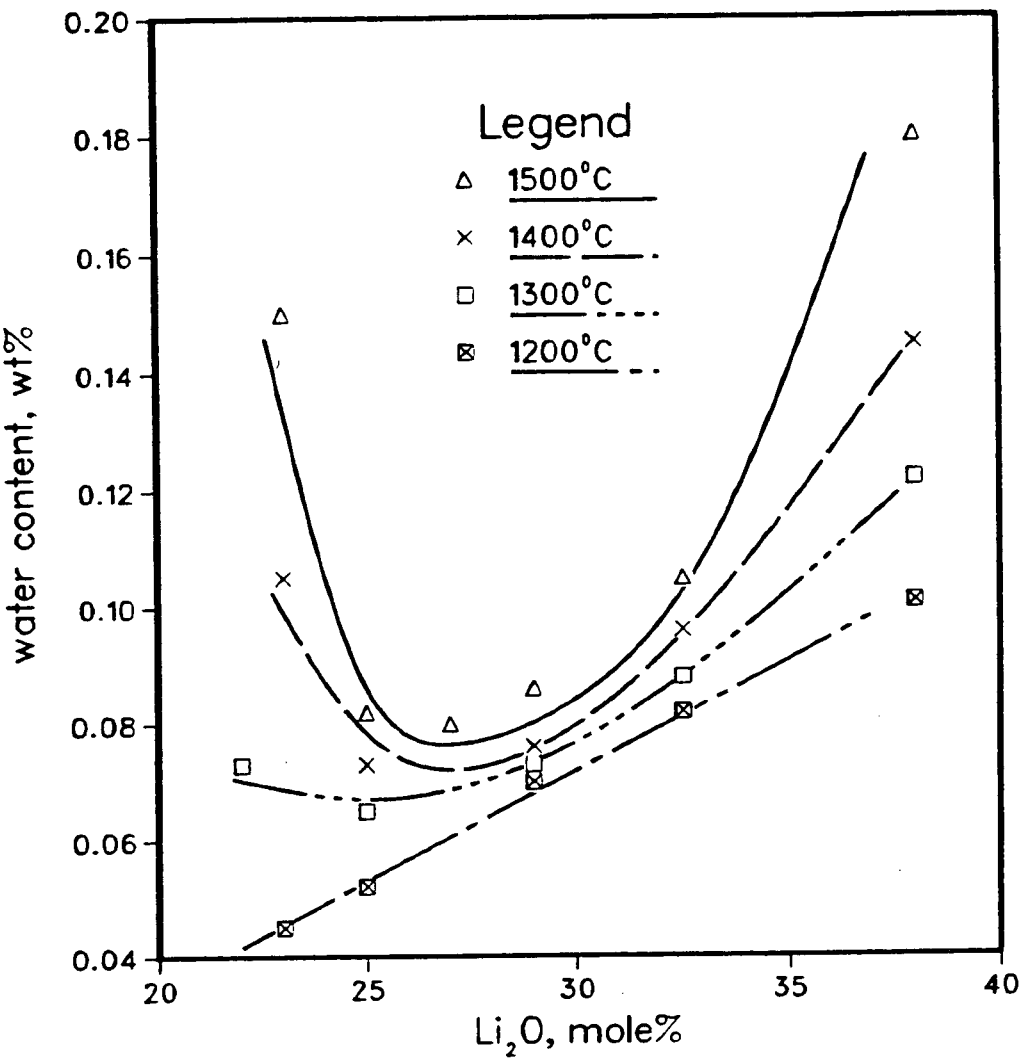

Fig. 2.8 Water solubility as a function of Li_2O content in Li_2O–SiO_2 system[30]

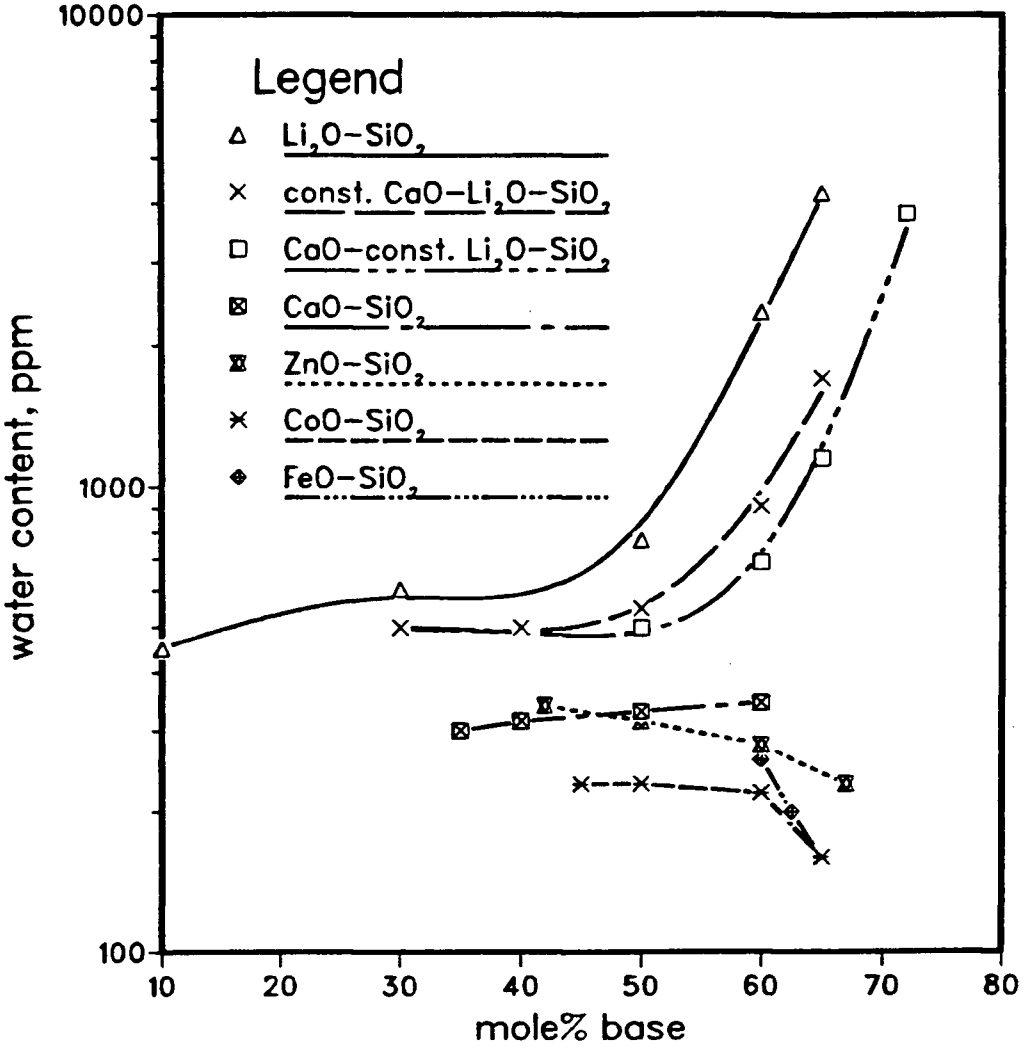

Fig. 2.9 Water solubility as a function of mole percent base in various silicate slags at p_{H_2O} = 146 torr Hg[31]

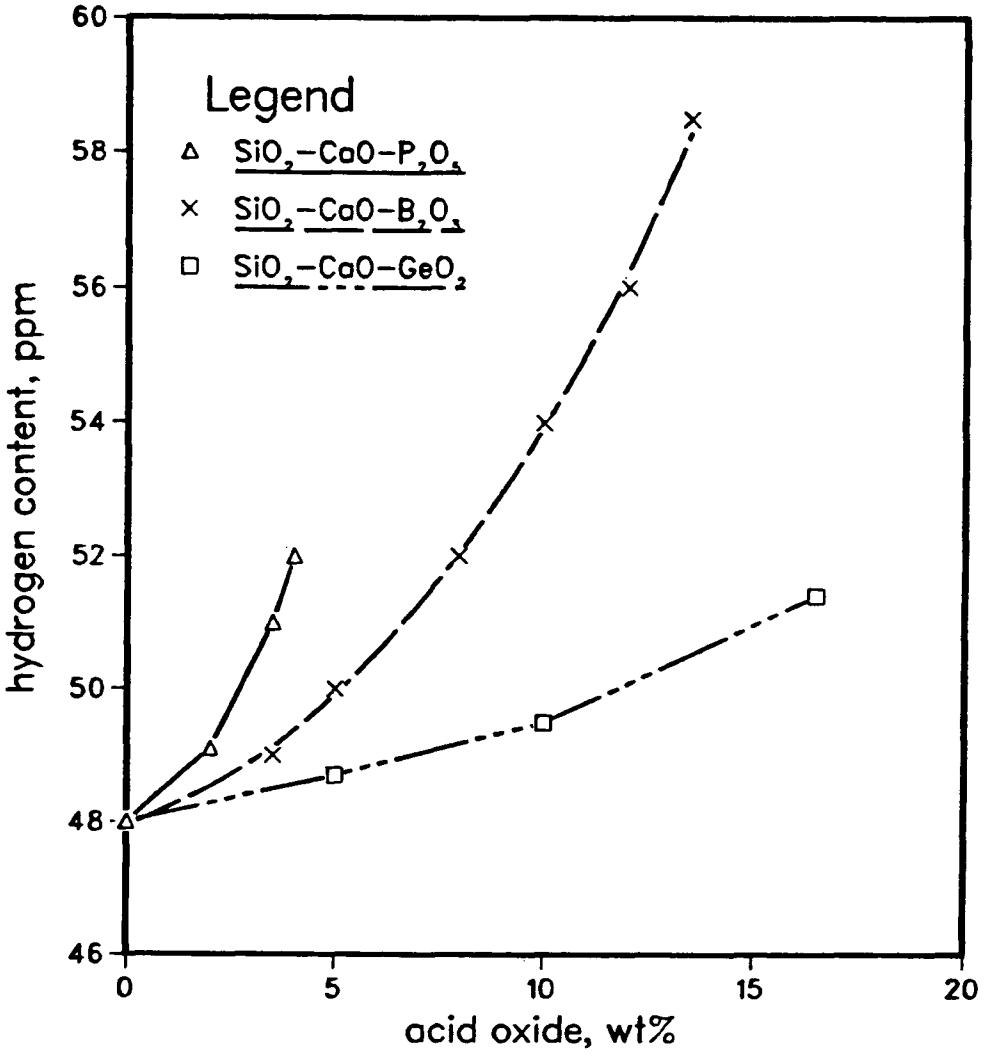

Fig. 2.10 Hydrogen solubility in various silicate slags containing acid oxide at 1500°C, CaO/SiO_2=0.59, p_{H_2O} = 289 torr[33]

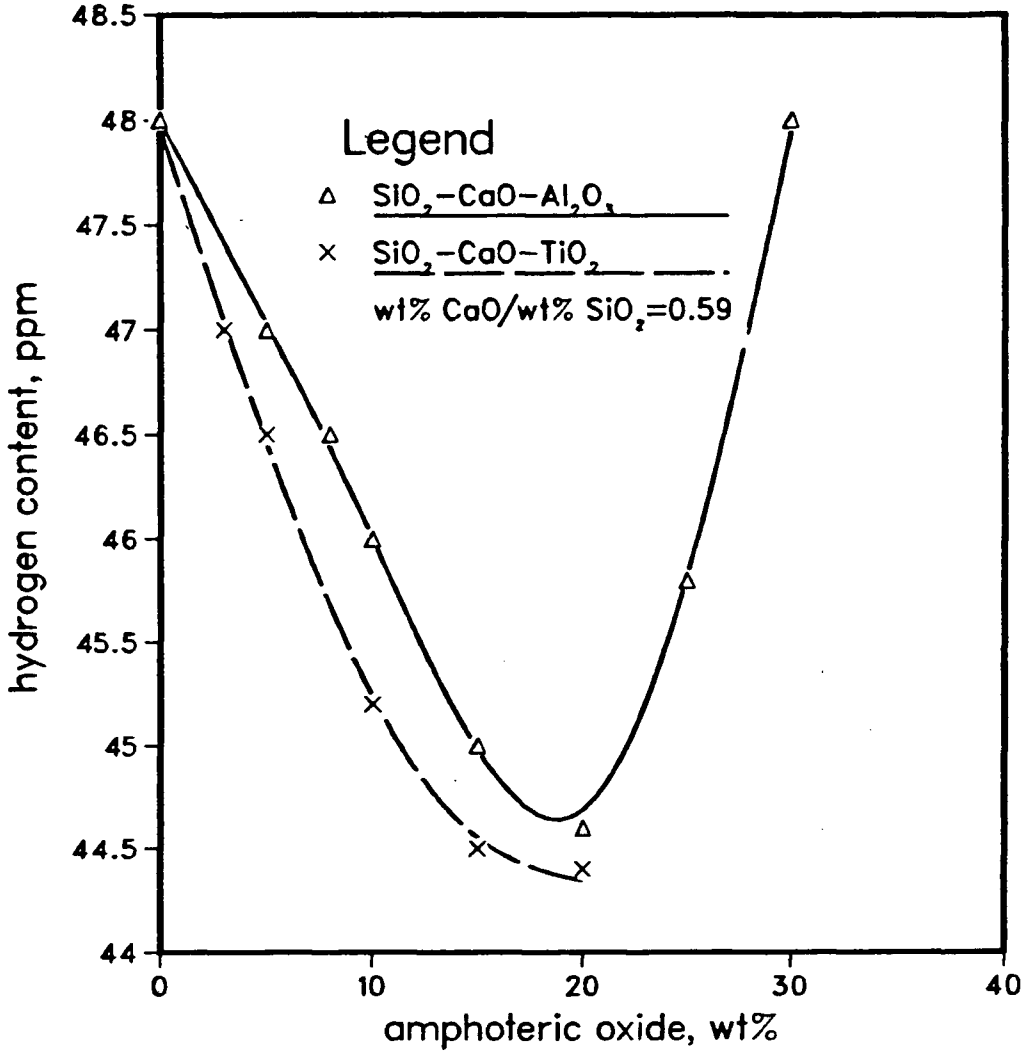

Fig. 2.11 Hydrogen solubility in various silicate slags containing amphoteric oxide at 1500°C, CaO /SiO_2=0.59, p_{H_2O} = 2.89 torr[33]

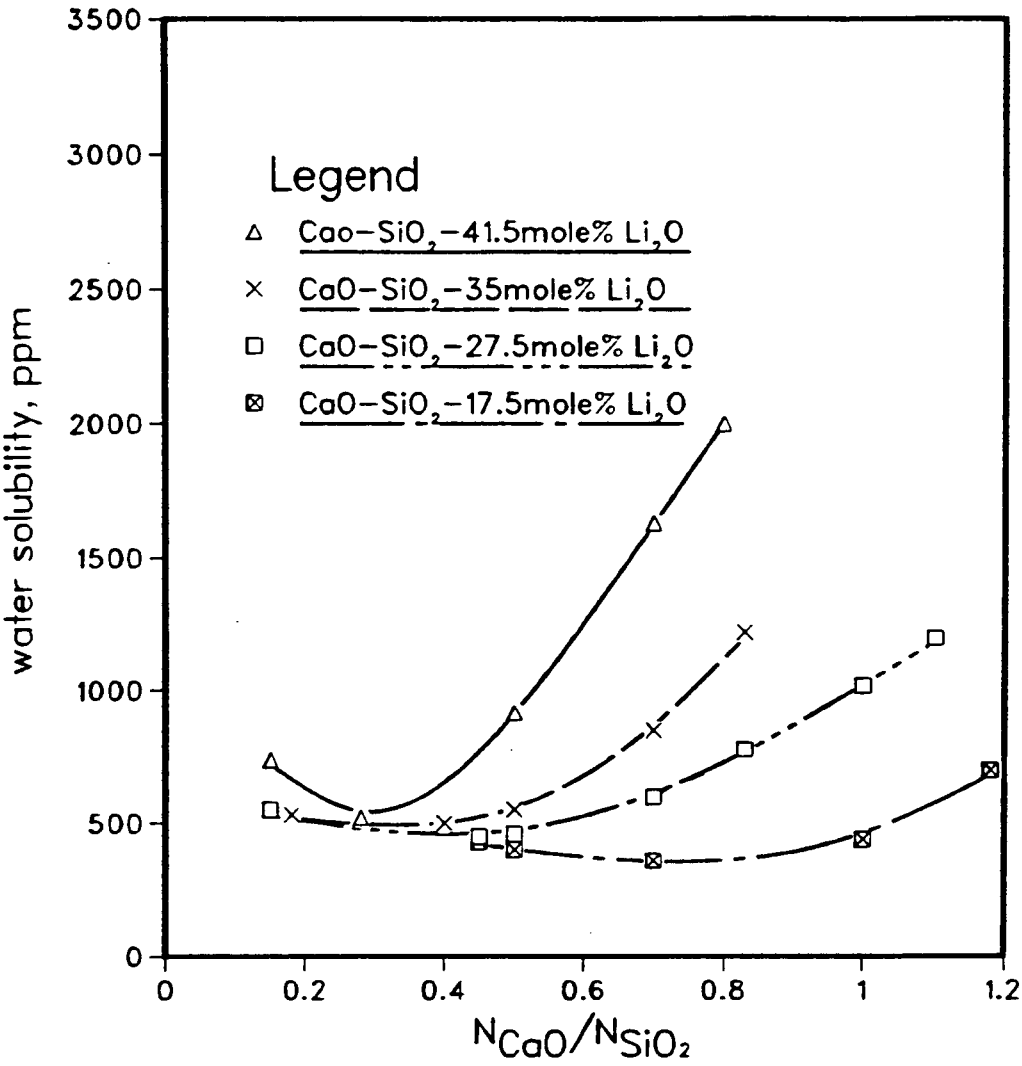

Fig. 2.12 Water solubility in the CaO $-SiO_2-Li_2O$ system[34]

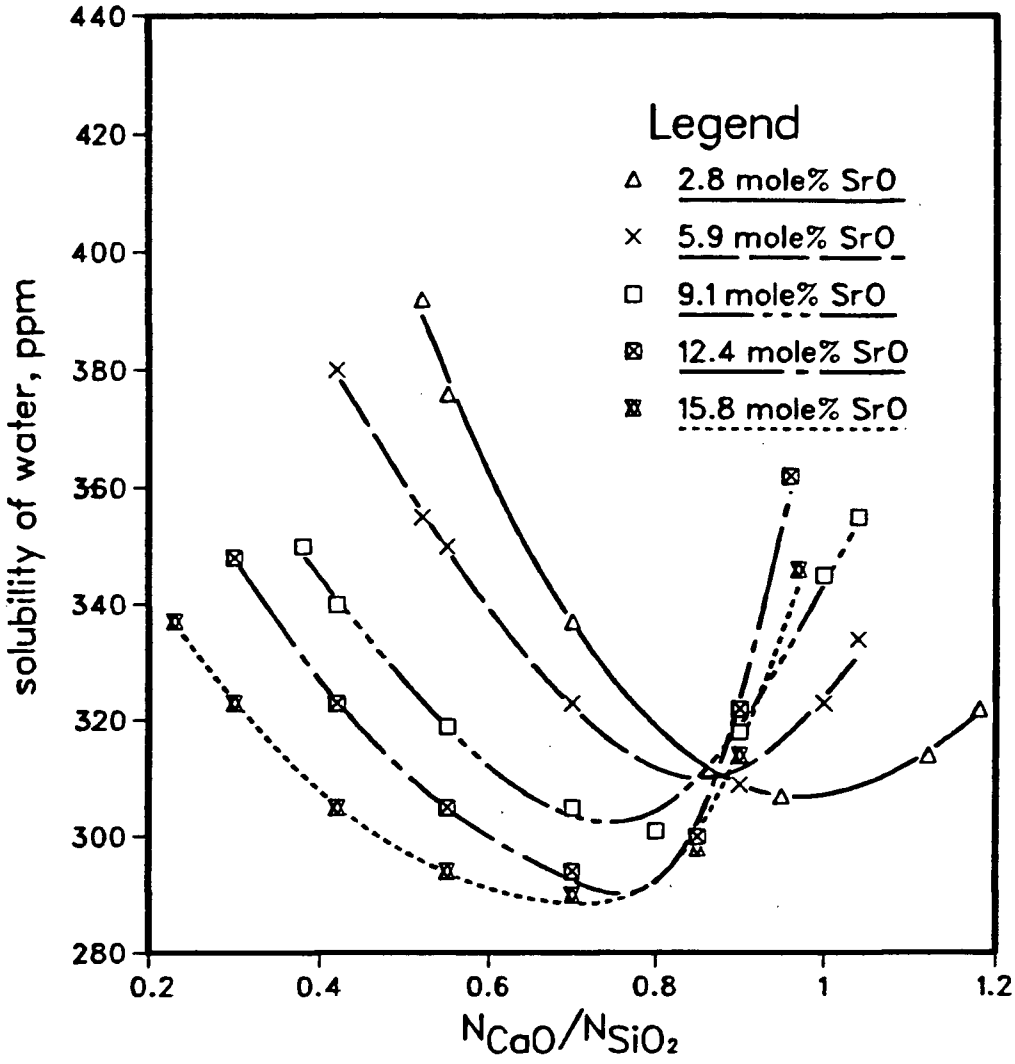

Fig. 2.13 Water solubility in the CaO $-SiO_2$-SrO system[34]

water solubility.[31,33,34]

2.2.1.3 MECHANISMS OF WATER DISSOLUTION

Infrared absorption spectra studies and the observation of minima of water solubility in these melts at least suggest that more than one mechanism of water dissolution operates to dictate the solubility level.

Fincham and Richardson[35] suggested that in liquid polymeric oxides such as silicates oxygen exists in three forms: doubly bonded O°, singly bonded O^{-}, and free oxygen ions O^{2-}. They equilibrate with each other, with concentrations depending upon melting temperature, characteristics of the cation and the oxide composition. There are four different reactions of water possible with these three oxygen species depending on the basicity of oxide melt. The reactions are as follows[33] (the equivalent expressions for silicate melts are also shown):

In the acid slag,

$$\begin{array}{c} | \quad\quad | \quad\quad\quad\quad | \\ -Si - O-Si - + H_2O(g) = 2-Si - OH \\ | \quad\quad | \quad\quad\quad\quad | \end{array} \qquad 2.6$$

$$O^{\circ} + H_2O(g) = 2OH^{\circ}$$

In the basic slag,

$$\begin{array}{c} | \quad\quad\quad\quad | \quad\quad | \\ 2\ (-Si - O^{-}) + H_2O(g) = -Si - O-Si - + 2OH^{-} \\ | \quad\quad\quad\quad | \quad\quad | \end{array} \qquad 2.7$$

$$2O^{-} + H_2O(g) = O^{\circ} + 2OH^{-}$$

$$\begin{array}{c} | \quad\quad\quad\quad\quad\quad | \\ 2\ (-Si - O^{-}) + H_2O = 2-Si - OH + O^{2-} \\ | \quad\quad\quad\quad\quad\quad | \end{array} \qquad 2.8$$

$$2O^{-} + H_2O(g) = 2OH^{\circ} + O^{2-}$$

In the highly basic slag,

$$O^{2-} + H_2O(g) = 2OH^-$$

One interesting feature of all the reactions is that the water solubility is proportional to the square root of p_{H_2O} in all the cases. Thus, the evidence of this relationship does not reflect the type of mechanism prevalent in different conditions.

Russel[28] considered the field strength of the cation to explain the temperature coefficient of solubility in disilicate glasses. The solubility decreases with increasing temperature for cations with low field strength whereas the opposite is true with cations of high field strength.

Ion-oxygen attraction (I) is another parameter considered by Uys and King[31] to explain the effect of composition and the general solubility behavior. This parameter I, can be defined as:

$$I = \frac{2Z}{a^2} \qquad 2.9$$

Where Z is the cation valency and a is the internuclear distance between the cation and oxygen in the appropriate co-ordination. In basic melts, cations with smaller ion-oxygen attractions dissolve more water and in acid system, larger ion-oxygen attraction shows higher water solubility. The ion-oxygen attraction for amphoteric oxides lies between these two extremes (table 2.2). On this basis, water itself can be considered as an amphoteric oxide. Thus it would act as an acid in a basic melt and as

Table 2.2 Ion-Oxygen Attraction in various Oxides

Oxides	Ion-Oxygen Attraction(I)
P_2O_5	3.31
SiO_2	2.44
B_2O_3	2.34
GeO_2	2.14
TiO_2	1.85
Al_2O_3	1.66
Fe_2O_3	1.50
H_2O	1.05
MgO	0.95
CoO	0.89
ZnO	0.88
FeO	0.87
MnO	0.83
CaO	0.70
Li_2O	0.50
Na_2O	0.36
K_2O	0.27

base in an acid melt.

2.2.2 WATER SOLUBILITY IN METALLURGICAL SLAGS

The type of slags included in this category are mainly lime-silicate containing various amounts of 'FeO', Al_2O_3 , MgO and MnO which are observed in the blast furnace and at different stages of steelmaking. The water solubility investigations include both industrial slags and synthetic slags, which are made from pure oxide ingredients. All studies show a proportional relationship of water solubility with the square root of water vapour pressure.

2.2.2.1 BINARY SLAGS

Many reports[9,33,36,37] are available on the water vapour dissolution in CaO -SiO_2 systems around 1500-1600°C. With the increase of basicity, the solubility increases slightly (650 to 750ppm) (figure 2.14) except in the case studied by Fukushima et al.[33], where a minimum is observed around the metasilicate composition. Fukushima et al.[33] also reported the increase of solubility with increasing temperature, but the effect was not great (figure 2.15).

In manganese silicate melts, as reported by Walsh et al.[9], the hydrogen solubility is slightly lower compared to that of lime silicates on a molar basis. At 64 mole percent basic oxide, the hydrogen solubility in manganese silicate is 65 ppm as against 75 ppm for the lime silicate when the water vapour pressure is 1 atm. A further reduction in hydrogen solubility is observed in the 'FeO'-SiO_2 binary[31,38] (figure 2.16). Uys and King[31] reported an almost constant hydrogen solubility up to the orthosilicate composition in the 'FeO' rich side and then the solubility is

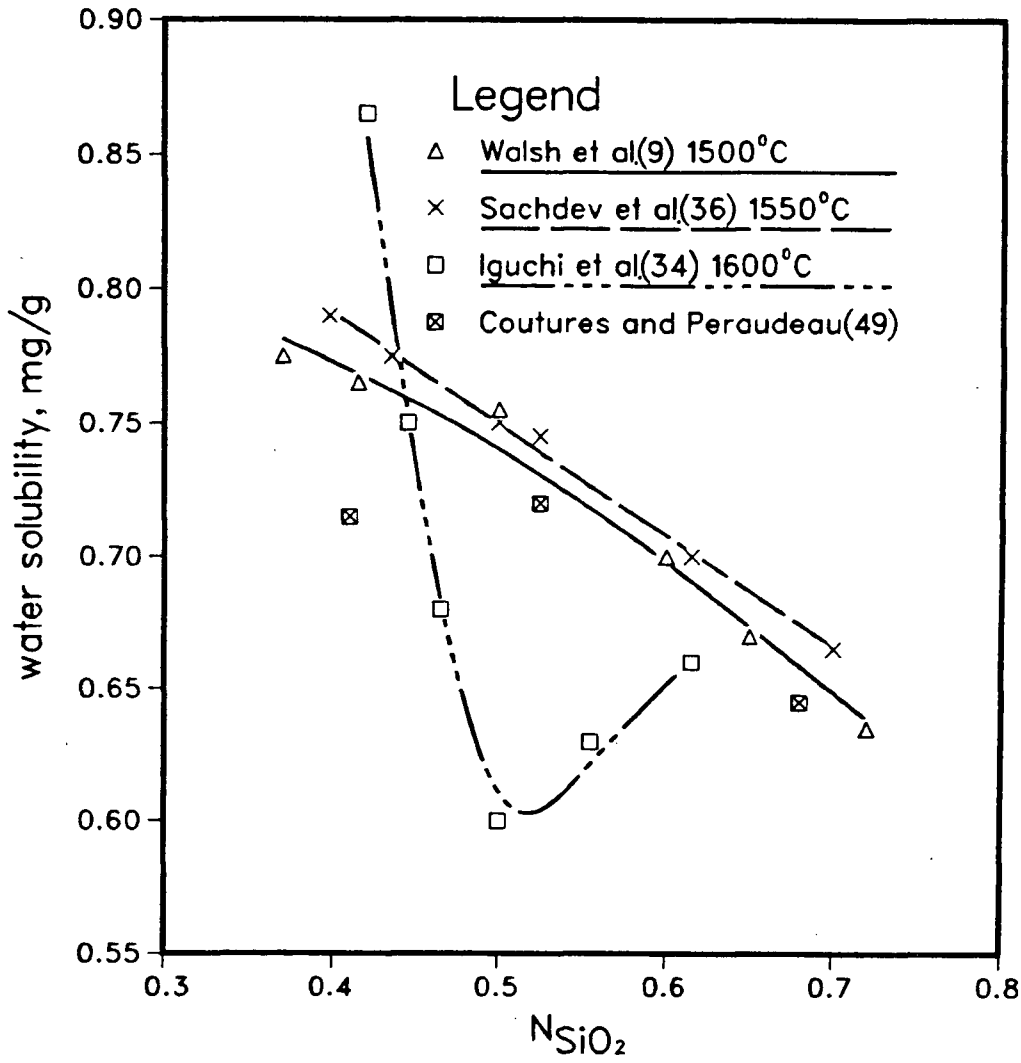

Fig. 2.14 Comparison of different water solubility data in CaO -SiO_2 system

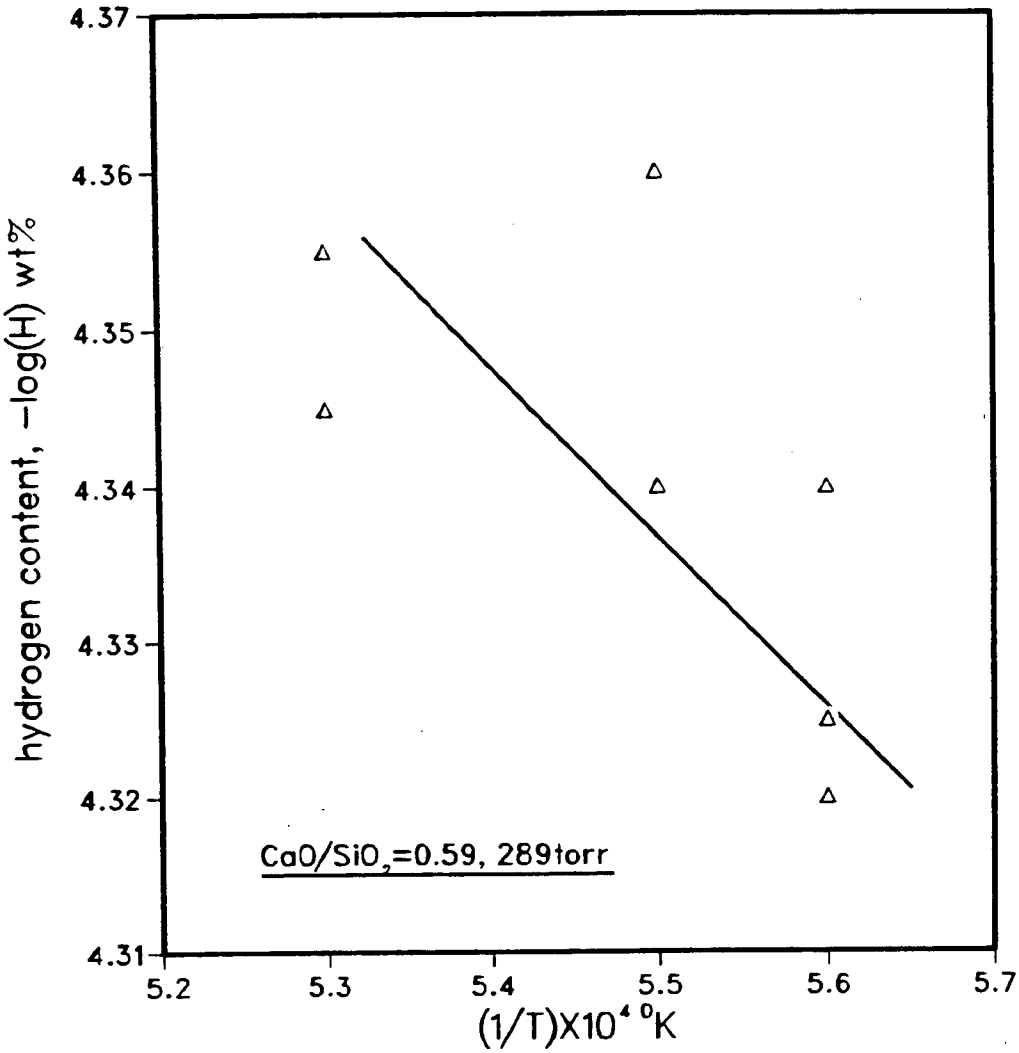

Fig. 2.15 Effect of temperature on hydrogen solubility in 63 SiO_2–37 CaO slag[33].

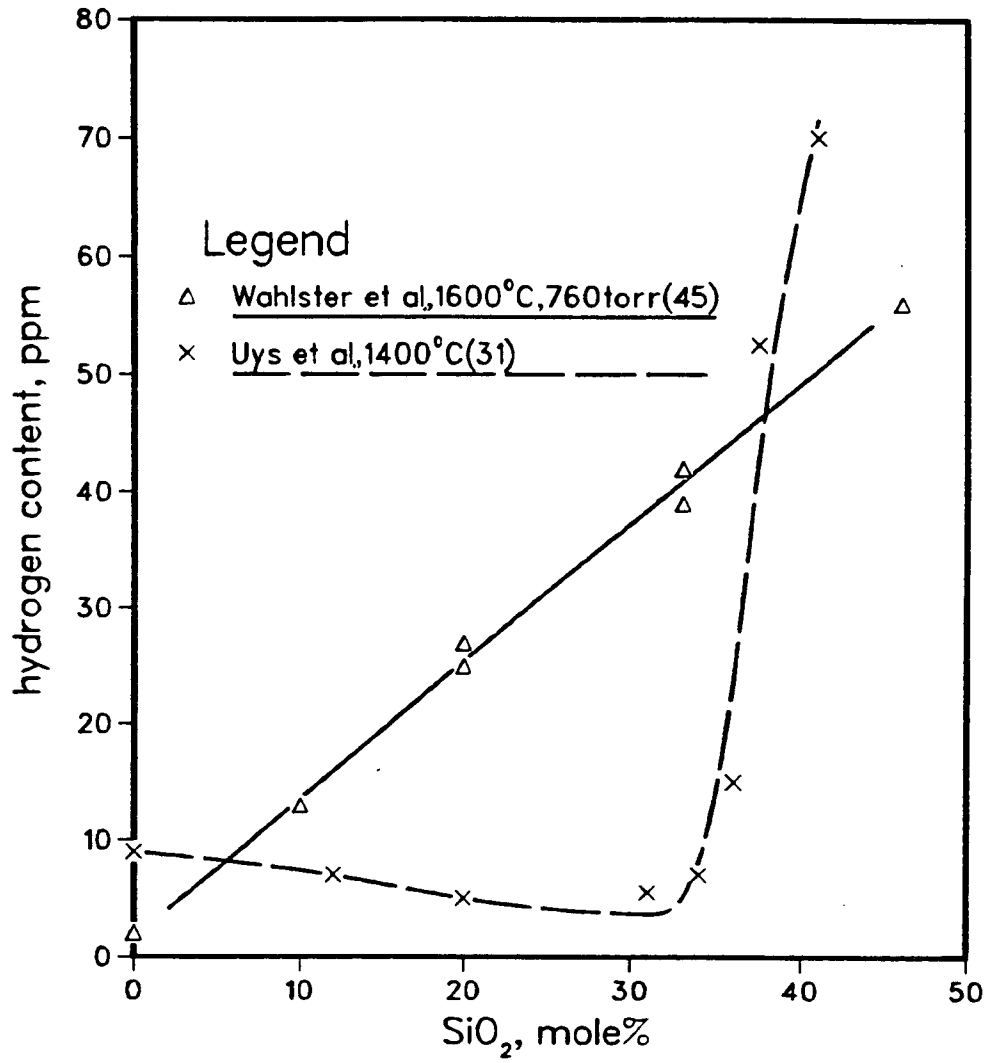

Fig. 2.16 Water solubility in 'Feo'-SiO_2 system[31]

increased very sharply; but in the same zone Wahlster and Reichel[38] observed a continuous and gradual increase of solubility. In silicate systems the trend of decreasing solubility in CaO $-SiO_2$, MnO$-SiO_2$ and 'FeO'$-SiO_2$ is very similar to that of the ion-oxygen attraction parameter, (I) (table 2.2), and I is thus a helpful indicator of water solubility.

In binary aluminates, CaO $-$ Al_2O_3 [39] shows a considerably higher solubility than that of SiO_2- Al_2O_3 .[40] At 35 mole percent Al_2O_3 the water solubility of calcium aluminate is 1200 ppm as compared to around 500 ppm for the silica-aluminate system. Again solubility increases with lime in CaO $-$ Al_2O_3 , but in SiO_2- Al_2O_3 it shows an initial increasing trend with alumina and later reaches a minimum around 90% Al_2O_3 . This unusual trend is explained in terms of Al/Si oxybridges and a phenomenon related to surface activity of SiO_2 in the SiO_2- Al_2O_3 melts.

In the FeO$-$ CaO [38] system, the water solubility is slightly higher than FeO$-SiO_2$ melts, but the solubility shows a similar relationship with composition.

2.2.2.2 TERNARY SLAGS

Extensive studies have been done on water solubility in the CaO $-SiO_2-$ Al_2O_3 system.[9,22,33,36,41] Even though there is a dispute over the absolute quantity of water dissolved (in 40 CaO $-40SiO_2-20$ Al_2O_3 slag 720ppm H_2O[9] against 540ppm[41] at 1400°C), the increase of basicity (CaO /SiO_2) shows an increase of solubility as reported by all the authors (figure 2.17). Sachdev et al.[36] and Fukushima et al.[33] also observed a minimum solubility around 20 wt% Al_2O_3 at a constant basicity. The effect of temperature is found to be insignificant in this system[156] and the

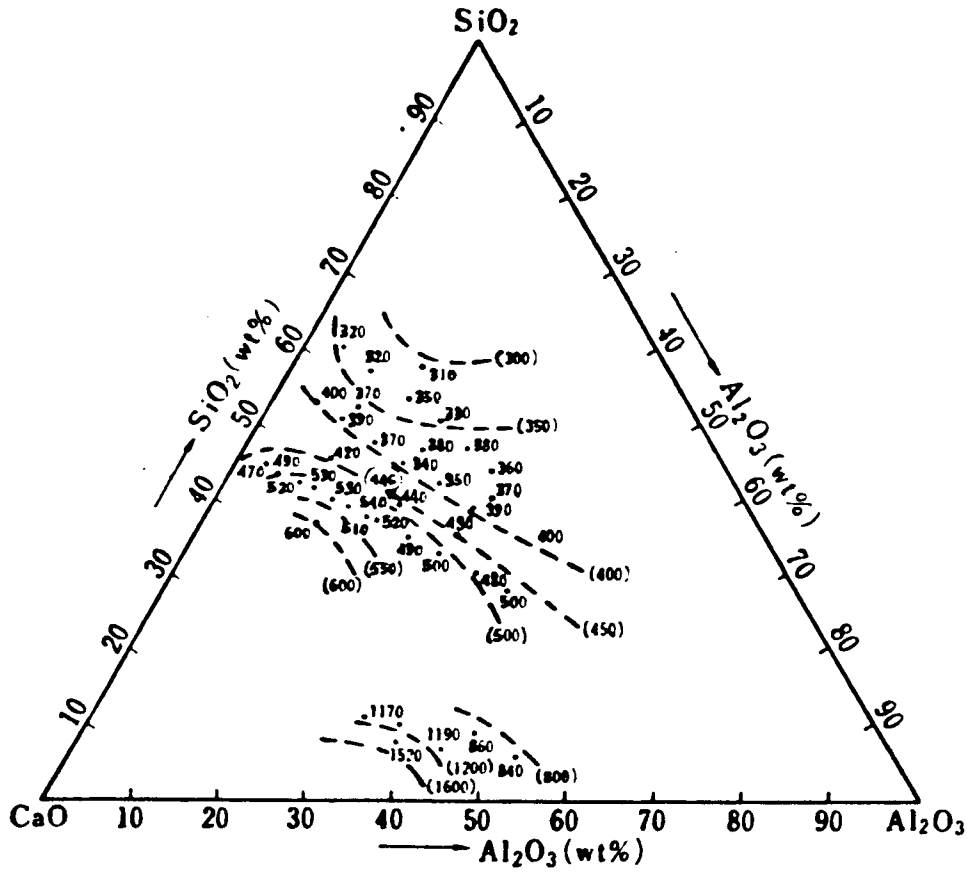

Fig. 2.17 water solubility (ppm H_2O) in CaO -SiO_2- Al_2O_3 system at 1550°C and p_{H_2O}=289 torr[22]

operating reactions with water vapour, according to Davies and Spassov[41] are:

$$4\ (-\overset{|}{\underset{|}{Si}}-O^-) + H_2O = 2\ (-\overset{|}{\underset{|}{Si}}-O^-.....H-O-\overset{|}{\underset{|}{Si}})- + O^{2-}..... \quad 2.10$$

$$2\ (-\overset{|}{\underset{|}{Si}}-O^-) + H_2O = (-\overset{|}{\underset{|}{Si}}-O^-....H-O-\overset{|}{\underset{|}{Si}}-) + OH^- \quad 2.11$$

Sachdev et al.[36] considered a new structural parameter, oxygen density, in view of the fact that these slags contain more than 90 vol. pct of oxygen ions. The oxygen density is defined as:

$$\text{Oxygen density} = \frac{\rho.L.No}{\bar{M}} \quad 2.12$$

where

ρ = density of the melt in gm/c.c.

L = Avogadro's number

No = mole fraction of oxygen atoms in the melt

$\bar{M}$ = average molecular weight of the melt calculated from the molar concentration of each melt component.

The water solubility linearly decreases with the increase of oxygen density (figure 2.18)

Considering the structural aspects of aluminosilicates, the sizes of the aluminum ion (r=0.5A) and the silicon ion (r=0.41A) and their charge levels are closely related. Consequently like a SiO_4^{4-} tetrahedron, Al^{3+} ion has also been suggested[36] to form AlO_4^{5-} as well as AlO_6^{9-} structures in liquid slags (even though simpler ionic complexes such as AlO_2^- and AlO_3^{3-} are plausible at high temperatures). When a small amount of Al_2O_3 is present in CaO $-SiO_2-$ Al_2O_3 slag, aluminium ions exist only in tetrahedral coordination. Thus similar to silicon ions, Al^{3+} acts like a network

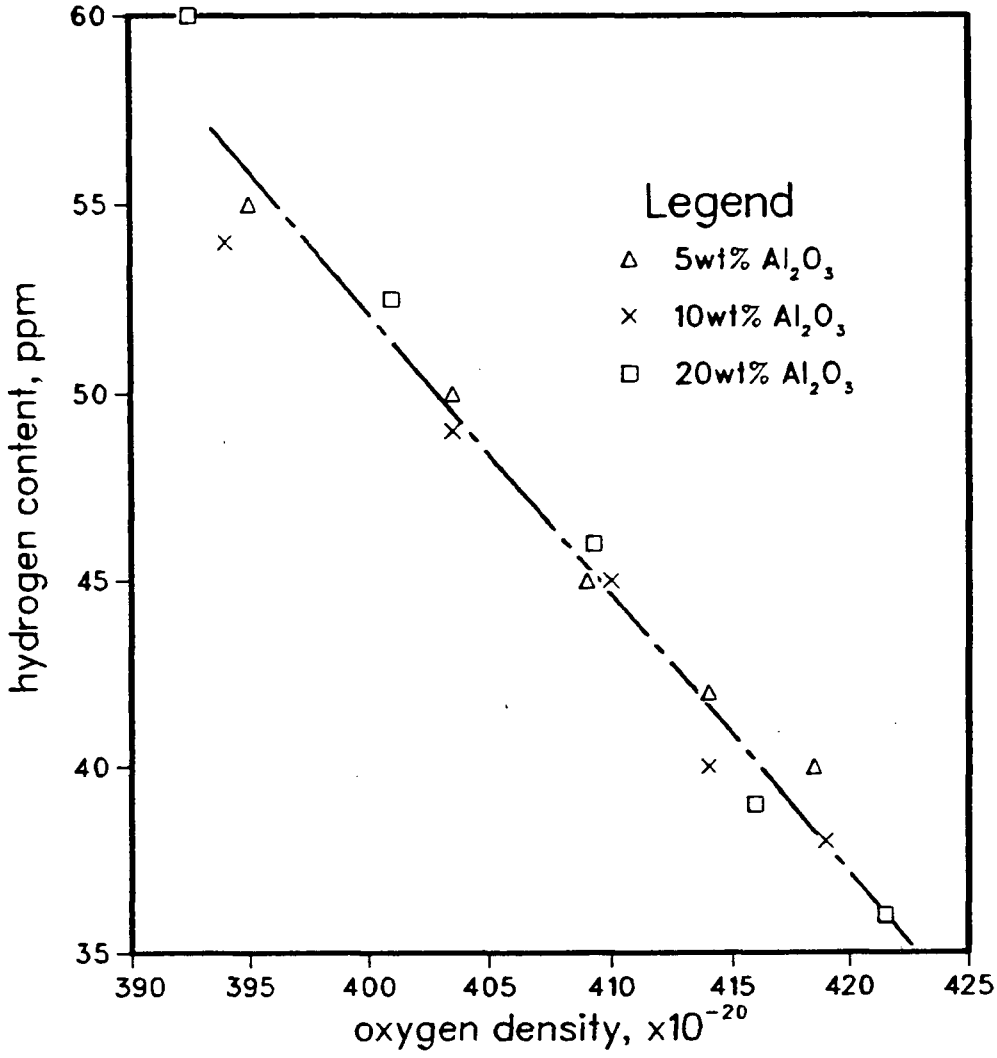

Fig. 2.18 Relationship between oxygen density and water solubility in CaO $-SiO_2-$ Al_2O_3 system at 1500°C and p_{H_2O}=190 torr[36]

connector and its further addition reduces the water solubility. Above 20 wt.pct. Al_2O_3 ,[36] this tetrahedral bonding becomes unstable causing a change to octahedral bonding, AlO_6^{9-} . As a result, a proportional amount of calcium ions is released from the structure making more free oxygen ions available for water solubility reaction., Thus the solubility of water is increased at this stage.

A similar conclusion can be drawn by considering ion-oxygen attraction (I) when the coordination number for the aluminum ion changes from 4 to 6 resulting in a weaker attraction of Al^{3+} ion.

The reports[22,31,38,42,43] on water solubility in CaO $-SiO_2-$'FeO' system are not at all consistent, possibly because of the difficulty in determining the form of 'FeO' present in the slag. Iguchi and Fuwa[43] reported a tendency of decreasing water solubility with the addition of 'FeO' in CaO $-SiO_2$ slag, whereas Wahlster and Reichel[38] observed an initial increase followed by a decrease upto 20 mole percent FeO, where the solubility starts rising again upto 60 mole percent FeO, and beyond that composition the solubility decreases (figure 2.19). Iguchi, et al.[22] reported somewhat similar behavior of 'FeO' with regard to the water solubility (figure 2.20). It was suspected that the increase of 'FeO' activity results in partial oxidation of 'FeO' to Fe_2O_3 which decreases the final water solubility. An increase of temperature is found to increase the solubility of water in these slags.[42]

$CaO-SiO_2-MgO$, another important ternary system, shows some apparent conflict on the effect of MgO on the water solubility. Iguchi and Fuwa[43] reported an increase of the water solubility with increasing MgO addition, but Zuliani et al.[18] who studied the same system by a

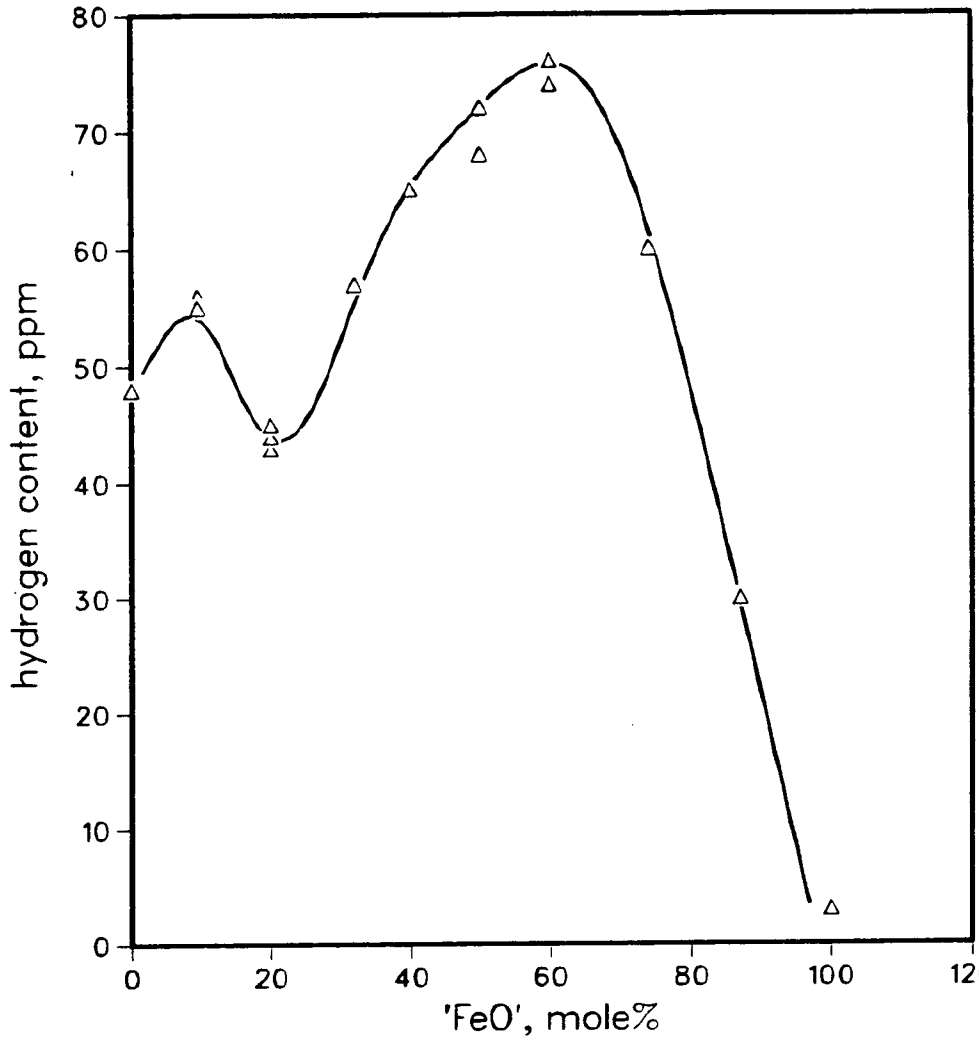

Fig. 2.19 Water solubility in CaO -FeO-SiO_2 system at 1600°C, CaO /SiO_2=1 and p_{H_2O} = 760 torr[38]

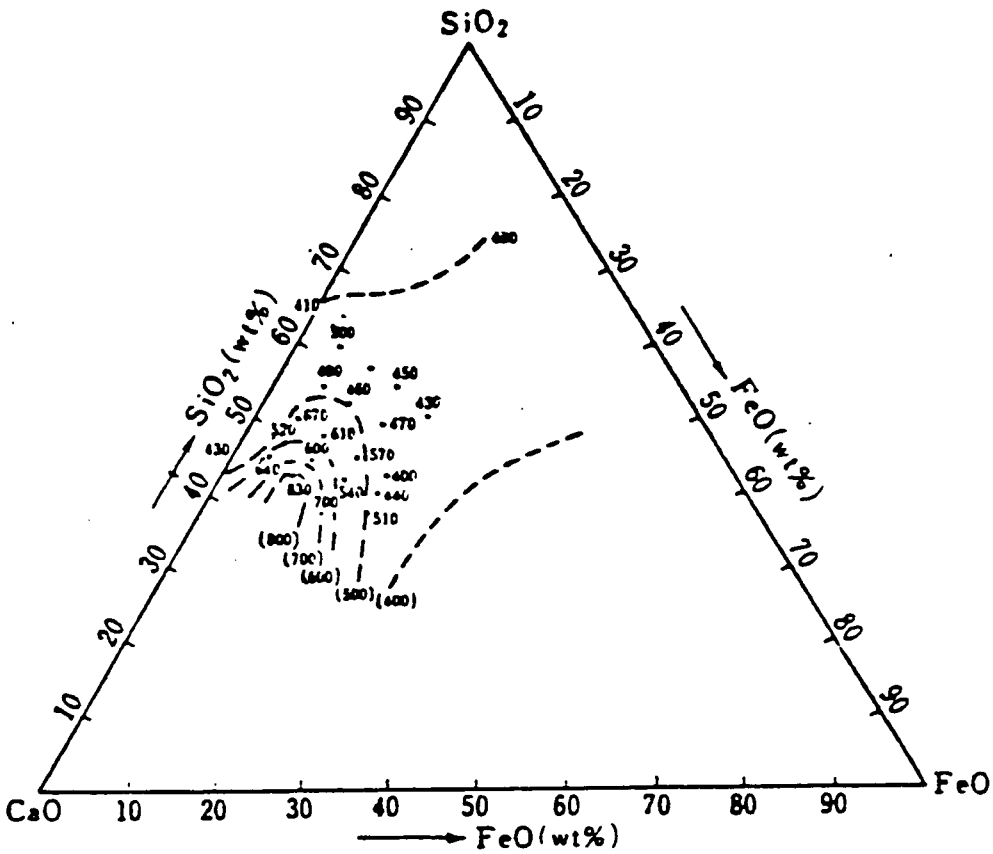

Fig. 2.20 Water solubility (ppm H_2O) in CaO –SiO_2–FeO system obtained at 1550°C, p_{H_2O}=289 torr[22]

thermogravimetric method did not find any effect of MgO, when it is replaced by CaO on a molar basis, although both the reports agreed upon a minimum solubility around unit basicity which is defined as $(N_{CaO} + N_{MgO}) / N_{SiO_2}$ (figure 2.21). Sosinsky et al.[44] found the inadequacy of this empirically defined basicity index, and instead they considered the activity of silica to resolve the above ambiguity (figure 2.22). They also obtained an empirical relationship to estimate water solubility in terms of the activity of silica, and it was given by:

$$(H_2O)ppm = (1095 - 2180 a_{SiO_2} + 3146 a^2_{SiO_2} - 1365 a^3_{SiO_2}) p^{0.5}_{H_2O} \qquad 2.13$$

Zuliani et al.[18] reported the independency of temperature from the water vapour solubility over the range of 1475 to 1575°C, while Iguchi and Fuwa[43] obtained, different, though not very significant effects of temperature in the acid and basic ranges of slags. In the acid range, the solubility of water decreases with increasing temperature, while the opposite is true in the basic range.

Some results on slags used for different industrial processes are available.[9,41,45,46] Water dissolved in blast furnace slags is close to an equilibrium level[46] and it ranges from 11 to 48 c.c./100gm depending on the location in the furnace from which the slag is sampled. The water solubility in these slags is also found to vary linearly with basicity, which is defined as the ratio of (CaO +MgO) to (SiO_2+ Al_2O_3) and is studied in the range of 0.9 to 1.0.

In acid open hearth slags[9], the water content is considerably lower than that in the slags of other steel making practices, and the water content does not reach an equilibrium level with the furnace atmosphere.

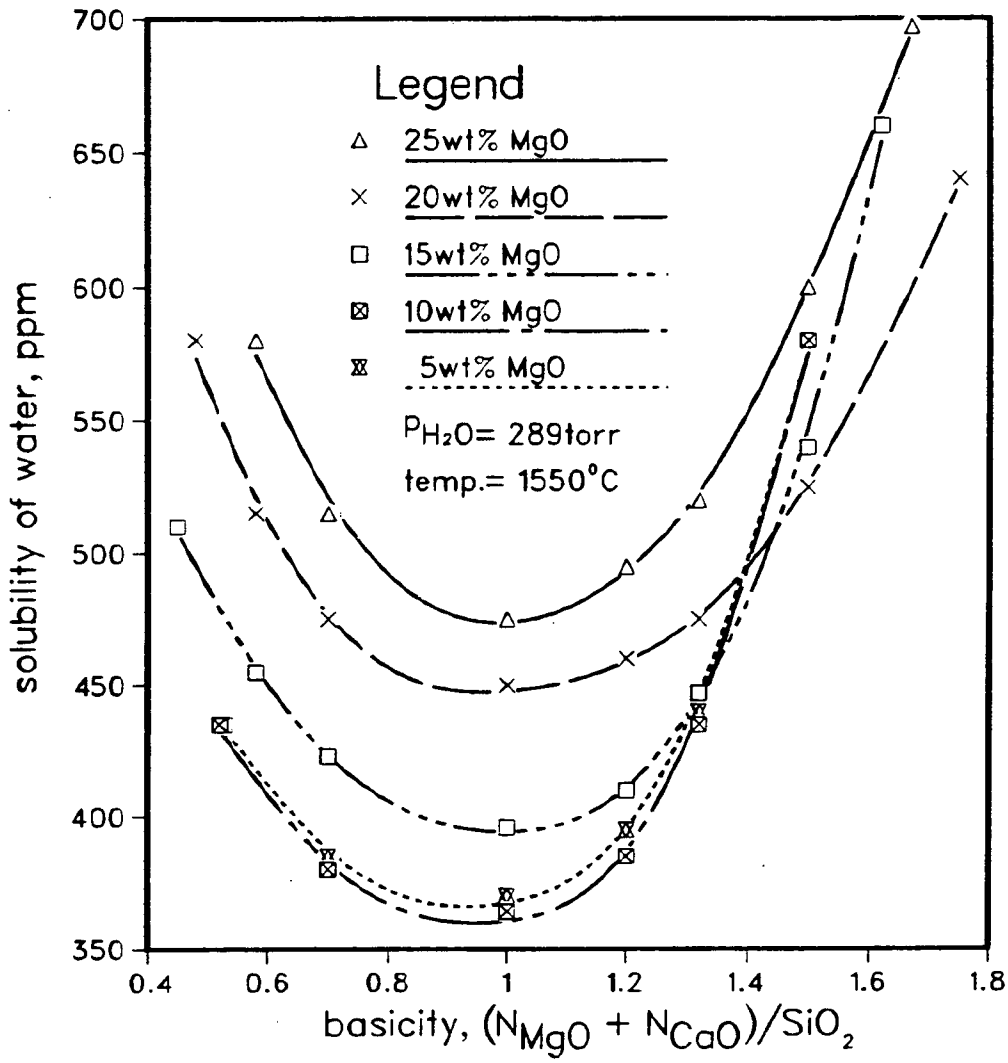

Fig. 2.21 Water solubility as a function of slag basicity and magnesia content at 1550°C and p_{H_2O}=289 torr[43]

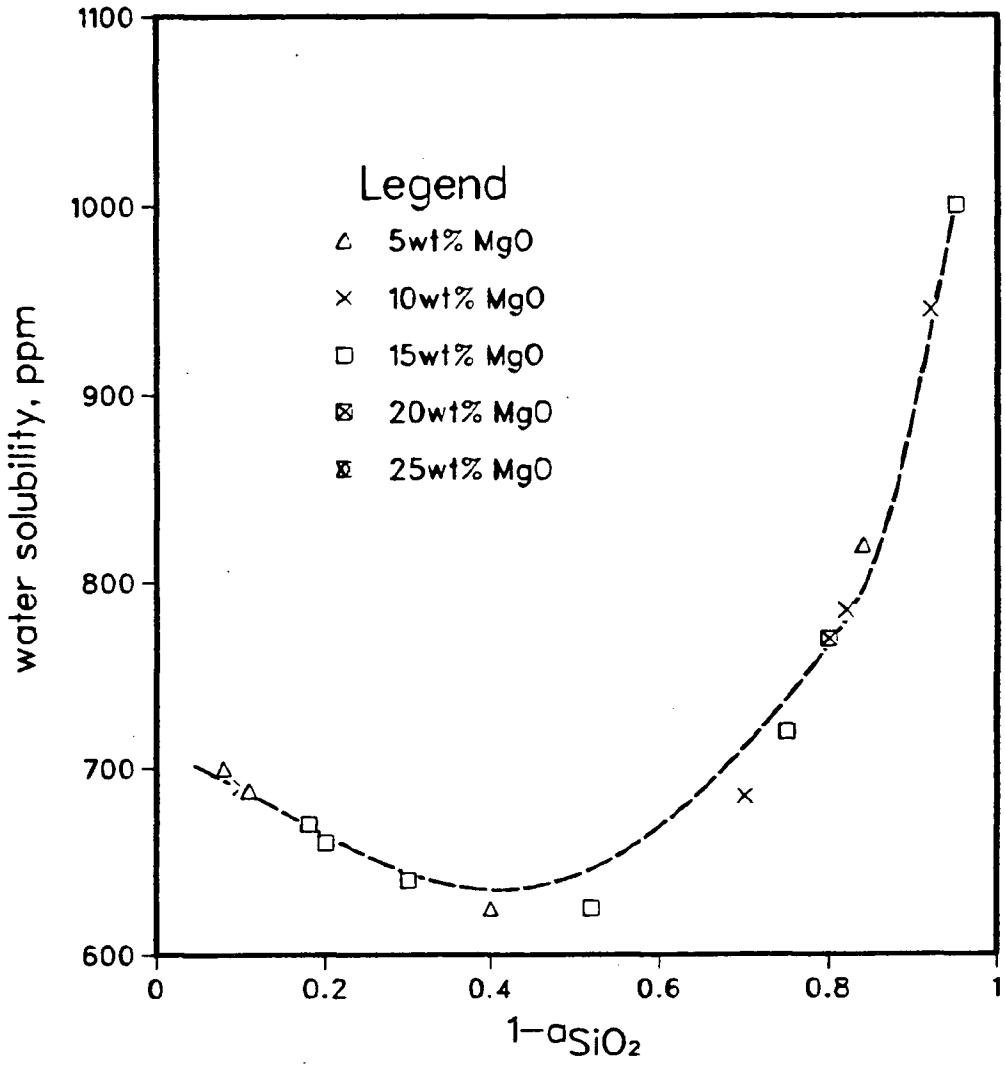

Fig. 2.22 Water solubility as a function of silica activity in the CaO -MgO-SiO_2 slags at p_{H_2O}=760 torr[44]

This is, presumably, due to the high viscosity of silicate slags. The water level in these slags is reported to be only around 115 ppm, about one third lower than the basic open hearth slags[9,45] which show almost the equilibrium value towards the end of a heat.

Electric furnace slags[9,45] contain about 200ppm water during the oxidizing period and are also close to equilibrium with the furnace atmosphere. In some cases,[9] the water level is reported to decrease during the heat.

These multicomponent complex industrial slags are difficult to study in order to extract the influence of different variables such as composition. Thus some investigations[41,46] involved multicomponent synthetic slags such as CaO $-SiO_2-$ Al_2O_3 $-MnO$[41] and CaO $-SiO_2-$ Al_2O_3 $-MgO$[46]. Davies and Spassov[41] obtained a small but significant effect of replacing CaO by MnO in the above quarternary system (table 2.3). At a constant MgO, the other quarternary slag has shown an almost similar effect with the increase of alumina and the subsequent decrease of lime.

2.3. HYDROGEN IN ESR INGOTS

The acceptable level of hydrogen for steel ingots destined for forgings with a relatively small forging reduction is around 2 ppm. Beyond this concentration, which is not that uncommon in ESR ingots, especially with a large cross-section, it is possible to produce small hairline cracks, also known as hydrogen flakes. The exact mechanics of this crack formation and propagation are debatable, although the critical role of hydrogen is very well recognized.

Table 2.3 Water Solubility in Different Silicate Slags[41]

Slag Composition, wt%				Temperature	Water Content
CaO	SiO_2	Al_2O_3	MnO	(Deg. C)	mg/g Slag
40	40	20	0	1400	0.536
Liquidus Temp.:1350				1450	0.536
				1500	0.539
				1550	0.546
				1600	0.417
30	50	20	0	1450	0.495
Liquidus Temp.:1350				1500	0.498
				1550	0.502
				1600	0.500
20	60	20	0	1450	0.476
Liquidus Temp.:1390				1500	0.473
				1550	0.465
				1600	0.472
35	40	20	5	1450	0.532
30	40	20	10	1450	0.521
20	40	20	20	1450	0.504
0	38	0	62	1350	0.379

Hydrogen, having a small covalent radius (0.32A), can dissolve as an interstitial solid solution in steels and other metals. Its solubility increases with temperature and attains a maximum in the austenite phase because of its FCC structure. Also, the solubility varies linearly with the square root of the pressure of H_2, suggesting that hydrogen dissolves atomically.

Hydrogen tries to effuse when it exceeds its solubility limit during rapid cooling of an ingot. In the case of large sections, the diffusion distance being considerable, hydrogen can be trapped in defect sites such as vacancies, dislocations, grain boundaries and inclusion-matrix interfaces[47]. The formation of hydrogen molecules at those sites would give rise to a very high pressure which, along with the thermal and transformation stresses, may result in rupture which appears as hydrogen flakes.

The molecular diffusion of hydrogen being very slow (diffusivity in iron at 100°C is $5x10^{-5}$ cm^2/sec) and the dissociation reaction, $H_2 \longrightarrow 2H$, being highly endothermic(103.3 Kcal/mol), it is extremely difficult to remove this hydrogen from the trapped sites. The slow cooling of ingots also does not help the escape of hydrogen since the hydrogen shows a tendency to segregate at the center. The isothermal heating at higher temperature (>200°C) is found to be a better method for hydrogen removal, even though it takes a great length of time.

Thus most of the previous investigations[1,7,11,25,48,49] in this area have focussed on understanding the reaction mechanism and the factors

controlling the final level of hydrogen in ESR ingots.

2.3.1 REACTIONS OF HYDROGEN TRANSFER

In view of the fact that the refined liquid metal in the ESR process is in continuous contact with the liquid slag, many authors[12,25,49] suggest that the final transfer of hydrogen to the metal takes place by the dissociation reaction of hydroxyl ion from the slag, and this reaction can be written as:

$$2(OH^-) + (Fe^{2+}) = [Fe] + 2[O] + 2[H] \qquad 2.14$$

Moreover, Medovar et al.[12] considered that the electrochemical discharge of hydroxyl ions at the anode caused the simultaneous increase of hydrogen and oxygen in the ingot,

$$(OH^-) = [H] + [O] + e^- \qquad 2.15$$

Holzgruber et al.[6] proposed a different hydrogen transfer scheme from the slag to the metal, which can be written as:

$$(OH^-) + e^- = (O^{2-}) + [H] \qquad 2.16$$

In case of the presence of protons (H^+) in the slag, the following cathodic reaction is also cited[12]:

$$(H^+) + e^- = [H] \qquad 2.17$$

However, considering the electrochemical reactions in ESR, the above reaction is highly unlikely since the overriding electrochemical reaction in this system would be:

$$Fe = Fe^{2+} + 2e^{-} \qquad 2.18$$

The reaction (2.18) would not only control the oxygen potential in ESR, but also limit the other reactions having higher potentials. Also the predominance of (OH^-) species in these slags, as observed in infrared studies, would make the last reaction (2.17) least important for further consideration.

From all the above reactions, it is very evident that in the case of a thermodynamic equilibrium that a constant distribution ratio of hydrogen in the slag and metal would be reached.

In a pilot plant study by Schurmann et al.[1], the distribution coefficient, (H)/[H], between the CaF_2-CaO-Al_2O_3 slag and the metal is investigated (figure 2.23). After about 30minutes, this coefficient, which is a function of the basicity of the slag, reaches a constant value. Similar observations are also reported by other authors[7,19,21] while studying other slag-metal systems. The initial hydrogen level in the metal, as observed at the bottom of an ingot, is normally higher than the equilibrium level which is reached after a certain time of operation[2]. If we consider a simpler form of hydrogen transfer reaction such as:

$$2(OH^-) = (O^{2-}) + [O] + 2[H] \qquad 2.19$$

and the presence of lower oxygen potential at the initial stage of remelting, the above reaction would shift towards the right giving rise to a higher hydrogen level at the bottom of the ingot.

Bagshaw[48] simplified the hydrogen transfer process, considering the overall gas-slag-metal equilibrium and the obvious following reaction:

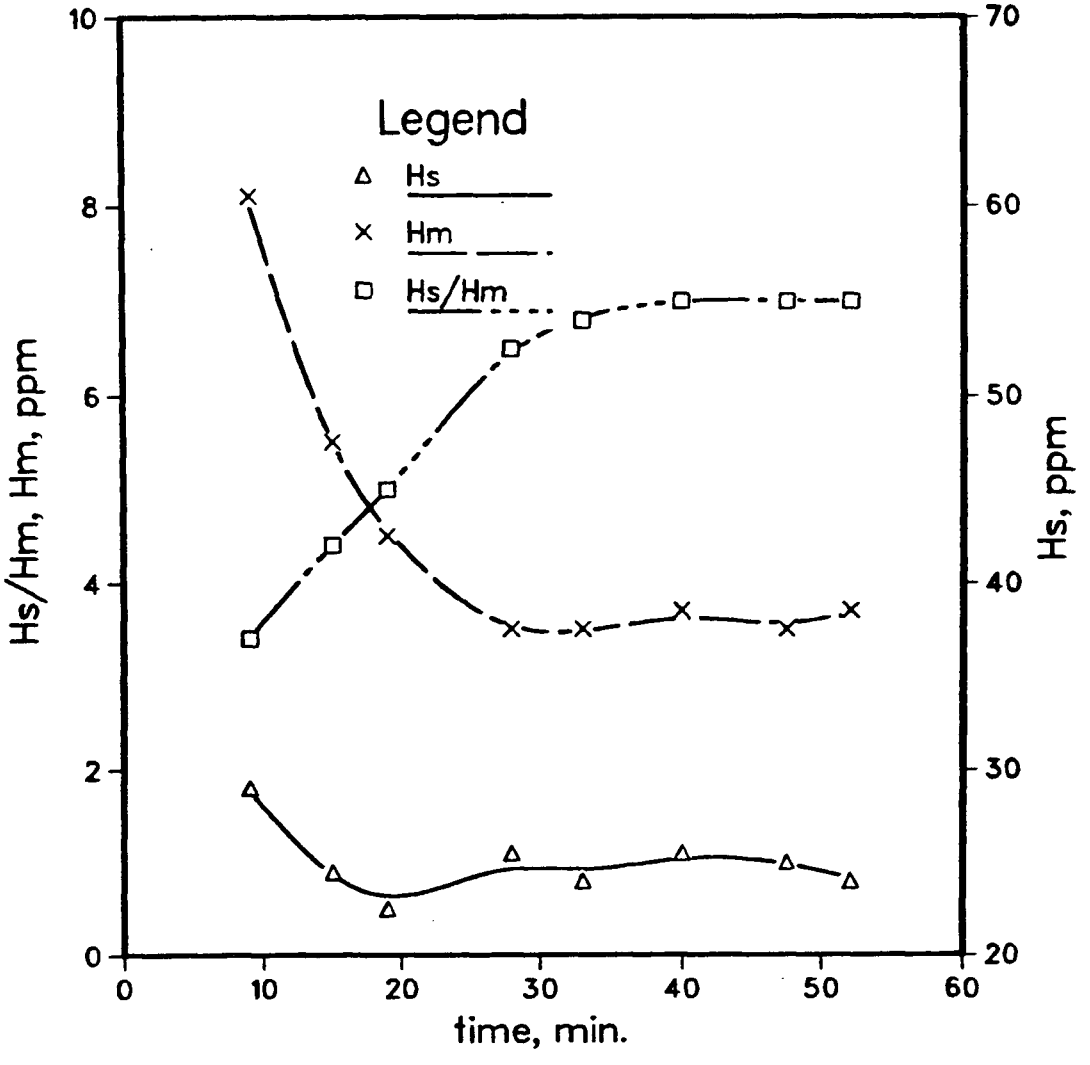

Fig. 2.23 Hydrogen equilibrium between slag and metal in an ESR operation, slag is 40 CaF_2 -30 Al_2O_3 -30 CaO , T=1780°C, p_{H_2O}=7 torr[1]

$$H_2O(g) = 2[H] + [O] \qquad 2.20$$

The oxygen potential in the system which directly controls the oxygen level in the ingot also influences the hydrogen level in the metal. For the above equilibrium, at a constant temperature, increasing the oxygen potential would reduce the hydrogen content in the metal. However, this would happen at the expense of lower desulfurizing power and higher oxidation losses of the alloying elements.

The consequent dependence of hydrogen in the metal on the water vapour pressure (figure 2.24) has been observed in different studies,[7,39,48] but by merely looking at this equilibrium, the vital capability of slag in controlling hydrogen transfer can not be estimated.

The estimation of equilibrium hydrogen solubility(%) can be made by the following expression[19]:

$$\log[H]_{max} = \log K_H\sqrt{p_{H_2}} - \Sigma e_H^i\,[i] \qquad 2.21$$

where

K_H = the equilibrium constant of solubility in iron,

e_H^i = the interaction parameter between hydrogen and the element i

[i] = the concentration of the element i, %.

Surprisingly, in the above formula, the partial pressure of hydrogen, p_{H_2}, is considered instead of a more relevant term i.e. water vapour pressure, p_{H_2O}.

The temperature dependence of the equilibrium constant, K_H, and the interaction parameter, e_H^i, are given by[19],

$$K_H = -1730/T - 1.688 \qquad 2.22\ \dagger$$

---

†The expression should be, $\log K_H = -1730/T - 1.688$

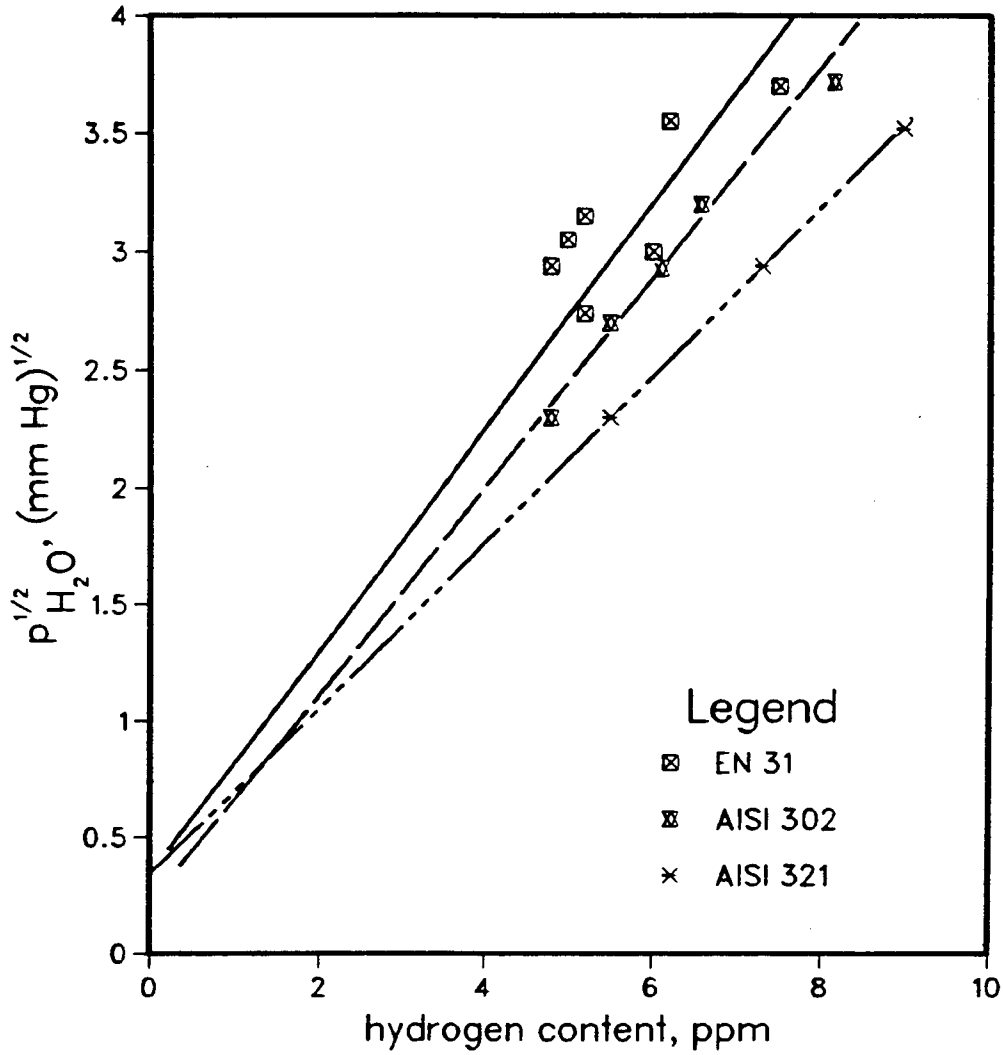

Fig. 2.24 Hydrogen solubility in ESR ingots as a function of water vapour pressure in the atmosphere[48]

$$e^{i}_{H}\ (T) = (3940/T-1.1)\ e^{i}_{H(1873)} \qquad 2.23$$

Vatolin et al.[15] analyzed the hydrogen transfer reaction using the available thermodynamic data to obtain an expression of the hydrogen distribution ratio between the slag and the metal as a function of temperature and the concentration of Fe^{2+} in the slag. Unfortunately, the expression predicted much lower values than those observed in practice, suggesting some flaws in the theoretical analysis.

2.3.2 FACTORS CONTROLLING HYDROGEN IN THE INGOT

Since the main sources of hydrogen in ESR are the moisture in the slag and in the atmosphere on top of the slag, reducing these two inputs would reduce the hydrogen in the remelted metal. Thus, all the factors limiting the hydrogen solubility in slag, as described previously, would in turn control the hydrogen level in the metal.

Moreover, Masui et al.[25] found that the gas/slag interface area, electrode hydrogen content, remelting rate and slag quantity are also controlling factors with regard to the hydrogen level in the ingot. The similar influence of remelting rate and metal/slag interface area is not evident in the work of Holzgruber et al..[6] They observed that the hydrogen at the bottom of the ingot is controlled by the moisture of the flux and at the top mainly by the hydrogen in the electrode and water vapour pressure in the atmosphere. This is probably because in their system the initial H_2O in the flux is very high.

The argon blowing through the slag and liquid metal helped Medovar el al.[12] to reduce the final hydrogen content by 2-2.5 times. In a regular practice, such a step would be too dangerous to implement.

Pocklington[7] did not get any benefit using direct current as the melting source, whereas Holzgruber et al.[6] found the use of superimposed DC component to be the most effective means of reducing the hydrogen level in a laboratory scale ESR unit. In AC remelting practice, Pocklington[7] stressed controlling the iron oxide levels in the slag for optimum concentration of hydrogen in the ingot. Both the steps, mentioned above, alter the oxygen potential of the system, which in turn, as discussed before, influence the final hydrogen level.

2.4. TECHNIQUES OF MEASUREMENT OF HYDROGEN IN SLAG

2.4.1 SAMPLING OF SLAG

The problem of hydrogen determination in slag begins at the sampling stage. Previous workers used mostly a copper[3] or tungsten[7,24] bar to collect representative slag samples from an experiment. The ESR slags being highly hygroscopic are prone to contamination while exposed in the air during handling. Also, due to the conducting nature of these slags and the harsh environment around the sampling area in an ESR unit, the electrical power must be disconnected during sampling. This practice introduces ripple marks on the surface of a solidified ingot which is otherwise remarkably smooth. Another effect is the change in thermal regime of the molten slag pool which changes the important physical and chemical characteristics of the slag.

Considering all these aspects, slag sampling using a quartz tube is envisaged,[3] but this has not previously been used due to the

suspicion that the silica might dissolve into the slag.

2.4.2 METHODS OF ANALYSIS

The accurate determination of hydrogen in ESR slag is a major obstacle to any study of the behavior of hydrogen in this system. The simple weight loss method of evolving water from the slag by heating around 500-600°C is not sufficient to remove all the hydrogen from the slag. Some chloride salts are found to retain water even at 1000°C[50]. Also fluoride-slags hydrolyze at high temperature and generate HF gas, thus making the weight loss analysis more complicated and uncertain. In the ESR slag, the hydrogen, present as hydroxyl ion, is chemically bonded to the structure and so is present as a stable solution at the high temperature. On the other hand, hydrogen forms a physical solid solution with steel; the effective species, being the hydrogen atom,[11] can diffuse out of steel easily when heated in a vacuum system. Thus, for the hydrogen analysis of slag, it is necessary to melt the slag in a vacuum to extract the dissolved hydrogen either in the form of molecular hydrogen or water vapour which should be analyzed immediately in a sensitive apparatus.

Various techniques have been developed to improve the confidence and accuracy of measurement. In the literature, most of the methods can be classified into two categories: vacuum extraction and extraction into a stream of carrier gas.[51] Again, among the vacuum extraction methods, there are two groups: vacuum heating[52] and vacuum fusion of slag.[3,53]

A mass spectrometric study[53] reveals that the hydrogen evolved from slag exists both as H_2O and molecular hydrogen. Therefore,

for quantitative measurement, all of it has to be either converted to H_2 with the help of reducing agents such as aluminum, ferromanganese, calcium carbide or oxidized to water vapour by some oxidant, such as CuO.

In determining hydrogen in fluoride slags by the carrier gas method, investigators[13,51] detected the presence of SiF_4 and HF in the gas stream evolving out of the slag at 1200°C because of the following reactions:

$$CaF_2 + H_2O = CaO + 2HF \qquad 2.24$$

$$4HF + SiO_2 = SiF_4 + 2H_2O \qquad 2.25$$

The interferences of HF and SiF_4 in the final adsorption tower are taken care of by passing the gas through a calcium oxide tube, kept at 500°C, and these gases result in the following conversions:

$$SiF_4 + 2\ CaO = SiO_2 + 2\ CaF_2 \qquad 2.26$$

$$2HF + CaO = H_2O + CaF_2 \qquad 2.27$$

Thus, the total hydrogen is determined gravimetrically in the form of H_2O by adsorbing in a magnesium perchlorate tower (figure 2.25).

The standard state decomposition temperature of calcium hydroxide is 580°C.[54] Therefore, keeping the calcium oxide tube at 500°C would give rise to some amount of moisture being trapped in the calcium oxide; and also, the cold parts of tubing, before the adsorption tower, would adsorb some moisture. These may be the reasons for getting a low value of hydrogen in ESR slags as analyzed by Schmidt.[51]

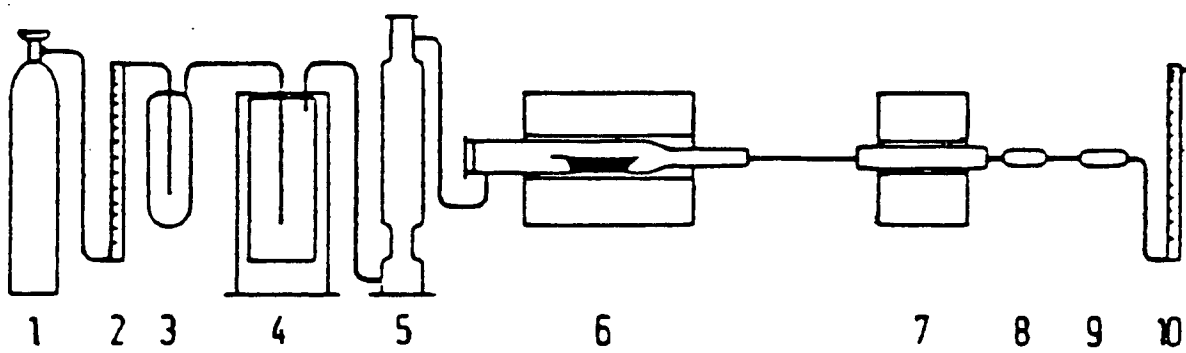

Fig. 2.25 Schematic diagram of the apparatus for determining hydrogen in ESR slags[51]. 1.Carrier gas (O_2) 2. flowmeter 3. H_2SO_4 4. furnace 5. soda lime+$Mg(ClO_4)_2$ 6. Pythagoras tube 7. CaO tube 8-9. absorption tubes 10. flowmeter

In a modified method,[17] (figure 2.26) the slag is melted in an MgO crucible inductively under the flow of oxygen as a carrier gas. The evolved gas is then passed through lime, kept at 500°C, and copper oxide, kept at 650°C, to obtain hydrogen in the form of water vapour. The quantitative detection of water vapour is done in a 'Keidel' electrolytic cell. The cell is equipped with a constant voltage source and platinum electrodes coated with P_2O_5 which reacted with water to generate H_3PO_4, which is also the electrolyte of the cell. At a constant potential, the change in current flow in the cell is proportional to the water reacted and hence to the hydrogen evolved from the slag.

The detection of hydrogen as water is less desirable because of its low vapour pressure and the high adsorptivity of water vapor on the walls of the tubes of an analyzer. In this regard, the analysis of hydrogen poses fewer difficulties while using a pressure gauge,[52] a mass spectrometer[3,53] or a commercially available gas analyzer such as LECO RH-1E and RH-2[2] and OMKF-71[8].

In developing a vacuum heating technique which requires, relatively, lower temperatures which do not melt the slag, Lloyd and Shanahan[52] found that a considerable amount of moisture from the atmosphere adsorbed on the basic slag surface and the system required initial heating of the sample at 150°C in a vacuum. Reproducible results are obtained in the vacuum apparatus, by evolving hydrogen from the slag sample at 900°C and measuring the resulting pressure changes by a piston-operated McLeod gauge (figure 2.27). Any water vapour, if present in the evolved gases, is converted to hydrogen by passing it through ferromanganese. The problem associated with this type of method is that it

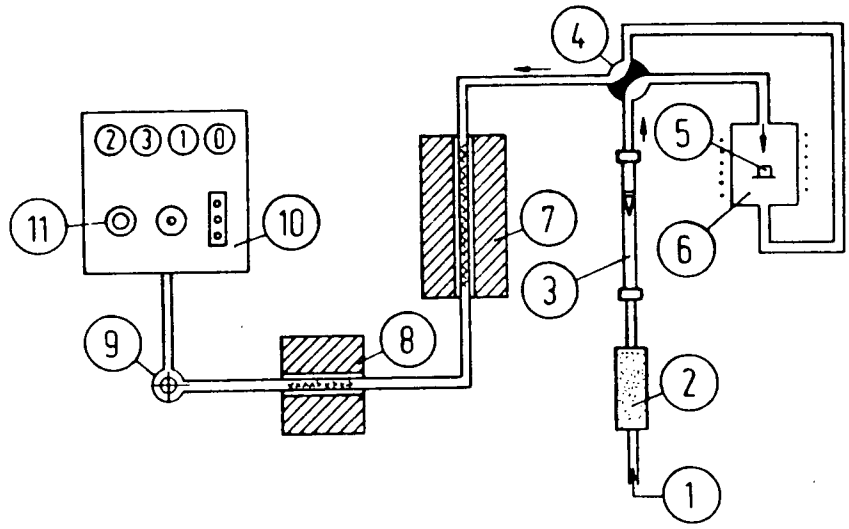

Fig. 2.26 Apparatus for determining hydrogen in slags[17]. 1.oxygen 2. P_2O_5 3. rotameter 4. 4-way stopcock 5. sample 6. induction furnace 7. CaO -reaction furnace 8. CuO-reaction furnace 9. calibrator 10. Electron gauge 11. 'Keidel' cell

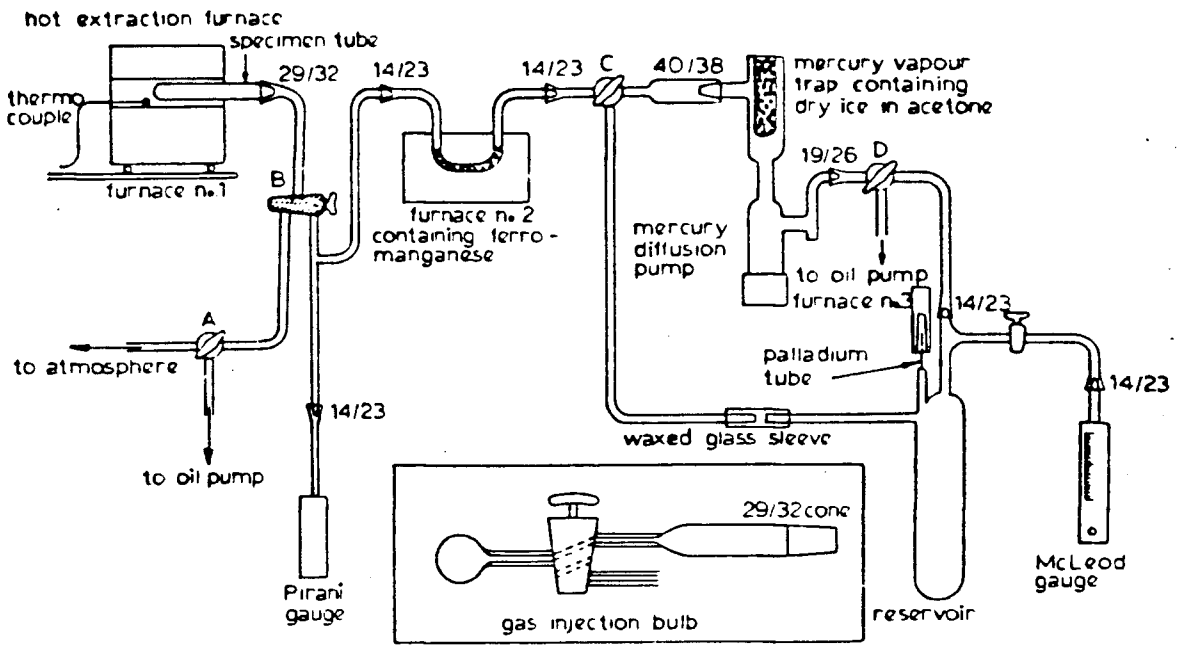

Fig. 2.27 Schematic diagram of hydrogen analyzer[52]

is difficult to confirm the complete evolution of hydrogen in a solid sample, and since it normally takes a longer time to analyze, there is the possibility of losing some hydrogen due to its very high diffusion coefficient.

The vacuum fusion method, even though the most complex, is used by many authors[3,9,24] to determine hydrogen both in steelmaking and ESR slags. Nakamura and Harashima[3] analyzed the hydrogen in ESR slags by inductively melting the slag in a molybdenum crucible along with aluminum followed by a collection of the generated gas in a reservoir which is later connected to a mass analyzer to detect the amount of hydrogen present. The use of a molybdenum crucible is not desirable as far as the analysis of hydrogen is concerned, since the metal can form volatile oxide[9] which can adsorb hydrogen and result in a lower determination of hydrogen in the slag.

2.5. THERMODYNAMIC PROPERTIES OF ESR SLAGS

The quantitative information of different thermodynamic properties, such as phase diagrams, chemical activities of different components in binary and ternary slags and solubilities of gases is very helpful in selecting a proper composition of slag for an ESR operation. Because of the highly corrosive nature of ESR slags at higher temperature, it is very difficult to carry out a controlled experiment for accurate determination of the above properties. Different experimental techniques are employed by a number of workers for a better understanding of phase diagrams and other thermodynamic behavior of ESR slags. Unfortunately in some cases, there are wide discrepancies among the reported results, presumably due to limitations and the different levels of accuracy in the

various experimental techniques. Errors may also creep in because of the high instability of fluoride slags in an open system with respect to chemical composition. This aspect is due to the presence of volatile species, such as CaF_2, AlF_3 and SiF_4, and the feasible chemical reactions are as follows (equation 2.28 is same as equation 2.24):

$$CaF_2 + H_2O = CaO + 2HF \qquad 2.28$$

$$3\ CaF_2 + Al_2O_3 = 2AlF_3 + 3\ CaO \qquad 2.29$$

Therefore experiments not designed to analyze the final composition of slag would probably give erroneous results.

2.5.1 PHASE DIAGRAMS

For a successful operation during electroslag remelting, slag should have a melting point at least 100°K lower than that of metal. The phase diagram is an important guide to judge this criterion and also the presence of any miscibility gap which would alter the physical and chemical characteristics of the melt drastically. Already phase diagrams of CaF_2-based slags, both for binary and ternary systems, are reported by many authors[55-61] However, considerable discrepancies exist with regard to the existence of different phases and the liquidus lines of various systems since they are obtained by experiments in some cases, such as DTA and quenching techniques,[61] and sometimes deduced from other results.[55] In the present context, only the aluminate and silicate slags containing CaF_2 will be reviewed.

<u>CaO – CaF_2</u>

So far it has been clearly established that this system forms a eutectic at 1360°C and around 16% CaO. Also, other authors (except

Baak[62]) agree well with the liquidus line on the CaF_2 rich section before the eutectic. Baak[62] reported the existence of a miscibility gap in the range of 1-8% CaO on the basis of the measurements of electrical conductivity (figure 2.28). The reason for this discrepancy may be due to the formation of CaC_2 phase, which is most likely for an experiment carried out in a graphite crucible. Therefore the results obtained by cryoscopic studies as carried out by Kojima and Masson[63] can be taken as a more reliable reference in this region (figure 2.29). Also there is wide scatter of data beyond the eutectic point,[56] but the reports by Kor and Richardson[55] and Ries and Schwerdtfeger[64] agree well to serve as a guideline in this zone.

<u>CaF_2 - Al_2O_3</u>

This system can be considered binary only when experiments are carried out in a sealed cell. Otherwise the following reaction tends to make it a CaF_2-CaO-Al_2O_3 ternary(same reaction as in 2.29):

$$3\ CaF_2 + Al_2O_3 = 2AlF_3 + 3\ CaO$$

The above reaction is a typical displacement equilibrium reaction in a simple reciprocal salt system where the variation in composition with respect to all four ions, such as, Ca, Al/O, F changes the proportions of salts in the mixture. This variation can be properly represented by four composition axes with polythermal profiles. However, the representation becomes much more complicated when there are more than two salts and when some stable compounds are formed.

Ries and Schwerdtfeger[64] verified the existence of the above reaction by performing experiments both in an open cell and a sealed cell (figure 2.30). The same reason can be attributed to the discrepancies in

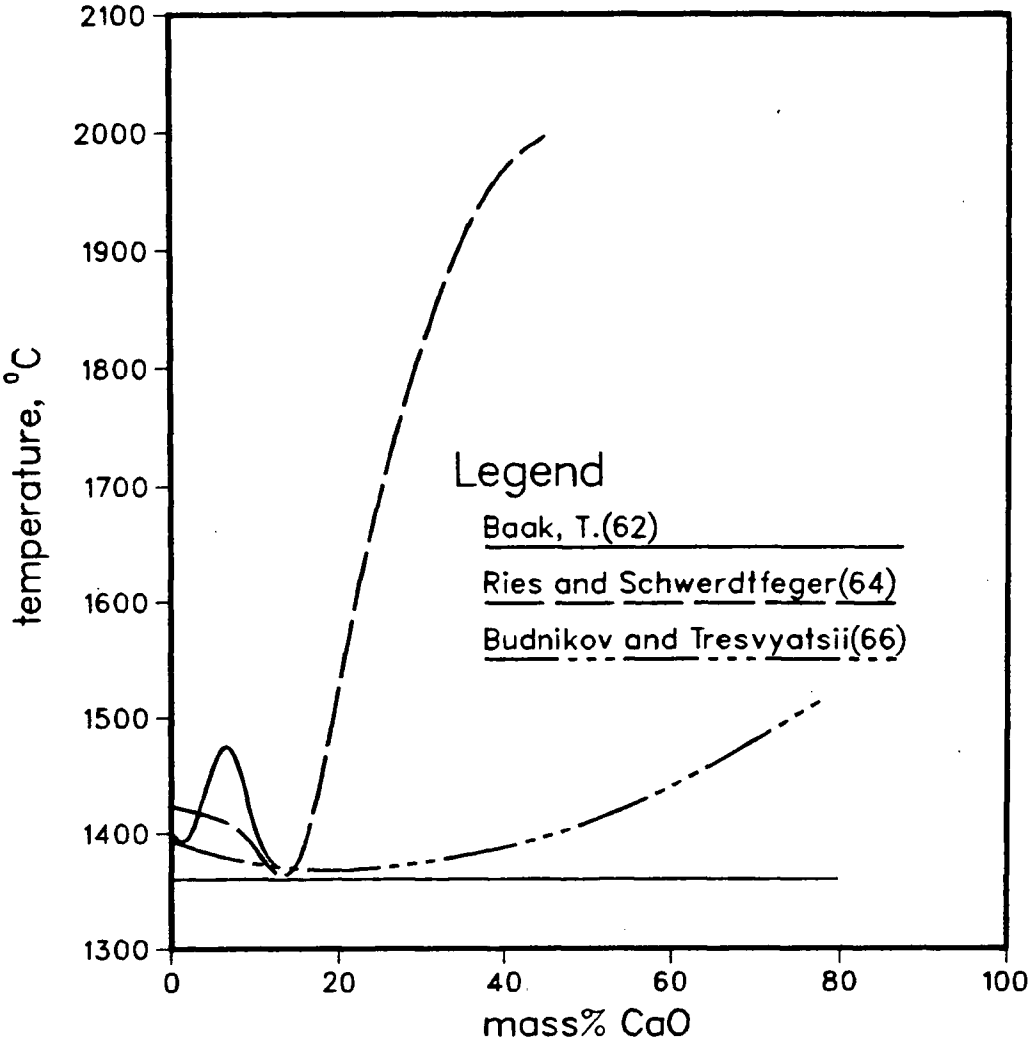

Fig. 2.28 Phase diagram for CaO – CaF_2 system

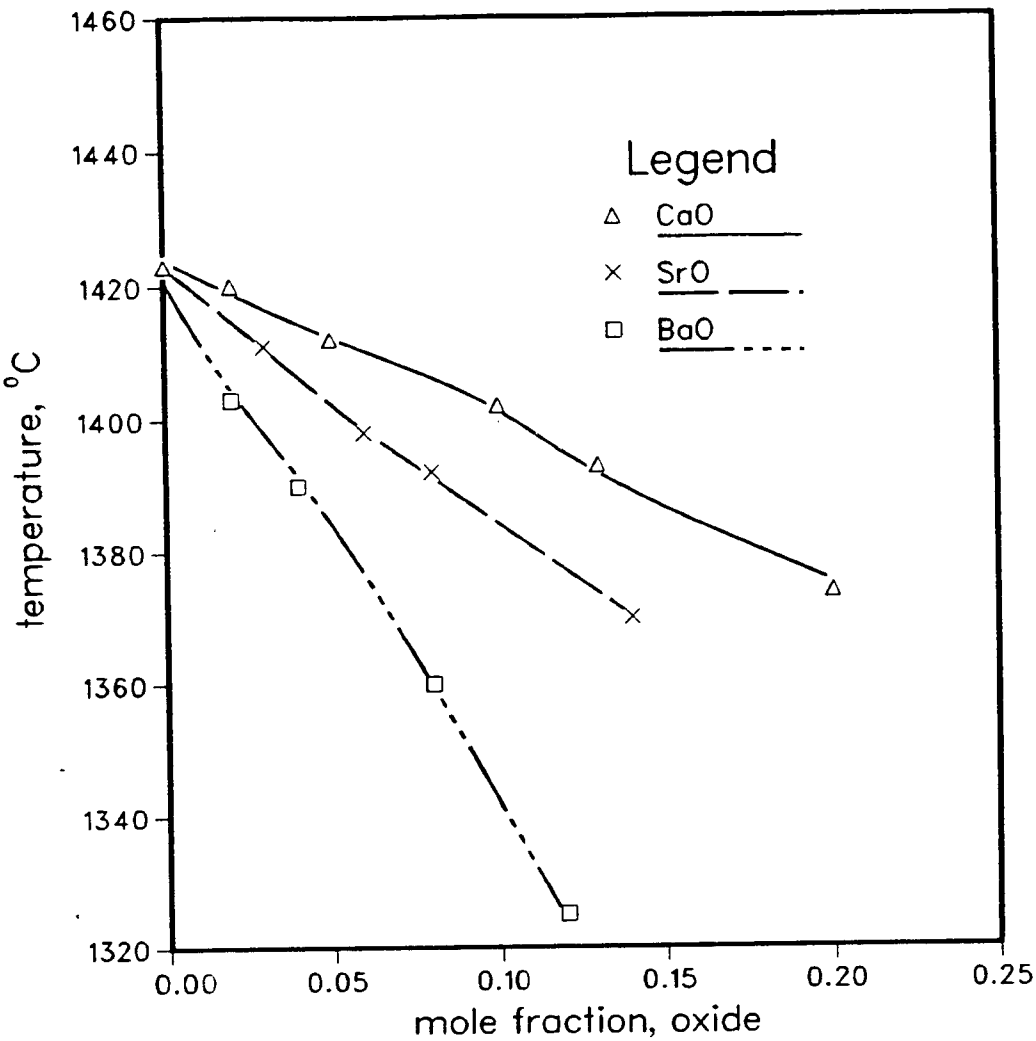

Fig. 2.29 Depression of freezing point of CaF_2 by CaO , MgO and SrO[63]

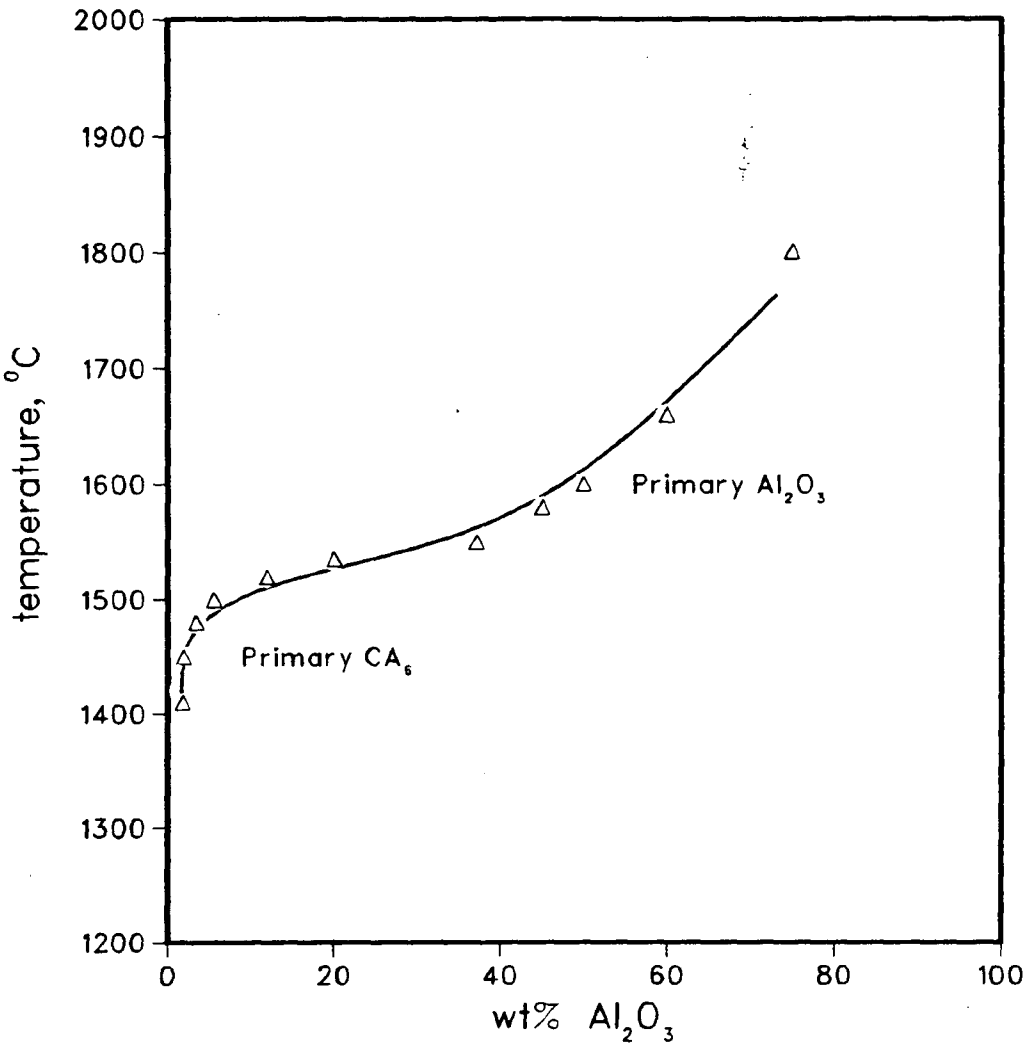

Fig. 2.30 Liquidus line of CaF_2 – Al_2O_3 melts according to Ries and Schwerdtfeger.[64] The melts are probably substantially contaminated with CaO.

phase diagrams reported by Kuo et al.[65] and Mitchell et al.[60] (figure 2.31). The extent of difference would depend on the amount of CaO formed due to the above reaction. 70wt% CaF_2 - 30wt% Al_2O_3, a widely used ESR slag, is investigated by Ries and Schwerdtfeger.[64] The evaporation of AlF_3 at temperatures 1600-1750°C changes the system to a ternary and the liquid separates into a two-phase mixture arising out of the miscibility gap which will be dealt with in detail in the next section.

<u>CaF_2 - CaO - Al_2O_3</u>

This ternary slag system is very widely used in electroslag remelting and so has been investigated by several authors to study its equilibrium phases and the melt behavior at different temperatures. Both the open[59,64,67] and closed[64] systems are considered but Ries and Schwerdtfeger[64] reported no significant difference to be observed due to these different conditions. However, under open cell condition, the system should be considered as quarternary type, CaF_2-CaO-AlF_3-Al_2O_3.[56]

Different compounds, so far identified in this system[56] are: CA_6, CA_2, CA, C_3A, $C_{12}A_7$, $C_{11}A_7Fl$ and C_3A_3Fl (figure 2.32). Nafziger[58] studied this ternary system under a partial helium atmosphere, but did not observe any miscibility gap which is confirmed to exist by other reports[56,64] both under open and closed cell conditions. Further indirect evidence of miscibility gap can be deduced from the ultrasonic measurements, isodensity, isoviscosity and isoactivity contours in that composition range.[56]

The electrical conductivity is measured by Mitchell and Cameron,[68] and it is revealed that at higher CaF_2 contents, networks are based on $AlO_2F_2^{3-}$ and $AlOF_2^-$, and that lime additions to these melts release the fluoride ions and produce AlO_3^{3-} and AlO_2^- structures.

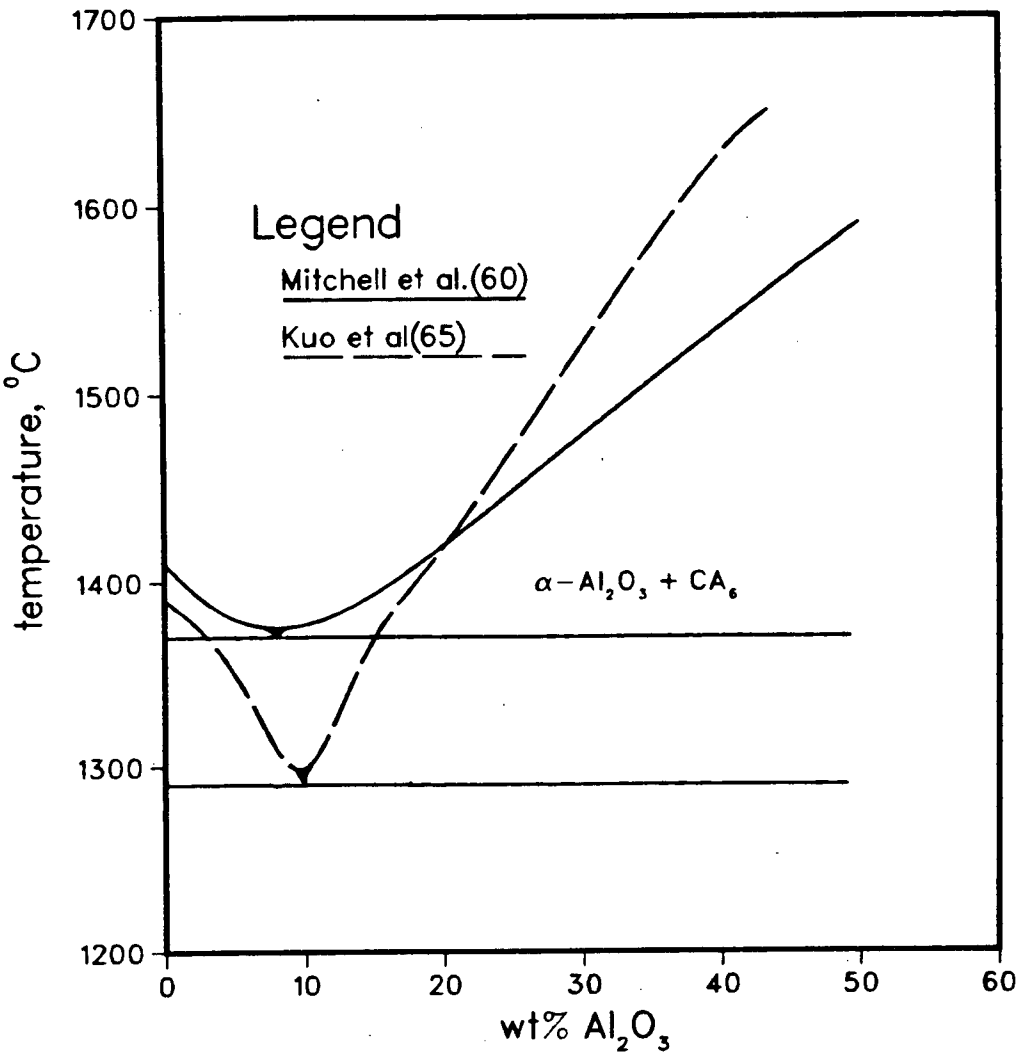

Fig. 2.31 Phase diagram for the system ` $CaF_2$ '- $Al_2O_3$ ; ` CaF_2 '= CaF_2 +2wt% CaO

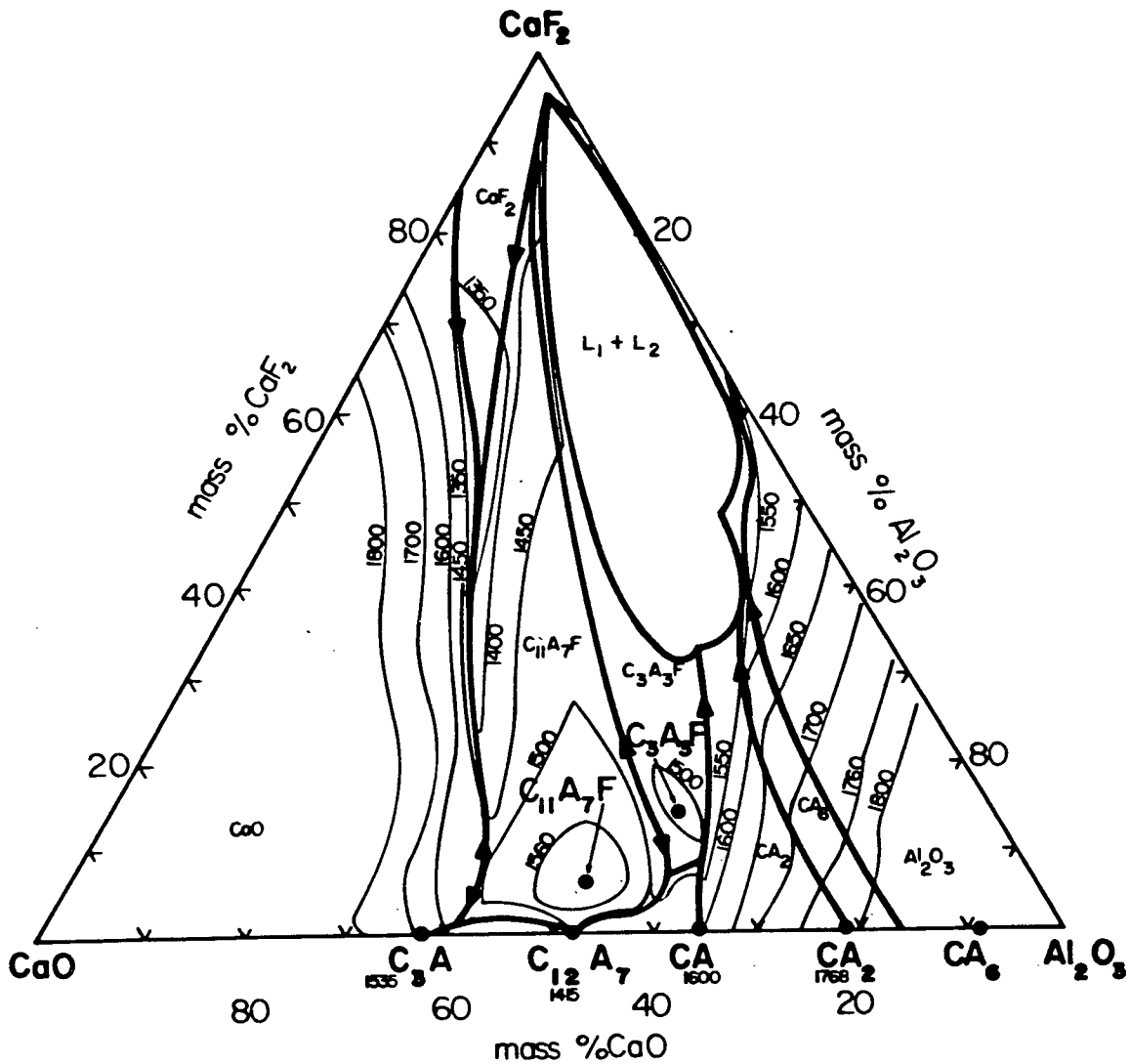

Fig. 2.32 Phase diagram for CaF_2 – CaO – Al_2O_3 system[56]

At low CaF_2 contents,[69] the molecules of $Al_3O_7^{5-}$ are bound by calcium ions and any additions of CaF_2 would tend to break the networks and subsequently the fluoride ions would fill the vacant sites.

The structural information further can be derived from the ultrasonic studies on the melts. At low levels of CaF_2 (0–30%) the melt consists of mainly Al–O structures which possess a considerable amount of covalent bonding. At high levels of CaF_2 (70–100%) the structure is predominantly ionic and at an intermediate concentration (30–70% CaF_2) both covalent and ionic types of structure co-exist.

CaF_2 – CaO – SiO_2

Several studies are reported[59,61,70-73] for this ternary system. Under open-cell conditions, it belongs to a strictly reciprocal system, CaF_2–CaO–SiF_4–SiO_2, but for all practical purposes, the established ternary phase diagram can be considered (figure 2.33). The compounds formed in this system are: CS, C_3S_2, C_2S, C_3S, CS_3FI, C_4S_2FI and C_9S_3FI. The different experimental conditions and techniques employed to study the phase diagram have resulted in some discrepancies. Salt[59] reported two separate two-liquid regions, but other authors[56,61,70] observed only one miscibility gap over a large composition range covering both the regions as proposed by Salt.[59] The thermochemical results[72] also support the wider and single zone miscibility gap.

Addition of CaF_2 in acidic silicate melt is believed to act as a network modifier, whereas in a basic melt it apparently behaves as a diluent as observed in weight loss and viscosity measurements.[71] This phenomenon is explained by Shinmei et al.[71] by the nature of competition between F^- and O^{2-} on the silicate network. The fluoride ion is far weaker

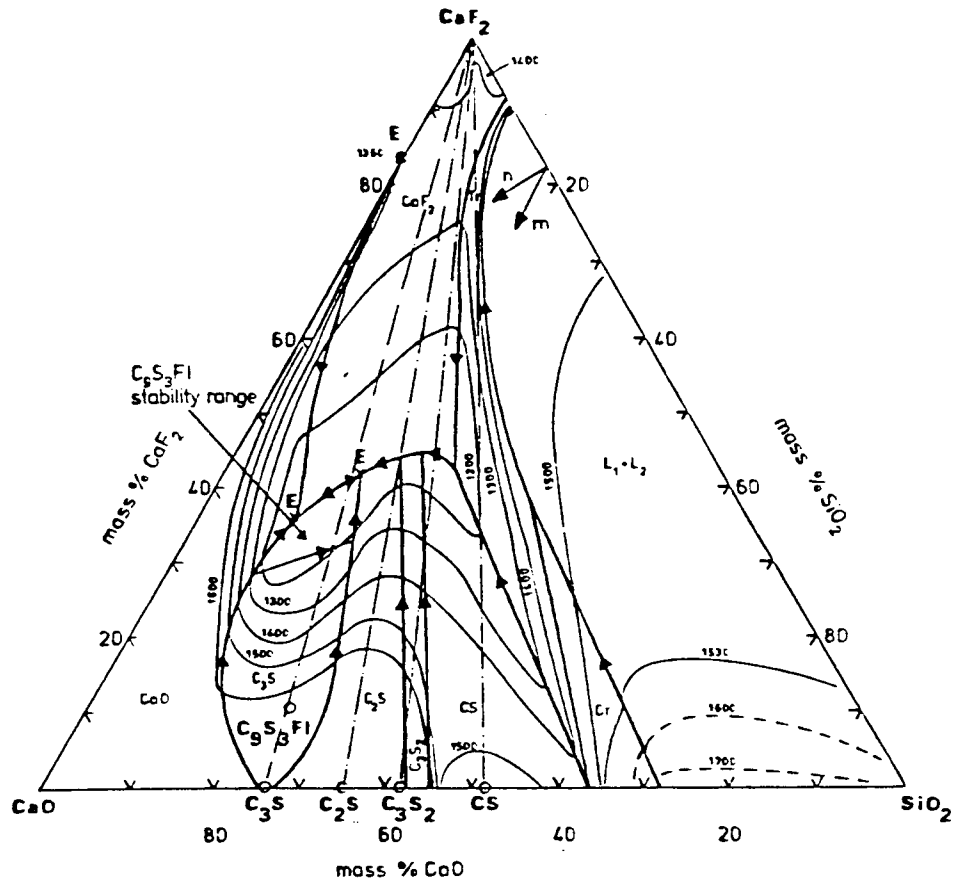

Fig. 2.33 Phase diagram for CaF_2 – CaO –SiO_2 system; Cr=Cristobalite, Tr=Tridymite[56]

than oxide ion in this respect and also Si-F is highly volatile at high temperatures.

The cryoscopic studies by Baak and Olander[70] and Suito and Gaskell[73] suggest the formation of trimeric ring metasilicate ion $Si_3O_9^{6-}$ and free F^- ions when $N_{CaO}/N_{SiO_2} > 1.5$. The latter report also suggests the formation of polyfluorosilicate anions such as SiO_3F^{3-}, $SiO_2F_2^{2-}$ or $SiOF_3^-$ when $N_{CaO}/N_{SiO_2} < 1.5$ in the melts, but there is no experimental evidence to prove the existence of these complex anions.

2.5.2 BASICITY AND ACTIVITY OF ESR SLAGS

2.5.2.1 CONCEPT OF BASICITY

There is no single method or index to define the basicity of metallurgical slags which are mainly a mixture of different oxides. Different practical methods are only applicable to a certain range of compositions and components. The use of the V-ratio is limited to a range within Blast Furnace related slags which normally contain varying proportions of CaO , SiO_2, Al_2O_3 and MgO. Even at the extreme ranges of the above components (acid or basic), these concepts lose their significance as a proper guide to basicity. An improved version is the concept of 'excess base', which is defined as follows:

$$\text{Excess Base} = \sum_{\substack{\text{all} \\ \text{basic oxide}}} \frac{N_{BxO}}{x I_{BxO}} - \sum_{\substack{\text{all} \\ \text{acid oxide}}} \frac{N_{AyO}}{y I_{AyO}} \qquad 2.30$$

where N refers to mole fraction and I is the Ion-oxygen attraction for a

particular cation. The problem here is to distinguish between acid and basic components specially for a amphoteric oxide such as Al_2O_3 . Another drawback is with the Ion-oxygen attraction parameter which cannot be applied for a non-oxide component, such as CaF_2.

In this regard, the recent idea of optical basicity[74] is more elaborate and reflects much more of the fundamental nature of a slag. It is directly related to the chemical nature of oxide ions present in the slag and theoretically can be estimated from the known Pauling electronegativity of cations. However, for the transition metal oxides, the direct calculation of optical basicity is not possible. Also in a slag containing halide, such as CaF_2 -CaO, the concept of optical basicity is not established. For oxide slags, the optical basicity is found to be independent of temperature.

The measurement of the oxygen potential of a slag (related to the oxide ion activity) is also considered in the same way as measuring the pH of an aqueous solution. This concept is the most scientific and is widely acclaimed. However, the major problem is related to the design of a proper electrode which can be used at high temperatures and in all kinds of slags without any chemical attack. Again, like water, there is no reference solvent available as a standard. However, the latest development of a long-life oxygen sensor[75] (figure 2.34) using a ZrO_2-MgO solid electrolyte looks promising. The measurement of oxygen potential is directly related to the oxide ion activity due to the following relation:

$$1/2\ O_2 + 2e = O^{2-} \qquad 2.31$$

Now for a known concentration of oxide ion, $N_{O^{2-}}$, the activity data would allow us to calculate $\gamma_{O^{2-}}$, an indicator for the deviation from

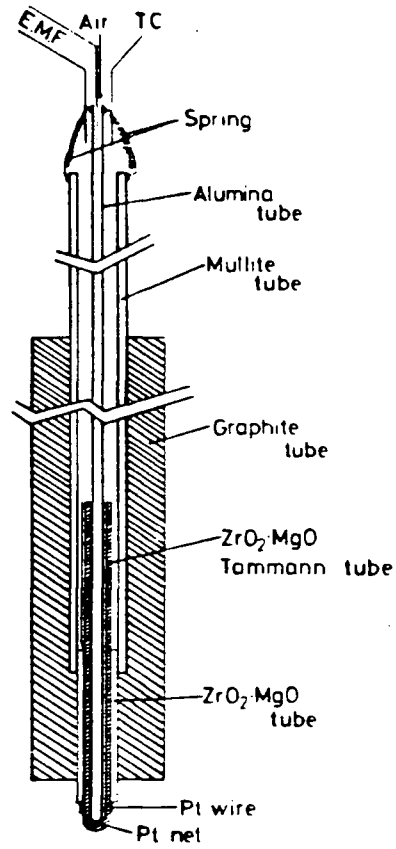

Fig. 2.34 Long-life oxygen sensor for measuring oxygen potential of slag[75]

ideality that reflects upon the ionic structure of the slag.

Wagner[76] proposed a new definition for basicity on the basis of carbonate capacity of a slag, defined as:

$$B_{carb} = C_{CO_3^{2-}} / C^{*}_{CO_3^{2-}} \qquad 2.32$$

where the carbonate capacity of a given slag $C_{CO_3^{2-}}$ can be expressed as:

$$C_{CO_3^{2-}} = \frac{wt\%\ CO_3^{2-}}{P_{CO_2}} \qquad 2.33$$

The $C^{*}_{CO_3^{2-}}$ is the carbonate capacity in a reference slag. The choice of the reference slag i.e. 0.4 CaO $+0.4SiO_2+0.2$ Al_2O_3 ,as proposed by Wagner,[76] seems unjustified,[77] since from the optical basicity relationship this slag is likely to have a very negligible carbonate capacity.

This concept of basicity should be very useful if $\gamma_{CO_3^{2-}}$ does not vary much with composition, as expected due to the big ionic size of a carbonate ion. Unfortunately, there are very few experimental data available in the literature for verification. Like the carbonate capacity, the sulfide, phosphate and hydroxyl capacities depend on the oxide-ion activity. Therefore, the variation of oxide ion activity should show a similar trend in these capacities and as a consequence they also should be interrelated.

2.5.2.2 ACTIVITY IN ESR SLAGS

The information on activity of a component in the slag not only corroborates the previously mentioned phase boundaries but also reflects the stability and the possibility of a chemical reaction under different conditions occurring during electroslag remelting. The experimental techniques employed and the assumptions made for the determination are very critical to obtain reliable activity data. In a way similar to the

experiments related to the phase diagram determination, the analysis of final slag composition is essential for fluoride-based slags. Lack of these precautions has resulted in a wide variation in activity data reported in the literature. However, some activities and the trend of variation are reliable enough to discuss as a guide line for future work.

CaF_2 - CaO

Different authors have calculated the activity of lime in this binary by different methods. Instead of experiments, Muratov,[78] Mehrotra et al.[79], and Kor and Richardson[55] employed particle interaction energy, statistical thermodynamics, and basic thermochemical data, respectively, to calculate the lime activity in this system. The values given by Muratov are not acceptable since the author used erroneous melting points in the melt data. The other two values, even though similar, do not correlate properly with the phase diagram. Kor and Richardson[55] derived the activity data at any temperature using the following relation:

$$\log a_{CaO}\ (\text{liquid}) = \frac{-6.6(2873-T)}{4.575\ T} \qquad 2.34$$

Hawkins et al.[80] estimated lime activity by assuming regular solution behavior and measuring the CaO saturation at 1500°C. They obtained $a_{CaO} = 1$ at $N_{CaO} = 0.26$ which matched well with the phase diagram. Edmunds and Taylor[67] measured the p_{CO} for the equilibrium reaction:

$$CaO + 3C = CaC_2 + CO(g) \qquad 2.35$$

Using a known equilibrium constant and assuming negligible solubility of CaC_2 in the melt, these authors estimated a lime activity which was very similar to that estimated by Hawkins et al.[80] (figure 2.35). However, at lower concentrations of CaO, increasing solubility of CaC_2 can affect this

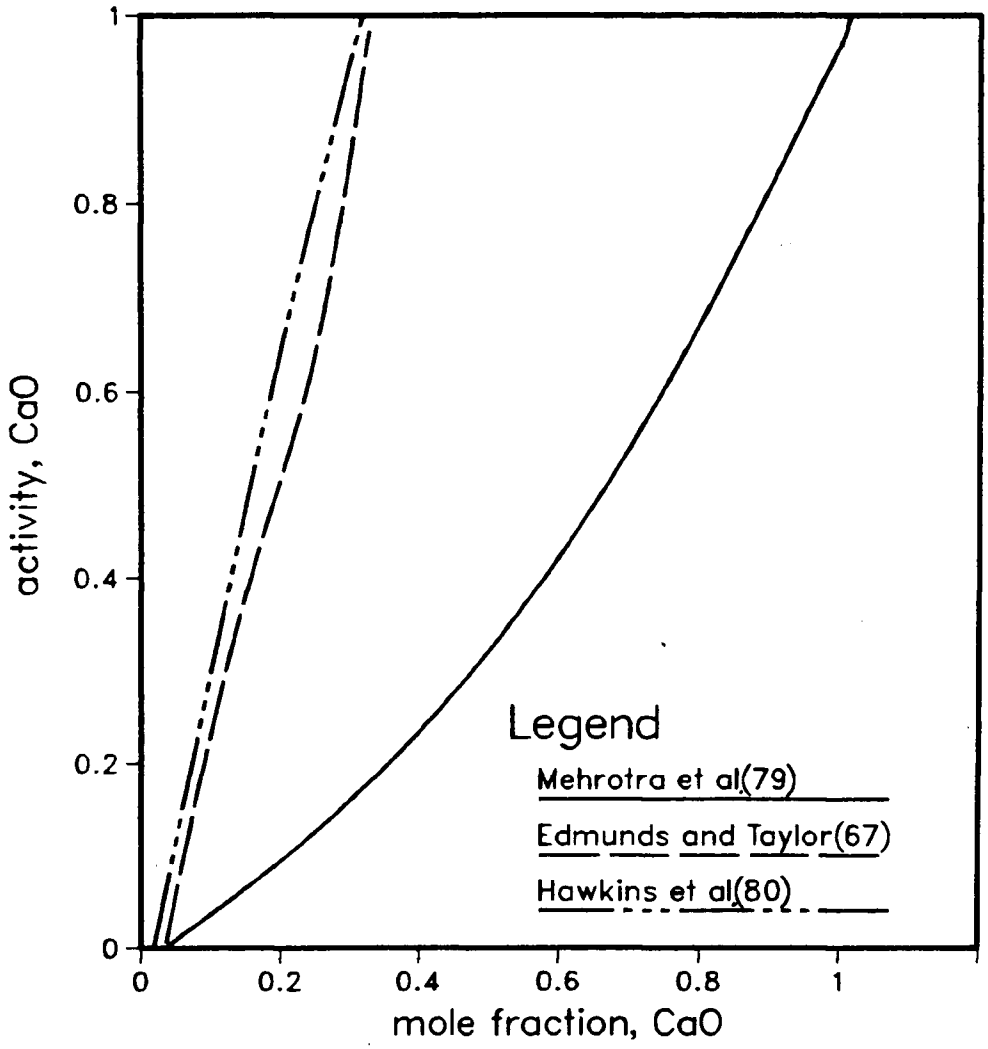

Fig. 2.35 Activity of CaO in CaO - CaF_2 system at 1500°C

estimation.[56] Cryoscopic measurments by Kojima and Masson[63] are a reliable method for estimating activity in this system, at least in the dilute solution region.

CaF_2 - CaO - Al_2O_3

The equilibrium reaction (2.35) is also employed to determine lime activity in this ternary by Edmunds and Taylor.[67] Similar activity data are also obtained by Zhdanovski[81] who considered the three binary phase diagrams in order to compute the equivalent activities in the ternary. Unfortunately, both these works are not in accord with the ternary phase diagram especially the miscibility gap region. Allibert and Chatillon[82] considered the following reaction:

$$CaO + AlF(g) + CaF_2 = 2CaF(g) + AlOF(g) \qquad 2.36$$

and used a mass spectrometer, connected to an effusion cell to determine the activity of CaO at 1600 and 1700K. There is a large discrepancy between these results and those of Edmunds and Taylor,[67] except when CaO activities are high (figure 2.36). Also, some of the activities do not correspond to a homogeneous liquid, but rather to two phase regions as evident in this figure.

CaF_2 - CaO - SiO_2

Sommerville and Kay[72] determined the silica activity in this system by monitoring p_{CO} of the following reaction:

$$SiO_2 + 3C = SiC + 2CO(g) \qquad 2.37$$

Subsequently, the activities of CaO are calculated by applying the ternary Gibbs-Duhem relationship (figure 2.37). Unfortunately, there are no direct independent lime activity data to use for comparison. However, the freezing

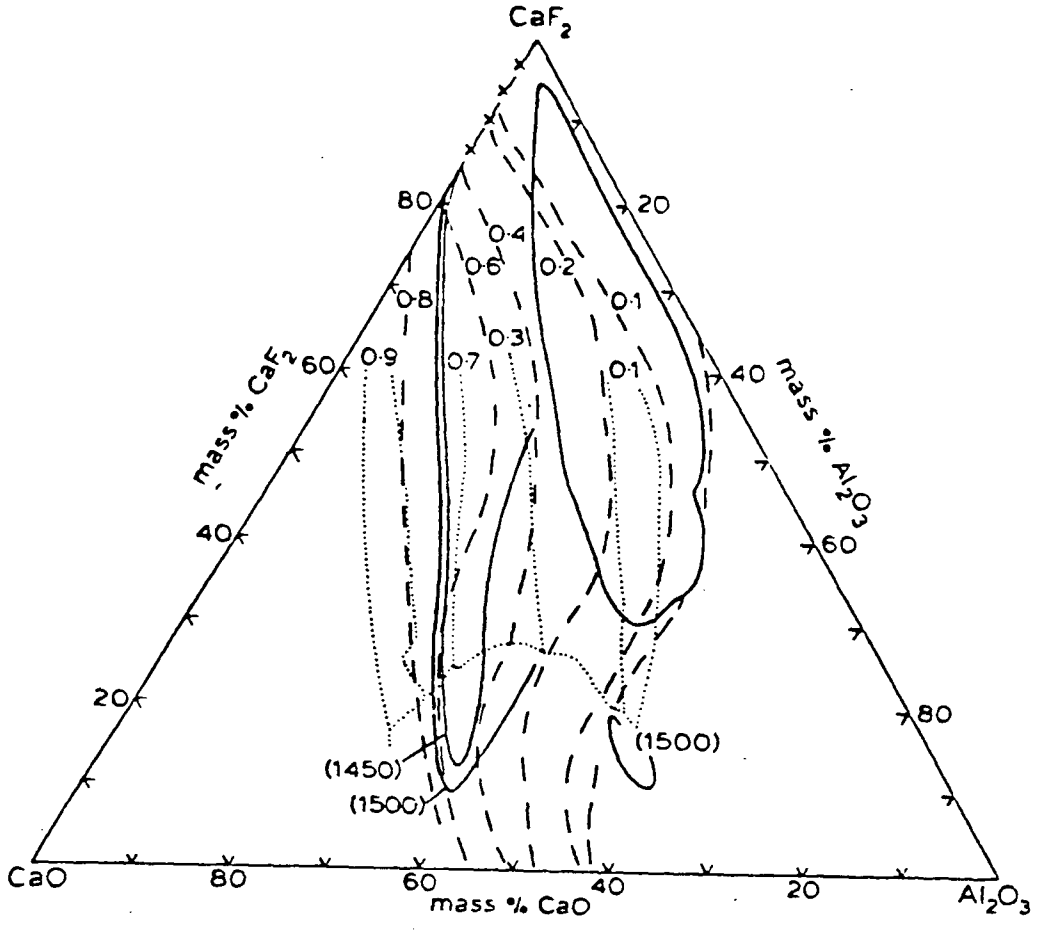

Fig. 2.36 Activity of CaO in CaF_2 – CaO – Al_2O_3 system:----,1500°C[67], ...,1427°C[82] ;----$t_{liq.}$

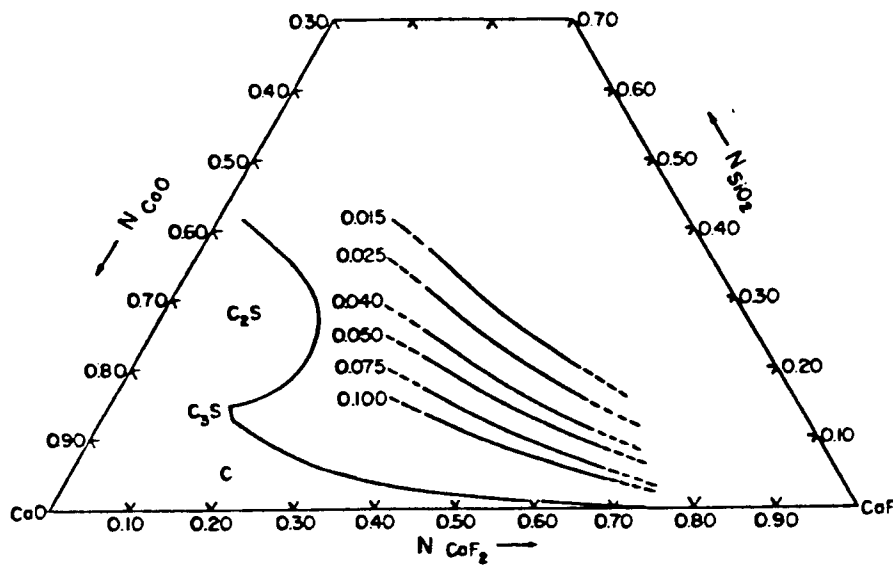

Fig. 2.37 Isoactivity of CaO in the CaF_2 - CaO -SiO_2 system at 1450°C

point depression measurements are carried out by Baak and Olander,[70] Kojima and Masson[63] and Suito and Gaskell[73] to determine a_{CaF_2}. The first work shows a smaller activity value compared to the other two and the difference becomes more significant at lower CaF_2 contents in the slag.

2.5.3 SOLUBILITIES

2.5.3.1 SOLUBILITY OF GASES IN MOLTEN SLAGS

In this area, principally the absorption of hydrogen, sulphur, carbon and nitrogen have been studied. The studies regarding the absorption of hydrogen have been discussed in detail in a previous section.

Kor and Richardson,[55] Hawkins et al.[80] and Raschev et al.[83] investigated the sulphur absorption in CaF_2 - CaO and CaF_2 - CaO - Al_2O_3 slags.

For CaF_2 - CaO slag, Hawkins et al.[80] obtained a much higher sulphur capacity value compared to the other two groups, but the dependence on CaO content is consistent in all the reports. A maximum sulphur capacity (0.15%)[55] is observed around 0.25 mole fraction of CaO. The replacement of Ca by Mg and Sr lowers the sulfide capacity. The increase of temperature also lowers the sulfide capacity, but the effect is not that significant.[80] In CaF_2 - CaO - Al_2O_3 , Raschev et al.[83] observed a 0.15% sulphur level at 1850°C which hardly varied with temperature.

Schwerdtfeger and Schubert[14] determined the nitrogen and carbon solubility in fluoride slags at 1600°C. Carbon is dissolved in the slag as CN^- and C_2^{2-}, whereas nitrogen is dissolved as N^{3-} and CN^-. In a

CaF_2 - CaO - Al_2O_3 slag, the total soluble carbon is 0.25% and the corresponding nitrogen level is 0.13%. Nitrogen was also found to obey the Sievert's law relationship. The addition of CaF_2 in CaO - Al_2O_3 slags results in higher cyanide and carbon solubilities.

2.5.3.2 SOLUBILITY OF GASES IN FUSED SALTS

The noble gases (He, Ne, A and Xe) are sparingly soluble in molten fluoride salts because of their very weak interactions with the solvents. The solubility increases with the increase of pressure (Henry's law), temperature and with the decrease in the size of the gas atom. For example, at 1 atm gas pressure, the solubility of He in 0.53mole NaF+0.47mole ZrF_4 melt is only 21.6×10^{-8}mole/ml of melt at 600°C and increases upto 42.0×10^{-8} mole/ml of melt at 800°C.[84]

Similar simple solutions are formed when carbon dioxide dissolves in molten alkali halides and the solubility increases with the increasing free volume of the salt. For instance, at 1 atm pressure, the solubility of CO_2 at 950°C is 7.0×10^{-6} mole/ml of KCl compared with 4.0×10^{-6}mole/ml of NaCl.[50] The molar volume of KCl is 51.4ml and that of NaCl is 38.9ml.

The gases which react with molten salts give rise to much higher solubilities. 0.75 mole of fluorine can be dissolved in the melt of 0.25mole $CuCl_2$ + 0.75mole KCl because of the following reaction[50]:

$$2CuCl_2 + 6KCl + 6F_2 = 2K_3CuF_6 + 5Cl_2 \qquad 2.38$$

Similarly, HF is also highly soluble in NaF-ZrF_4 melts and its solubility decreases with the increase in temperature.

CHAPTER 3

OBJECTIVES

The foregoing review reveals that the thermodynamics of reactions related to the hydrogen transfer in ESR system are still not very well defined. Therefore, the objectives of this work are directed toward the following:

1. Independent investigation of the oxide activity of binary and ternary fluoride-based slags and a comparison of the results with the available literature data.

2. Development of a new and reliable sampling technique of ESR slag for subsequent water analysis.

3. Design, fabrication and operation of an improved apparatus to carry out water analysis in slags so that the on-line monitoring of hydrogen in an ESR ingot can be made in future.

4. Analysis of the previous and new water solubility data to define the controlling parameter during Electroslag remelting with respect to hydrogen in the ingot.

5. Application of thermodynamics to clarify the critical reactions involved during the process and assessment of different slags in that perspective.

CHAPTER 4

EXPERIMENTAL

4.1. CO_2-SLAG EQUILIBRIUM

For all experiments, synthetic slags of different compositions were prepared by weighing appropriate amounts of reagent grade CaF_2 , Al_2O_3 , $CaCO_3$ and SiO_2.

All the equilibria runs were carried out inside a vertical super Kanthal furnace containing a recrystallized alumina tube ($36"x1\frac{3}{4}"\phi$ O.D). Both ends of the tube were closed and water cooled by brass plates and copper tubes respectively. The bottom end was connected both to a helium and to a carbon dioxide cylinder through a two-way valve. The on-line flow and pressure were checked by a calibrated flowmeter and a mercury manometer. The helium line was connected through an absorption tube containing 'ASCARITE' to eliminate CO_2 from the gas stream (figure 4.1). All the experiments related to fluoride based slags were done at 1400°C ± 5°C maintained by a temperature controller (Honeywell 'Continuous Balance' type).

Before each experiment, the set-up was flushed with CO_2 at least for an hour and the temperature of the furnace was stabilized at the set temperature. A 5c.c. platinum crucible containing 200mg slag introduced from the bottom end of the furnace was raised to the hot zone with the help of a platinum wire and a magnet assembly. During the experiment, the

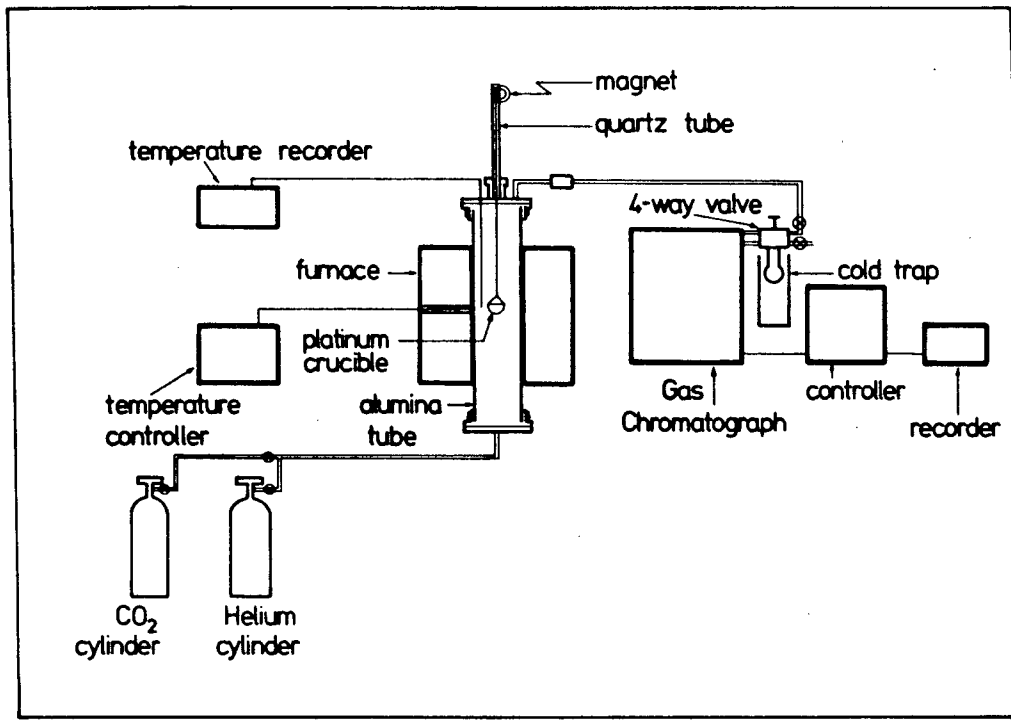

Fig. 4.1 Schematic diagram of the apparatus for carbonate equilibrium studies

CO_2 flowrate was maintained constant at 500c.c/min. Each run lasted for an hour after which the liquid slag in the crucible was quenched by quickly lowering it onto the water cooled brass plate.

The CO_2 solubility in the slag was determined in the same furnace which was purged with helium overnight. The next morning the gas composition was checked for any trace of CO_2 by a Pye-Unicam gas chromatograph (series 104). Actual analysis was postponed until all the CO_2 in the assembly was flushed out.

To analyze CO_2 in the slag, the platinum crucible containing the equilibrated slag was again raised to the hot zone of the furnace, but with helium flowing at the rate of 200ml/min. The gases exiting from the furnace were delivered directly to the Gas Chromatograph sample loop(2ml). The evolved CO_2 from the slag was cold trapped in that loop which was dipped in the liquid nitrogen. The CO_2 evolution was found to be completed within 30 minutes. This was confirmed by extending the time of cold trapping and also by adding some B_2O_3 to the slag. Later, the frozen CO_2 was evolved by removing the cold trap and its quantity analyzed in the Gas Chromatograph.

The analyzer column of the Gas Chromatograph was modified by a 1/4"ϕ copper tube, 2" of which was filled with silica gel (mesh 80/100) in order to improve the detection limit and the response time. Before each set of experiments the instrument was calibrated repeating the same procedure, but taking different amounts of $CaCO_3$ instead of slag in the platinum crucible (figure 4.2). The analysis error is found to be within 10% of the content when the attenuation was at 20x, carrier gas (helium), flowrate 50ml/min, detector oven temperature 100°C, column temperature

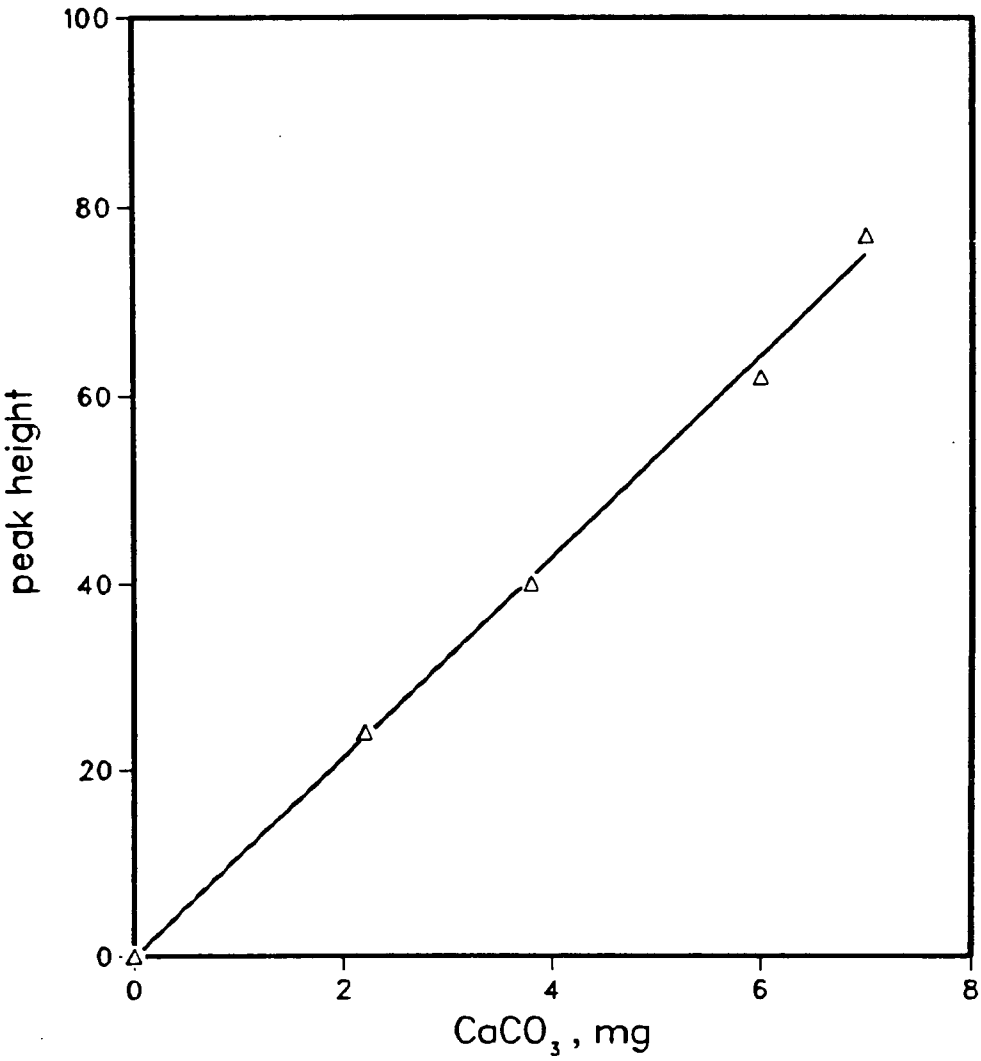

Fig. 4.2 Typical calibration plot for carbonate analysis.

70°C and the detector filament current 100 mA.

For chemical analysis of slags, identical CO_2 equilibrium experiments were repeated. The slags were analyzed by the standard fusion method (Na_2CO_3+ZnO) where Ca, Si and Al were analyzed by atomic absorption spectrophotometer (Perkin Elmer 306) and the fluorine analysis was done by fluoride-ion selective electrode (Appendix I).

4.2. D_2O-SLAG EQUILIBRIUM

The vertical super kanthal furnace which was used for the previous set of experiments was modified to carry out the water vapour-slag equilibrium (figure 4.3). A bigger platinum crucible (50c.c.) was placed in the hot zone on a smaller diameter alumina tube. With a bucketlike arrangement it was possible to quickly retrieve the crucible from the top with a molybdenum wire hook. The top port, previously used for the magnetic lowering and raising device, was converted to a sampling port.

A constant temperature magnetically stirred water bath was made to generate different levels of D_2O vapour partial pressures in the furnace. Helium, used as a carrier gas for D_2O vapour, was first dried by magnesium perchlorate before entering the water bath, whose temperature was maintained by a Thermistemp Temperature Controller (model 71). The temperature of helium was also raised by passing it initially through a coil of copper tubing (1/4"ϕ) which was immersed in the water bath. Next, the carrier gas was passed through a series of closed test tubes containing D_2O at greater than 99.9% purity and bubbling through a gas dispersion tube in each case. To prevent condensation of the D_2O saturated gas stream, the

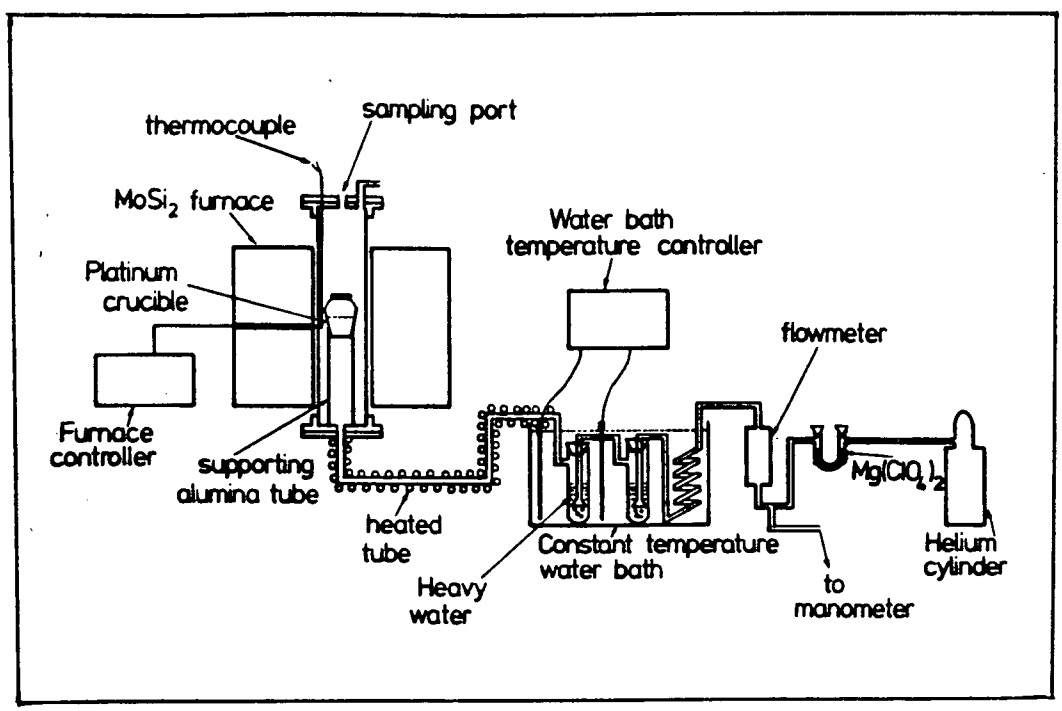

Fig. 4.3 Schematic diagram of the apparatus for D_2O-slag euilibrium water vapour pressure

remainder of the copper tubing connected to the furnace, was heated above 100°C by means of a heating tape.

Initial trials were conducted to verify the generation of saturated water vapour pressure in the gas stream by collecting the water vapour at the end of the copper tube in an absorption column containing magnesium perchlorate. The results (figure 4.4) at different flowrates of helium were found to be quite satisfactory within the range of this investigation.

Bulk slags were prepared by mechanically mixing different pure reagent grade ingredients such as CaF_2 , $CaCO_3$, Al_2O_3 and SiO_2 in a mechanical shaker for 30 minutes. All the binary and ternary slags were equilibrated for one hour at two different partial pressures of D_2O (0.042 and 0.122 atm) at 1400°C and constant flow rate of helium (300ml/min). At the end of each run, a slag sample was collected through the sampling port in a quartz tube (5–7 mmϕ) by applying suction through a rubber bulb. This simple method was similar to the metal sampling technique, but has not been tried before because of the possibility of silica contamination of the slag. For this reason, during later slag analysis, Si analysis was conducted for non-silicate slags. There was no Si detected in those slags confirming the validity of this simple sampling technique. All the slag samples, so obtained, were stored in a desiccator for further composition and water solubility determinations.

The chemical analysis of slag was carried out by the same

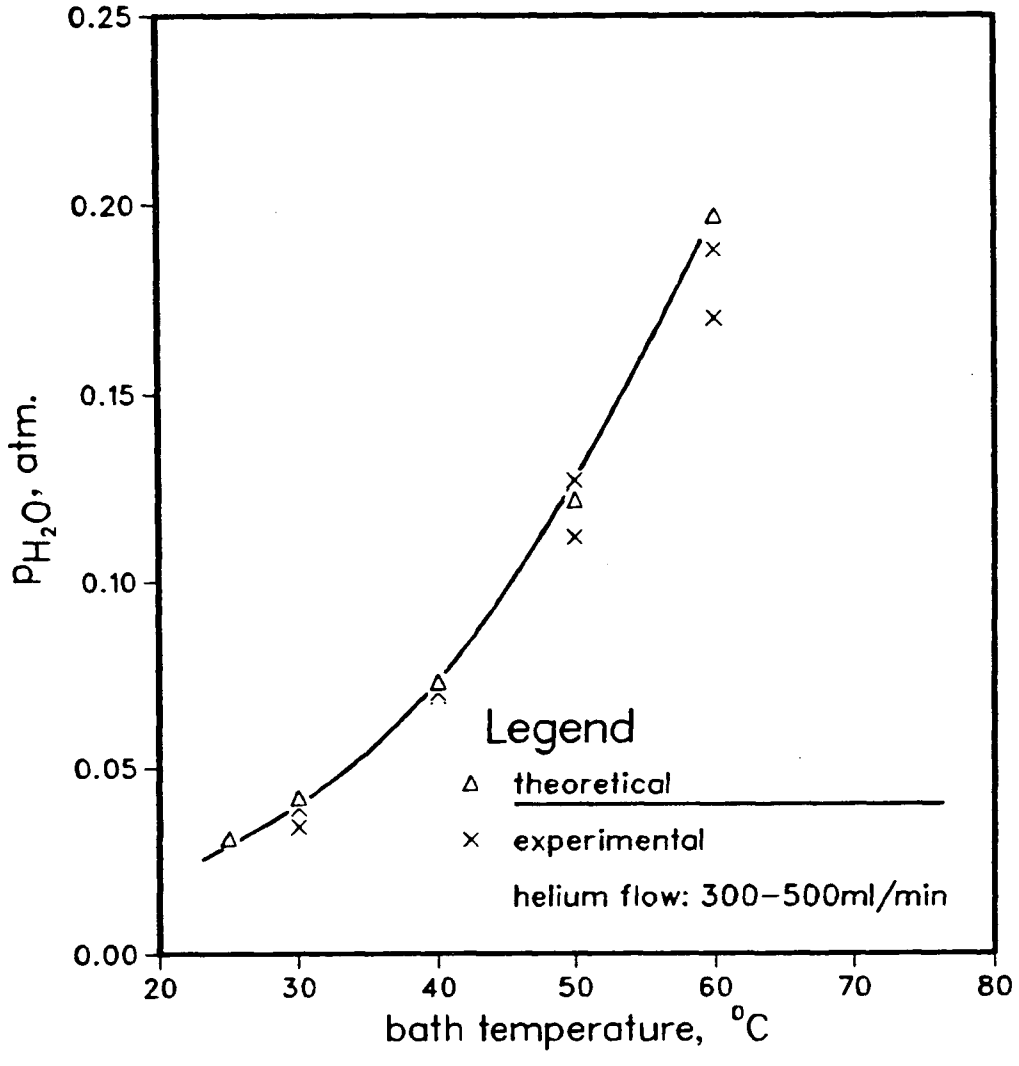

Fig. 4.4 Comparison of theoretical and experimental equilibrium water vapour pressure

fusion method as described in the section 4.1.

4.3. WATER ANALYSIS

Since there was no unique method for the analysis of water in fluoride slags, and in the literature it was observed that different techniques yield different results, it was considered necessary to design and fabricate a new experimental technique with due regard to the drawbacks of the previous methods. The trace quantity of water could be detected either as the total water evolved from the slag or as the equivalent hydrogen obtained by reducing the water. The detection of water as water had certain problems: water would condense on its way to the detection chamber if all the area is not adequately heated; moreover, most materials absorbed a certain quantity of water and it was difficult to ensure that a system was 'water-free'.

The obvious conclusion from the above facts was that it would be possible to design an apparatus in which the water could be analyzed as hydrogen. For detection of any element as a trace quantity, the mass spectrometer was an ideal tool, which unfortunately requires a high vacuum environment. Again, in a vacuum system, hydrogen was found to be one of the predominant species (small wonder since it makes up more than 90% of all atoms of the universe!) besides nitrogen and water. Therefore, the high background level of hydrogen again made this method questionable.

Fortunately, hydrogen has two isotopes, deuterium and tritium, and isotope detection techniques were not only clean and reliable but also removed the doubts surrounding the origin of the test material. The hydrogen, besides being introduced during equilibrium experiments, may also

contaminate the sample as H_2O during its handling. On the other hand, the natural abundances of these isotopes (e.g 0.015% for deuterium) are too low to have any effect on the analysis . Among these two isotopes, the choice of deuterium was quite straightforward since it is non-radioactive and relatively much cheaper and easily available.

4.3.1 FABRICATION OF HIGH VACUUM APPARATUS

Even though the high vacuum system was to be connected to a metallic analyzer head of a mass spectrometer, a glass apparatus was built (figure 4.5) since it was a much cleaner system and also it could be easily connected to a silica reaction tube where slag samples would be inductively fused.

A water cooled mercury diffusion pump, which was backed by a mechanical rotary pump, was connected to the apparatus to maintain a vacuum of the order of 10^{-6} torr. A liquid nitrogen trap was employed to improve the efficiency of the system. A heating tape was wrapped around the glass tube close to the analyzer head to clean up the residual gases quickly and to keep the absorption of hydrogen-related species to a minimum. A glass-Kovar joint enabled the vacuum tight connection of the 70mm stainless steel flange of the analyzer head which detected different gases on the basis of their mass number with the help of a control unit(VG MICROMASS 1/2). The other end of the glass tube was connected to the silica reaction tube through a metroseal leak, a high vacuum valve and a quickfit joint (size 60/71).

The reaction tube area was also equipped with a sampling holding area and as a result, this area could be completely isolated from

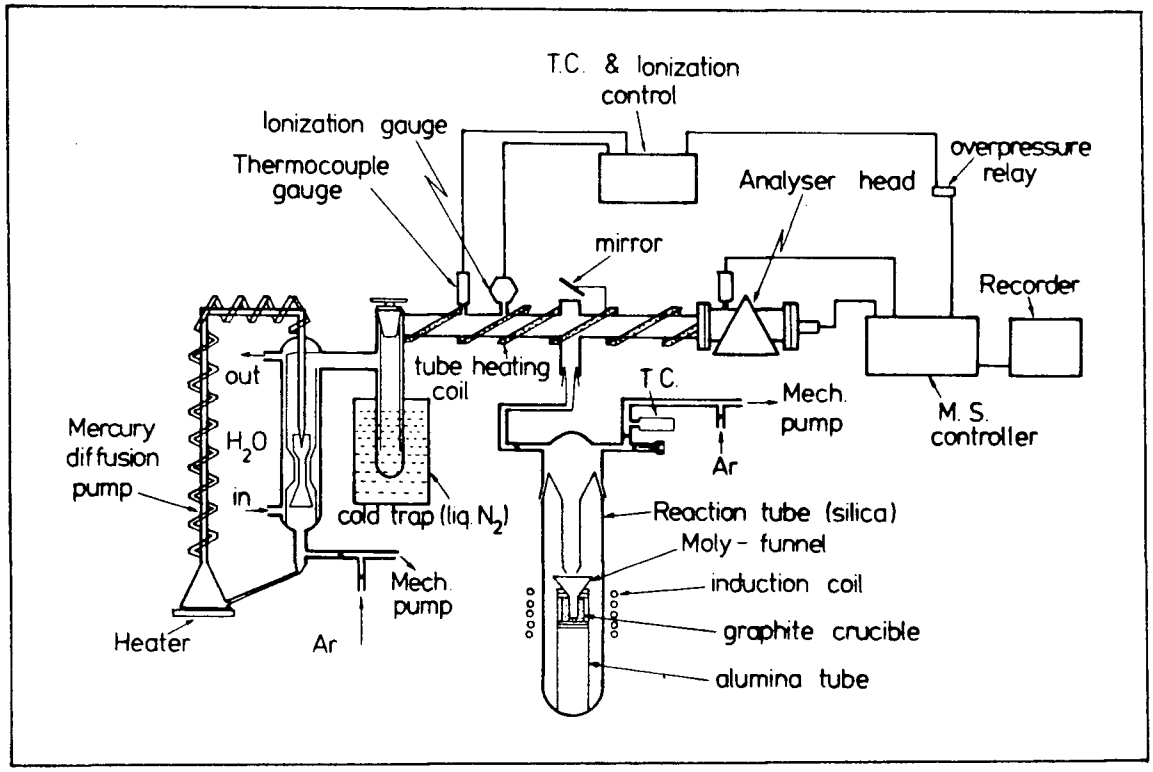

Fig. 4.5 Schematic diagram of the apparatus for water analysis of slag

the high vacuum mass spectrometer area and back filled by argon to enable sample loading and flushing of the system. This area was also connected to the mechanical pump to attain a vacuum around $5x10^{-2}$torr.

A graphite crucible was used as a susceptor for induction heating of samples. This crucible was wrapped by a graphite felt placed inside an alumina tube to reduce the overheating of the silica tube. A water cooled copper coil, connected to a high frequency induction supply, was placed around the quartz tube. In the sample holding area, one magnetic pusher was placed, so that the sample could be dropped into the graphite crucible without disturbing the vacuum.

4.3.2 PREPARATION FOR CALIBRATION

For proper calibration of this complex apparatus it was best to follow the same steps as was done for a slag. For this reason $Ca(OD)_2$ was prepared by the following method.

50 c.c. of pure D_2O was taken in a beaker and placed inside a nitrogen flushed desiccator(no desiccant inside). About 35gm of $CaCO_3$ was taken in a crucible and heated to 1200°C for 3 hours inside a muffle furnace to generate pure CaO. The pure lime, so obtained, was transferred into the beaker containing D_2O, this beaker being left inside a nitrogen flushed glove box overnight for the complete conversion to $Ca(OD)_2$. The equilibrium constant of this reaction involving H_2O ($2.7x10^{11}$ at 300K)[54] strongly favours the production of $Ca(OD)_2$. Later this compound was dried off on a hot plate and stored carefully inside the glove box.

For calibration, a small known quantity of $Ca(OD)_2$ was placed in a capsule along with a sufficient amount of reducing agent, such as

aluminum. After initial trials, about 0.5" long, one end closed tubes were made by drilling a 0.089" bore in a 1/8" mild steel rod. A measured quantity of $Ca(OD)_2$ and aluminum was packed inside the tube and the open end was sealed off by a 3/32" ball bearing. This procedure ensured the complete reduction of D_2O to D_2 since no peak was observed at mass 20 while using helium as the back filling gas.

4.3.3 CALIBRATION AND SLAG ANALYSIS FOR WATER

For both the calibration and the slag analysis the following steps were taken. The high vacuum area was warmed up and cleaned so that the pressure was steady at a 10^{-6}torr range and it was isolated from the silica tube area which was then inductively heated for 5 minutes. The crucible was then cooled for 15 minutes. Consequently, the blank gas analysis of the silica tube area was made by opening the high vacuum valve which connected the mass spectrometer area. A similar procedure was followed after dropping a sample into the graphite crucible. Before each set of slag analysis a calibration plot of p_{D_2} versus the amount of $Ca(OD)_2$ was obtained (figure 4.6) for estimation of water in the slag. Also at the end of a set of slag samples, a calibration capsule was introduced and the system was checked for any inconsistency.

For slag analysis, about 100–300mg of ground slag (depending on the estimated water level) was wrapped in a cleaned (acetone and carbon tetrachloride) aluminum foil. After analysing 10–15 slag samples it was necessary to clean the silica tube which was by then coated with a substantial quantity of vaporized aluminum. It was possible for this aluminum to absorb some H_2 and D_2 and thus yielding lower values of partial pressures of these two species.

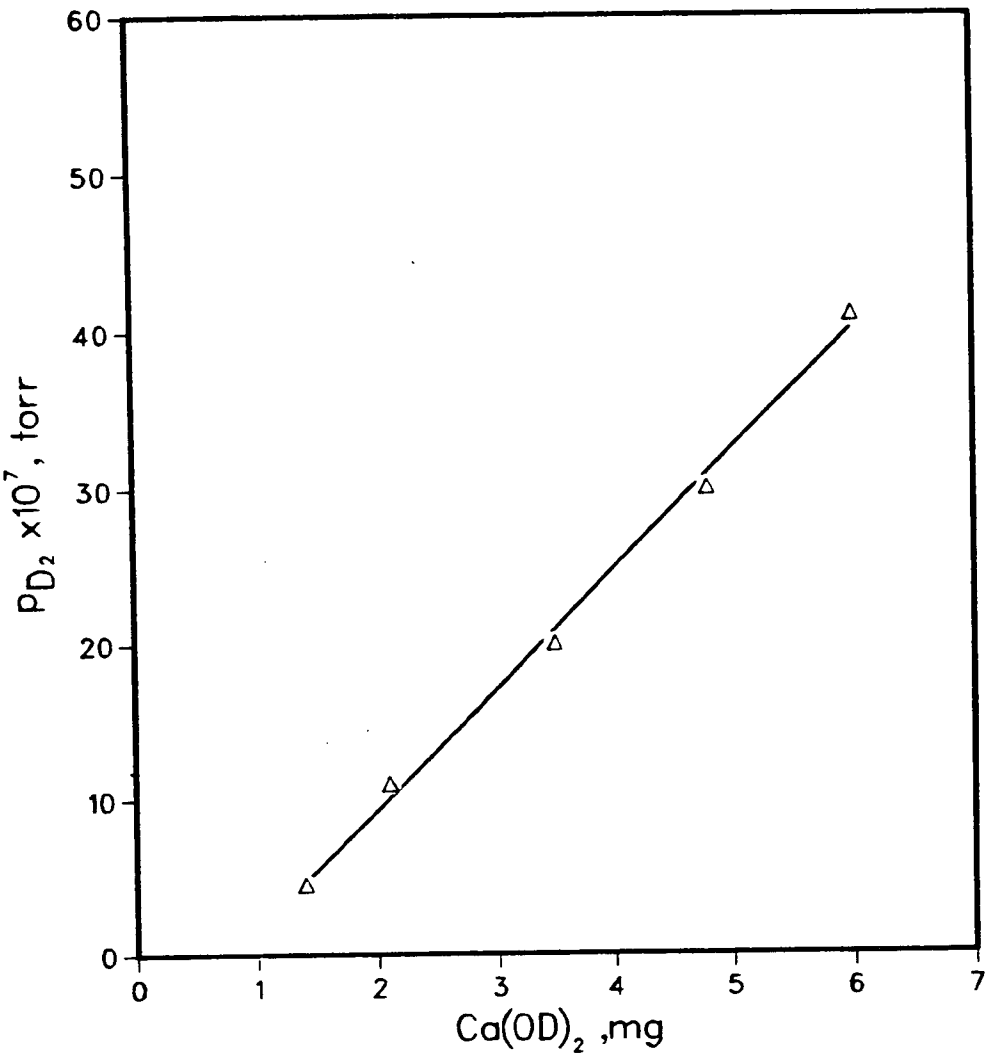

Fig. 4.6 Typical calibration plot for water analysis

This new analytical tool was subsequently verified by analysing water solubility in known binary non-fluoride systems (table 4.1). In both cases, the agreement was quite good with respect to the previous data. Also, the repetition of the same slag samples showed that the reproducibility of the analysis was within 10% of the content. A few slags (both binary and ternary) were also equilibrated with H_2O under the same conditions which were maintained for D_2O-slag equilibrium. These slags were also sampled in quartz tubes and later sealed in evacuated glass tubes to prevent any moisture pick-up from the atmosphere. These encapsulated slag samples were sent out to Vereinigte Edelstahlwerke (VEW), Austria, for an independent analysis of water solubility in ESR slags by a different method. The analyses, so obtained, are discussed in the next chapter.

Table 4.1 Verification of Water Analysis by Isotope Tracer Technique

Slag No	Composition				Literature	This method
	% CaO	% Al_2O_3	% SiO_2	P_{H_2O} torr	(H_2O) ppm	(H_2O) ppm
1	50.4	49.6		150	900[39]	1178
2	37		63	289	429[22]	526

CHAPTER 5

RESULTS AND DISCUSSIONS

5.1. OXIDE ION ACTIVITY IN ESR SLAGS

From the ionic theory of slag, we formulate a_{CaO}:

$$a_{CaO} = a_{Ca^{2+}} \times a_{O^{2-}} \qquad 5.1$$

$$= a_{O^{2-}} \text{ , if } a_{Ca^{2+}} = 1$$

In the present systems this assumption is quite valid since the ESR slags studied are highly basic and the only cation is the calcium ion. Also, in the ternary systems containing Al_2O_3, it is highly probable that the cations remain only as calcium, since aluminum is probably present only as complex anions such as AlO_2^-, AlO_3^{3-}. The same reasoning is applicable to the silicate systems used in ESR slags.

5.1.1 CARBONATE EQUILIBRIUM IN FLUORIDE SLAGS

The determination of oxide ion activity can be done by studying the following equilibrium:

$$CO_2(g) + (O^{2-}) = (CO_3^{2-}) \qquad 5.2$$

for which, the equilibrium constant is,

$$K = \frac{a_{CO_3^{2-}}}{p_{CO_2} . a_{O^{2-}}} = \frac{N_{CO_3^{2-}} . \gamma_{CO_3^{2-}}}{p_{CO_2} . a_{O^{2-}}} \qquad 5.3$$

In the presence of calcium, the change in the free energy can be written

as[85]:

$$\Delta G^\circ = -40248.6 + 34.4T \quad \text{cal/mole}$$

where T is temperature in K.

To calculate the activity of CaO, the activity coefficient of carbonate ion is estimated by combining the cryoscopic data of Kojima and Masson[63] and the data from the binary slag–CO_2 equilibrium experiment of the present work, and the slag is assumed to be regular in view of the fact that these coplanar carbonate ions are too large to have any significant interactions with other anions such as AlO_2^-.

The final determination of the oxide ion activity in binary fluoride slags shows a positive deviation, whereas the deviation is negative in ternary, CaF_2–CaO–Al_2O_3 and CaF_2–CaO–SiO_2, slags (table 5.1 to 5.3). It is also observed that the activity of lime is a strong function of basicity (more specifically, the ratios of lime and silica or alumina depending on the type of slag).

The activity of CaO can also be deduced from the information available in the literature. These data are presented in figure 5.1 to 5.3, but since their computation involves certain assumptions, they are not very reliable in certain cases.

In the CaF_2–CaO binary system, the activity of CaO at 1400°C is computed by the Gibbs-Duhem Integration method (figure 5.1). The cryoscopic experimental data of Kojima and Masson[63] are used and the system is assumed to follow regular solution behavior. The experimental

Table 5.1 Activity of CaO in CaF_2 - CaO system at 1400°C

N_{CaO}	a_{CaO}	γ_{CaO}
0.136	0.24	1.77
0.138	0.25	1.82
0.17	0.29	1.76
0.19	0.38	1.99

Table 5.2 Activity of CaO in CaF_2 - CaO - Al_2O_3 system at 1400°C

N_{CaO}	a_{CaO}	γ_{CaO}	$N_{CaO}/N_{Al_2O_3}$
0.403	0.05	0.13	3.05
0.47	0.09	0.183	3.14
0.52	0.09	0.19	3.08
0.56	0.1	0.18	3.1
0.22	0.08	0.386	3.9
0.38	0.17	0.448	4.99
0.41	0.18	0.439	6.27
0.32	0.22	0.687	7.02
0.26	0.24	0.92	7.67

Table 5.3 Activity of CaO in CaF_2 - CaO -SiO_2 system at 1400°C

N_{CaO}	a_{CaO}	γ_{CaO}	N_{CaO}/N_{SiO_2}
0.62	0.11	0.18	3.3
0.52	0.17	0.33	3.02
0.37	0.18	0.48	3.1
0.22	0.13	0.60	3.4
0.51	0.013	0.025	2
0.45	0.019	0.041	2
0.38	0.098	0.26	2.3
0.26	0.03	0.102	2.9

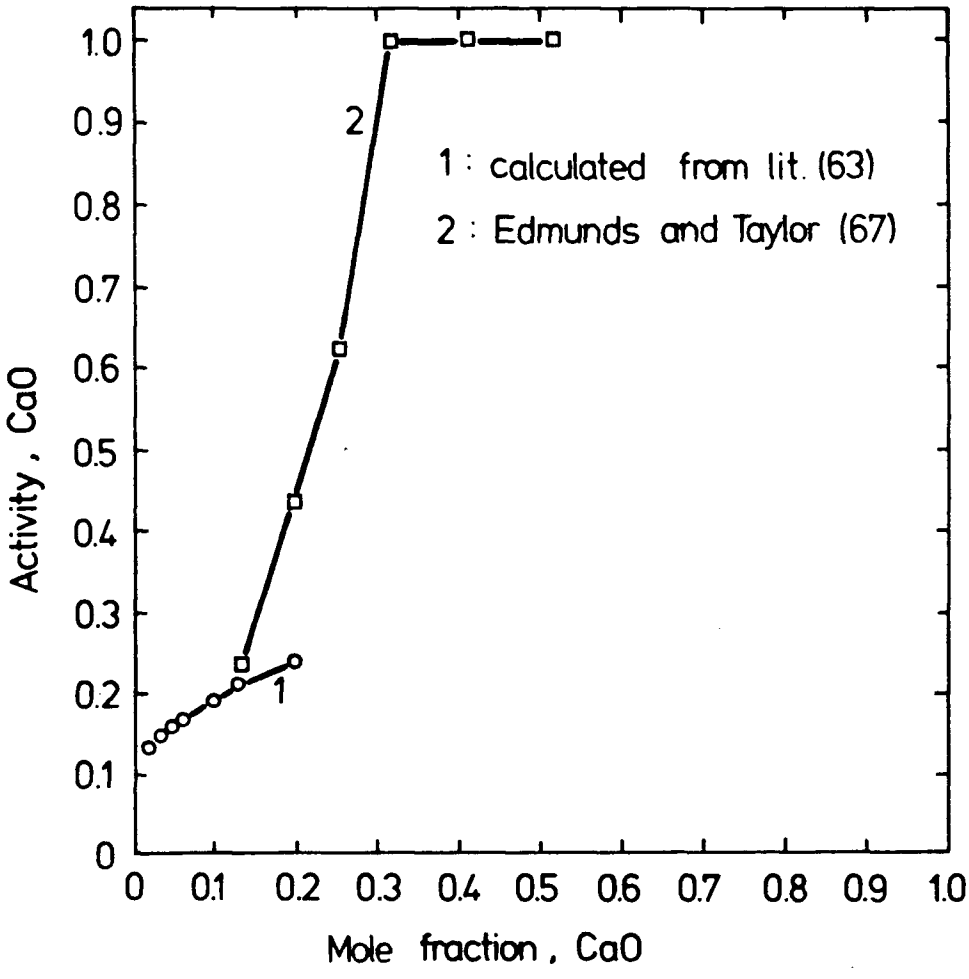

Fig. 5.1 CaO activity in the CaO - CaF_2 -binary slag system

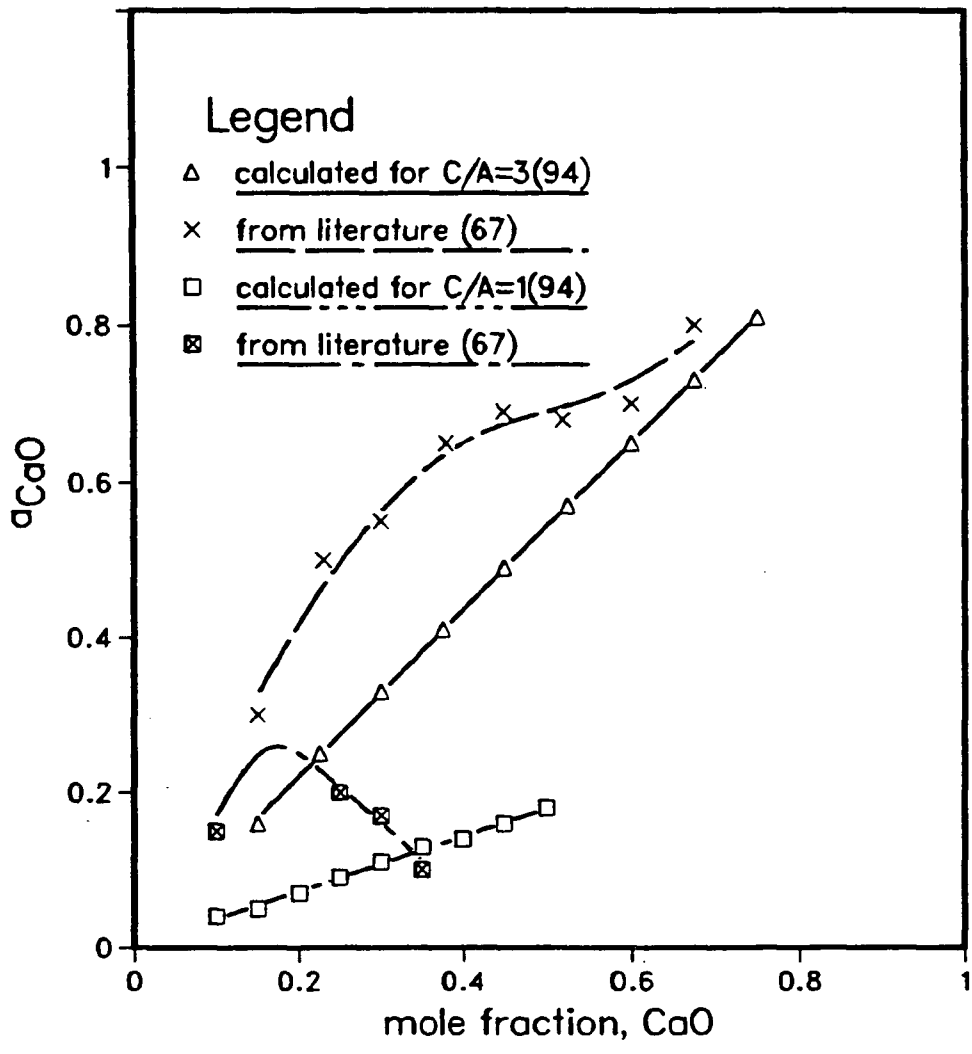

Fig. 5.2 CaO activity in the CaO - Al_2O_3 - CaF_2 ternary slag

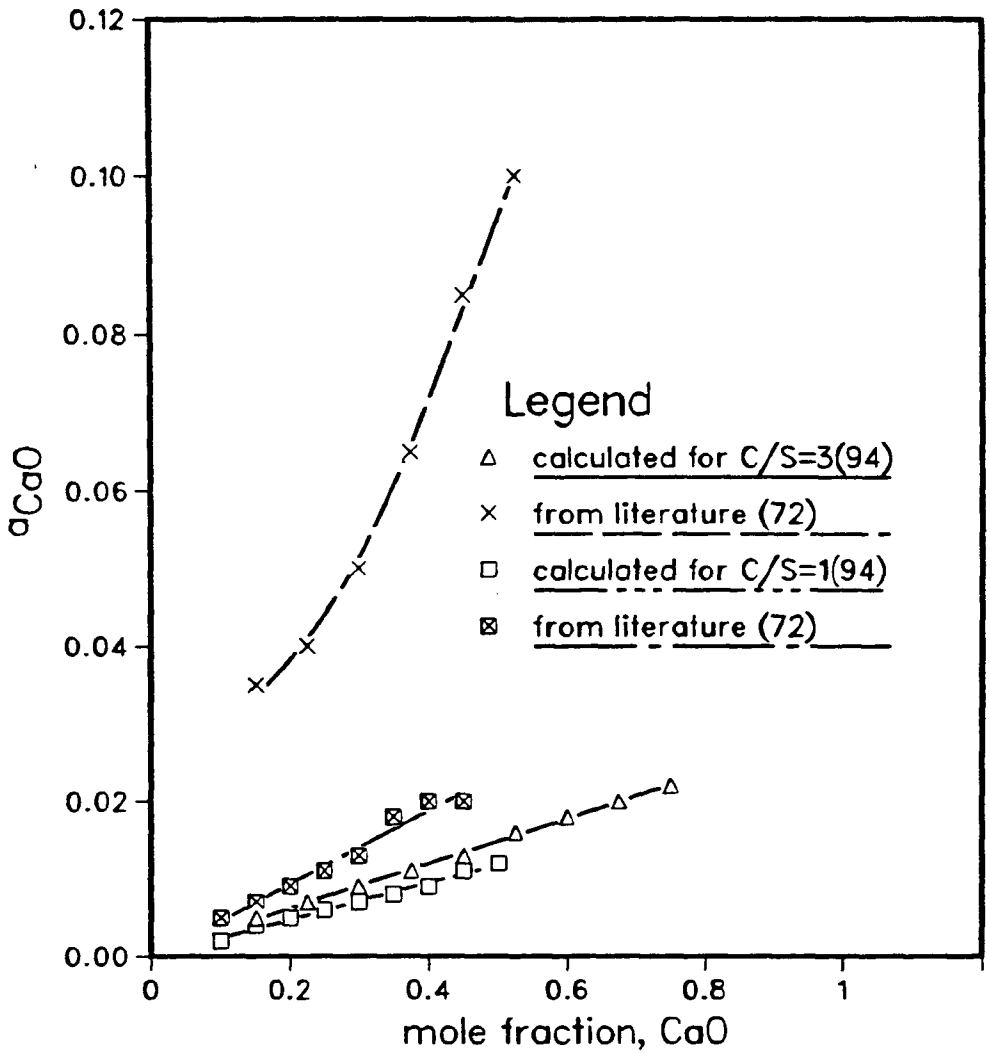

Fig. 5.3 CaO activity in the CaO -SiO_2- CaF_2 ternary slag

data of Edmunds and Taylor[67] are also considered here. The equilibrium they studied is:

$$CaO + 3C = CaC_2 + CO \qquad 5.4$$

It is also assumed that CaC_2 is completely insoluble in the slag, but this is not true in fluoride slag systems.[86] The CaF_2–CaC_2 system is reported to form a eutectic at 1240°C and $N_{CaC_2} = 0.14$. Thus, assuming unit activity for CaC_2 in the above equilibrium reaction would result in higher values for lime activity data. A similar argument is applicable in the determination of silica activity in the CaF_2–CaO–SiO_2 system by the following equilibrium[77]:

$$SiO_2 + 3C = SiC + 2CO \qquad 5.5$$

Even though the solubility of SiC in CaF_2–slag is highly unlikely, the available CaO would react to form CaC_2 and make the slag more than a 3 component system. Hence the activity measurements obtained by measuring the P_{CO} would be in error. However, the activity data so obtained can still be considered for comparison.

In the CaF_2–CaO–Al_2O_3 ternary system, CaO activity is calculated from the data of the CaO–Al_2O_3 binary by assuming that CaF_2 is an inert diluent (figure 5.2). These data may not be very reliable because of the complexity of the aluminate system containing fluoride ions, as observed by Hara and Ogino.[87] However, the data can serve as a reference for comparison with the experimental data and the data from Edmunds and Taylor.[67]

The experimental data show a substantial negative deviation even at a molar ratio of CaO/Al_2O_3 = 3 and approach ideality only at higher molar ratios (table 5.2). The calculated data and the values from the literature[67] (figure 5.2) show a similar trend but the calculated data approaches ideality at a ratio lower than 3. When the molar ratio is 3, both of these data show a positive deviation. Since the ionic radii of oxygen (1.4A) and fluorine (1.36A) anions are similar, it can be presumed that the fluorine would gradually replace the oxygen from an aluminate bond, with the progressive addition of CaF_2. However, the structure is much more complex in CaF_2 saturated melts where two separate liquid phases exist (figure 2.32, ternary diagram of C-A-Fl).

In the CaF_2-CaO-SiO_2 ternary system, the activity of CaO is calculated from the data of CaO-SiO_2 binary, assuming CaF_2 is an inert diluent (figure 5.3). The similar behavior of CaF_2 in this ternary is also observed by Shinmei et al.[88] and Hara et al.,[89] Sommerville and Kay[72] studied the reaction(5.5) to determine the silica activity. The modified Gibbs-Duhem equation is used to calculate the lime activity in this ternary system. All these activity data show a substantial negative deviation at all molar ratios of CaO/SiO_2. Also the inert diluent characteristics of CaF_2 in the silicate melt are evident in the experimental data.

5.1.2 VERIFICATION OF CARBONATE EQUILIBRIUM

In order to validate the assumption that the carbonate ions behave regularly in slag solution, similar carbonate equilibria experiments are carried out at 1500°C, in the binary systems with known oxide ion activity such as, CaO-Al_2O_3 and CaO-SiO_2. The results obtained in these experiments are shown in table 5.4. The activity coefficient of the

carbonate ion shows apparent regular solution behavior in the binary aluminate and silicate slags, but the activity coefficient is a different order of magnitude in different types of slags, being smaller in the aluminate slags. The activity coefficient in fluoride slag is between the values obtained in the aluminate and silicate slags.

5.1.3 ACTIVITY CALCULATION FROM THE SULFIDE CAPACITY DATA

The calculation of the activity of CaO from the sulfide capacity data[55] in the CaF_2–CaO–Al_2O_3 system can be done assuming the regular solution behavior of CaS. The results in table 5.5 are compared with the experimentally determined values. It is clearly evident that the discrepancy which exists at lower $N_{CaO}/N_{Al_2O_3}$ ratios gradually diminishes at higher ratios. In this case, the reason may be that the assumption of the regular solution behavior of CaS in this melt is not completely valid. This argument can further be justified after comparing the ionic radii of O^{2-}(1.40A) and S^{2-}(1.84A) and their electronic configuration and the subsequent variation of γ_{CaO}, observed in the CaF_2–CaO–Al_2O_3 system (table 5.2).

The differences in activity data also occur because some of the previous studies are based on the initial slag composition, and do not allow for changes during the equilibration. In the case of fluoride slags, substantial composition changes occur during the course of an experiment because of the presence of volatile species such as CaF_2, SiF_4, AlF_3 etc; therefore, all high temperature equilibrium experiments concerning fluoride-based slags require final analysis of the melts to determine more accurate thermodynamic data. The present work is consistent in this way. The only problem in this technique is to extract the oxide ion activity at a

Table 5.4 Variation of $\gamma_{CO_3^{2-}}$ in Binary Aluminate and Silicate Slags at 1500 °C

Slag No.	X_{CaO}	a_{CaO}	N_{CaCO_3}	$\gamma_{CO_3^{2-}}$
CA-1	0.58	0.2	4.57×10^{-3}	0.12
CA-2	0.65	0.4	5.798×10^{-3}	0.19
CA-3	0.68	0.7	9.2×10^{-3}	0.21
CS-1	0.57	0.02	6.28×10^{-3}	8.8×10^{-3}
CS-2	0.5	0.005	2.74×10^{-3}	5.1×10^{-3}
CS-3	0.4	0.003	3.49×10^{-3}	2.4×10^{-3}

Table 5.5 Comparison of Experimental Activity of CaO with calculated one Obtained from Sulphide Capacity Measurements[55] in CaF_2-CaO-Al_2O_3 Slags at 1400°C; $\gamma_{CaS} = 3.4$

Slag No.	N_{CaO}	$N_{CaO}/N_{Al_2O_3}$	Experimental a_{CaO}	Calculated a_{CaO}
1	0.4	3.05	0.05	0.16
2	0.47	3.14	0.09	0.19
3	0.52	3.08	0.098	0.199
4	0.56	3.1	0.1	0.198
5	0.22	3.9	0.09	0.106
6	0.38	4.99	0.17	0.275
7	0.41	6.27	0.18	0.368
8	0.32	7.02	0.22	0.309
9	0.26	7.67	0.24	0.23

specific composition of a slag, since it is difficult to estimate the final composition from the starting material for a particular equilibrium experiment. However, these activity data would be useful particularly for a region where activities are not very composition sensitive.

5.1.4 IMPORTANCE OF THE CARBONATE EQUILIBRIUM

The study of the carbonate equilibrium, in spite of the fact that it does not have the direct implication of studies related to P and S, can be correlated to some important thermodynamic properties. Already, it has been shown that the data on carbonate equilibrium can be used to obtain the oxide activity of the slag, which, in a way, indicates the behavior of the slag with respect to different chemical reactions. Also, compared to other equilibria, such as those of sulfide and phosphate, the carbonate equilibrium is much more simplified in nature since at unit atmospheric pressure of CO_2, we have to consider only the carbonate ion activity and the reaction equilibrium constant to determine the oxide activity. Moreover, it is safe to assume regular solution behavior of the carbonate ion because of its large ionic size and low solubility in many slag systems. As a consequence, the major obstacle in studying this equilibrium is the accurate detection of carbonate in the slag. The experimental design should be done in such a way that the minimum CO_2 evolved can be analyzed accurately in an apparatus operating within tolerable experimental error.

The partial molar heat of dissolution of oxide can also be computed if the corresponding activity data are available over a temperature range. However, in the present case, due to the constraints of the operating temperature range of the apparatus and the limited range of

liquid phase region of the slag systems studied, this thermodynamic parameter can not be computed.

5.1.4.1 CARBONATE CAPACITY AND BASICITY OF SLAG

The carbonate equilibrium also can be employed to calculate carbonate capacity of a slag, which is defined as:

$$C_{carb} = \frac{N_{CO_3^{2-}}}{P_{CO_2}} \qquad 5.6$$

Wagner[76] proposed that the basicity of slags, involving O^{2-} ions as reactants, can be defined as(same as in equation 2.32):

$$B_{carb} = \frac{C_{carb}}{C^{*}_{carb}} \qquad 5.7$$

where C^{*}_{carb} is the carbonate capacity in a reference slag. He also suggested that the slag, $0.4CaO+0.4SiO_2+0.2Al_2O_3$, be deemed as a reference slag. In a recent investigation, Sosinsky et al.[77] concluded on the basis of optical basicity that this slag would have too low a carbonate capacity to be considered as a reference slag. Unfortunately, there is no direct experimental evidence to verify this and to select some other slag as a reference to define basicity according to the equation (5.7). In such a case, carbonate capacities of different slags can be compared and their variation with the change of composition plotted (figure 5.4). Since the sulfide capacity[90] is also a similar function of oxide ion activity, the change in carbonate capacity with respect to the composition shows a similar trend. The carbonate capacity is the highest in the binary $CaO-CaF_2$ slag, and the addition of CaF_2 in the silicate and aluminate slags increases the carbonate capacity. Similar effects were realised in the sulfide capacity investigations.

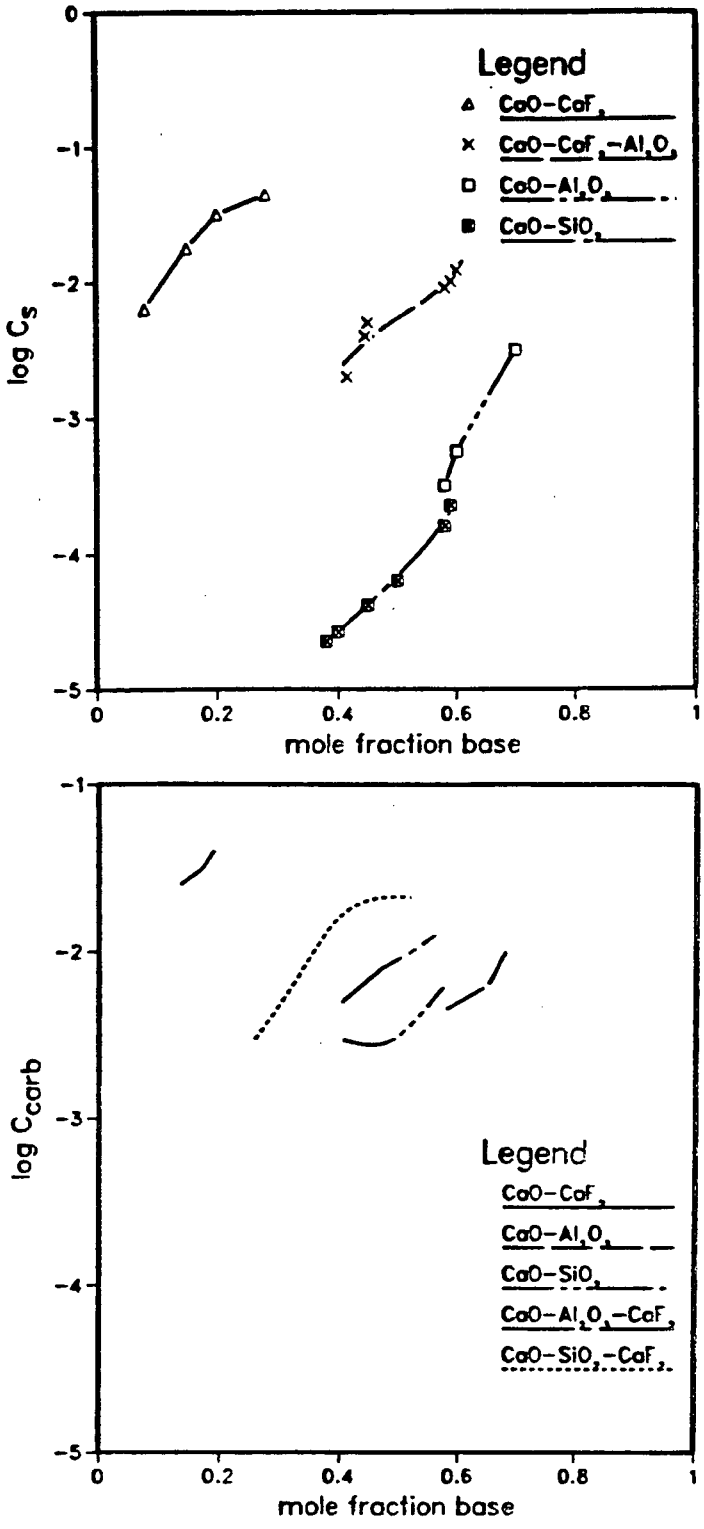

Fig. 5.4 Comparison of carbonate capacity and sulphide capacity[90] of silicate, aluminate and fluoride slags

From these observations on carbonate and sulfide capacities, it can be said that the addition of CaF_2 opens up the structure of slag, resulting in the greater capacities of S^{2-} and CO_3^{2-} ions in the slag.

As mentioned before, carbonate equilibrium data can be utilized to deduce the oxide ion activity of the slag. Some authors[91] have also tried to determine oxide ion activity from the EMF measurements of a concentration cell. Since most slags do not show ideal behavior, the cations cannot be assumed to have constant activity. Consequently, the relation as follows is not valid:

$$\frac{a''_{O^{2-}}}{a'_{O^{2-}}} = \frac{a''_{Na_2O}}{a'_{Na_2O}} \qquad 5.8$$

where $a''_{O^{2-}}$ and $a'_{O^{2-}}$ are the oxide ion activities of slags placed in a concentration cell, a''_{Na_2O} and a'_{Na_2O} are the activities of Na_2O of the respective slag in the same cell. The above equation can be true only when $a''_{Na^+} = a'_{Na^+}$. Goto et al.[92] performed both the carbonate equilibrium and EMF measurements on the Na_2O–SiO_2 slag. These data can be employed to calculate $a_{O^{2-}}$ and a_{Na_2O} (table 5.6) and the discrepancy becomes evident as the concentration changes. The contribution from any irregular solution behavior of carbonate ion, even if there is any, would be much smaller than the differences observed in the values of $a_{O^{2-}}$ and a_{Na_2O} as a result of the variation in the cation activity.

Rewriting the expression for oxide ion activity from the equation(5.3):

$$a_{O^{2-}} = \frac{N_{CO_3^{2-}} \cdot \gamma_{CO_3^{2-}}}{p_{CO_2} \cdot K} \qquad 5.9$$

Table 5.6 Variation of Oxide Ion Activity in Na_2O-SiO_2 Slags at 1373K obtained by Carbonate Equilibrium and EMF Measurements[92]

$X_{Na\ O}$	log X_{CO_2}	$X_{CO_3^{2-}}$	Carbonate Equilibrium, Activity, O^{2-}	EMF Experiment, Activity, Na_2O
0.5	-1.93	0.012	1.00×10^{-6}	1.00×10^{-6}
0.6	-0.9095	0.123	1.03×10^{-6}	3.20×10^{-5}
0.7	-0.592	0.256	2.10×10^{-5}	1.00×10^{-3}
0.8	-0.456	0.350	2.90×10^{-5}	0.01

or,

$$\log a_{O^{2-}} = \log \frac{N_{CO_3^{2-}}}{p_{CO_2}} + \log \frac{\gamma_{CO_3^{2-}}}{K} \qquad 5.10$$

Here the term $N_{CO_3^{2-}}/p_{CO_2}$ is equivalent to the carbide capacity (C_{carb}) and $\gamma_{CO_3^{2-}}/K$ is a constant for a specific slag system, thus

$$\log a_{O^{2-}} = \log C_{carb} + Q \qquad 5.11$$

where

$$Q = \log(\gamma_{CO_3^{2-}}/K)$$

Therefore, the plot of $\log a_{O^{2-}}$ versus $\log C_{carb}$ would be a straight line with unit slope and the intercept Q is equal to $-\log C_{carb}$ at unit oxide ion activity. The carbonate capacity and the oxide activity data in $CaO-CaF_2$, $CaO-Al_2O_3-CaF_2$ and $CaO-SiO_2-CaF_2$ at 1400°C are plotted in figure 5.5. The slope of the line is very close to unity and from the intercept $\gamma_{CO_3^{2-}}$ is calculated to be 0.043. In a similar exercise, Maeda et al.[93] plotted the activity of Na_2O at 1200°C, and the graph shows a similar slope (figure 5.6). The activity coefficient of carbonate ion, $\gamma_{CO_3^{2-}}$, can also be calculated here assuming the only cation to be Na^+, in which case K is equal to 2.4×10^4 atm^{-1}. Thus, $\gamma_{CO_3^{2-}}$ is found to be 15.1, representing a positive deviation and a significant interaction with the melt, which is not at all expected considering the big size of carbonate ions.

In $CaO-SiO_2$ slag, $\gamma_{CO_3^{2-}}$ is calculated from the CO_2 solubility

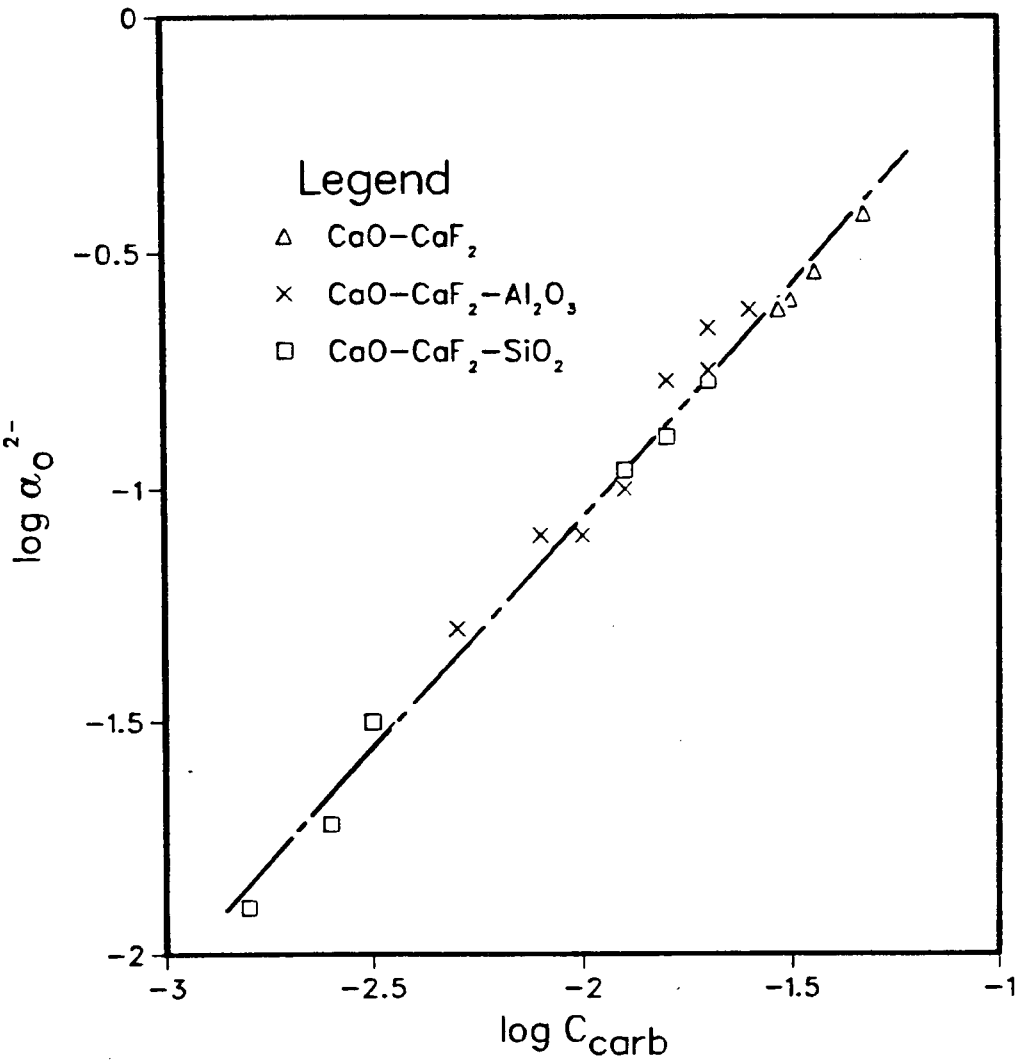

Fig. 5.5 Relationship between carbonate capacity and oxide ion activity in fluoride slag at 1400°C

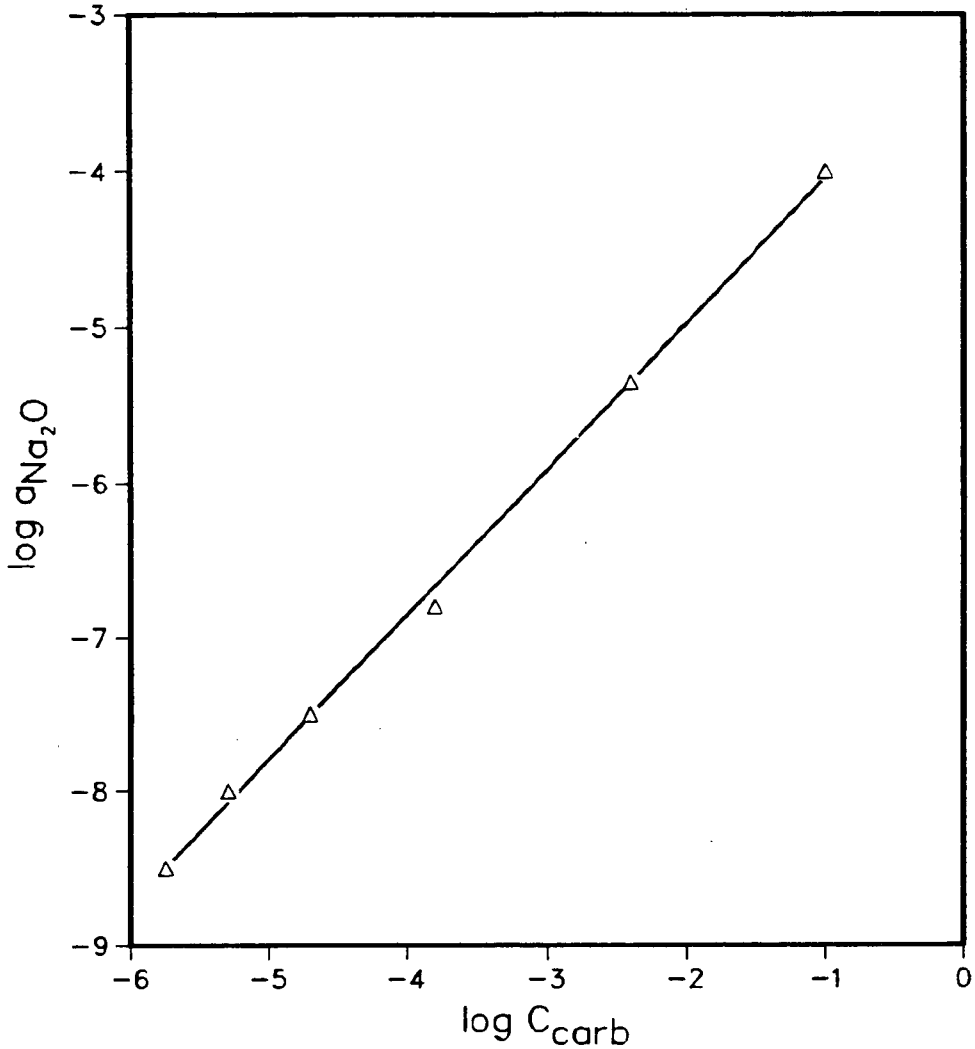

Fig. 5.6 Relationship between carbonate capacity and sodium oxide activity in Na_2O-SiO_2 slag at 1200°C [93]

experimental measurements at 1500°C. It is in the range of $2x10^{-3}$ to $9x10^{-3}$.

5.1.4.2 CARBONATE CAPACITY AND OPTICAL BASICITY

In oxide slags, optical basicity(OB) has been related to sulfide capacity data ($-\log C_S$)[74] and thus considered to be a parameter for clear characterization of a slag. As shown earlier, the sulfide capacity and the carbonate capacity exhibit similar trends in both fluoride-free and fluoride based slags. It is expected that optical basicity also can be correlated with the carbonate capacity of different slags.

At this stage, it is not possible to calculate optical basicity of CaF_2-CaO slag. Therefore, only ternary fluoride slags, such as CaF_2-CaO-SiO_2 and CaF_2-CaO-Al_2O_3, are considered where CaF_2 is assumed to play an inert role with respect to optical basicity. The binary silicate and aluminate slags for which the carbonate equilibrium data are available are also included in this plot. The final figure reflects an increasing trend of optical basicity with increase of carbonate capacity (figure 5.7). However, no simple linear relationship can be derived as observed in oxide slags with respect to sulfide capacity. It seems that optical basicity is not a very sensitive parameter in highly basic and fluoride slags, whereas oxide ion activity or carbonate capacity can be considered to be more suitable parameter to characterize a slag.

5.2. WATER SOLUBILITY IN ESR SLAGS

The newly developed deuterium tracer detection technique, as described in the previous chapter, was employed to analyze water solubility in all ESR slags. All solubility data vary from about 9000 to 1000 ppm

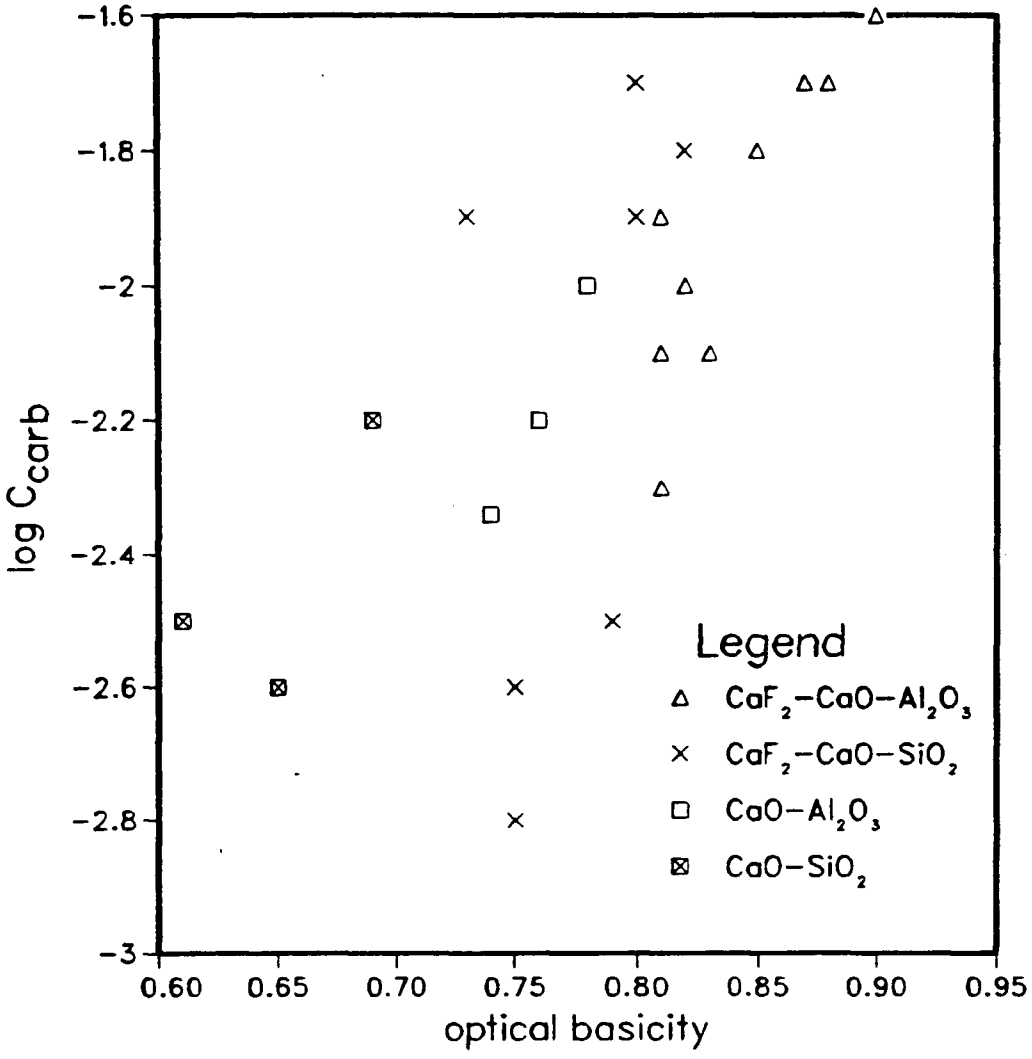

Fig. 5.7 Relationship between optical basicity and carbonate capacity in binary silicate, aluminate and ternary fluoride slags

and are much higher than those reported in the literature. Since the use of this new technique of solubility measurement is the major reason for the discrepancy, it is necessary to detail both the advantages and drawbacks of this novel method of analysis.

5.2.1 ADVANTAGES AND DISADVANTAGES OF THE DEUTERIUM TRACER DETECTION TECHNIQUE

The major concern for a regular water analysis of slag is the contamination of the sample. In a normal situation, if the slag after sampling is exposed to air, it adsorbs moisture. The same problem arises during the storage of the sample, thus requiring a moisture-free, inert atmosphere in the storage area. However, in the case of deuterium having natural abundance only 0.015%, one can be sure about the source of this isotope being analyzed. Once the slag has been equilibrated with D_2O, there is no possibility of contaminating the sample with any measurable quantity of deuterium.

Moreover, the reliability of analysis of a species in a mass spectrometer depends on the resolution of the instrument. If there is no helium source present in the system, the separation of masses of H_2 and D_2 (the percentage mass difference is considerable) can easily be done in a simplified version of a mass spectrometer. Also the analysis of deuterium is much more reliable, since there is no noticeable blank correction required for this measurement. Deuterium is not a radioactive isotope like tritium, therefore this analysis does not require any special handling, location or licensed personnel.

On the other hand, this technique calls for special preparation of the calibration sample, to ensure that $Ca(OD)_2$ is completely reduced to D_2 instead of D_2O. Moreover, the apparatus is designed in such a way that the graphite crucible, which heats up the slag and capsules, gradually becomes loaded with used slag and steel. Also, aluminum vapour deposits with increased proportions around the silica tube. The combined effect is the deviation of the apparatus from calibration level, but this becomes evident only after analyzing around 15 samples. Thus the technique requires very frequent, time-consuming and elaborate setting-up procedures.

5.2.2 WATER SOLUBILITY IN BINARY AND TERNARY FLUORIDE-BASED SLAGS

Binary slags containing different proportions of CaF_2 and CaO , which have been equilibrated at 1400°C and water vapour pressures of 31.8 torr and 92.5torr, are analyzed for water solubility (table 5.7-5.8). The solubility of water increases with the increasing CaO content of the slag and the water vapour partial pressure. The solubility level ranges from about 2400 to 8700ppm. There are no data available in the literature to compare the solubility levels for this type of slag. However, by comparing the sulfide capacity data and similar oxide ion behavior, these slags can be presumed to have a maximum level of water solubility.

Ternary slags of the type CaF_2 - CaO - Al_2O_3 are also analyzed for water solubility after performing the equilibrium experiment at 1400°C and water vapour partial pressures of 31.8torr and 92.5 torr (table 5.9-5.10). In the ranges of composition of these slags, analyzed water solubility varies from 1800 to 4200 ppm. The maximum solubility is obtained at a higher partial pressure of moisture and at 0.21 mole fraction

Table 5.7 Water Solubility in Binary Slags at 1400°C

Slag No.	(H_2O), ppm	
	P_{H_2O} = 31.8 torr	P_{H_2O} = 92.5 torr
SL-1	2400 ± 120	2500 ± 130
SL-2	2500	4600
SL-3	3100	5000
SL-4	5400	8700

Table 5.8 Chemical Analysis of Binary (Fl-C) Slags

Slag No.	% CaF_2	% CaO
SL-1	88.1	11.9
SL-2	83.5	16.5
SL-3	81.5	18.5
SL-4	78.6	21.4

Table 5.9 Water Solubility in Ternary (Fl-C-A) Slags at 1400°C

Slag No.	(H_2O), ppm	
	P_{H_2O} = 31.8 torr	P_{H_2O} = 92.5 torr
SL-6	3800 ± 200	4200 ±200
SL-7	1800	2300
SL-8	2900	3400

Table 5.10 Chemical Analysis of Ternary(Fl-C-A) Slags

Slag No.	% CaF_2	% CaO	% Al_2O_3	N_{CaO}	$N_{CaO}/N_{Al_2O_3}$
SL-6	78.6	15.8	5.6	0.21	5.1
SL-7	62.8	24.7	12.5	0.32	3.6
SL-8	47.4	32.4	20.2	0.42	2.9

of CaO . The reason for such a high level of solubility at a low CaO content is the ratio of CaO to Al_2O_3 , which is maximum at that composition. Eight ternary slags of the type CaF_2 - CaO -SiO_2 are analyzed for water solubility after they have been equilibrated at 1400°C and 31.8 and 92.5 torr of water vapour pressures (table 5.11-5.12). These slags exhibit minimum water solubility compared to data for all the slags analyzed. Also the solubility increases with the increase of N_{CaO} /N_{SiO_2} ratio and the partial pressure of water vapour. The minimum solubility is obtained at 0.31 mole fraction of CaO and the molar ratio of CaO /SiO_2 at 2.2. Presumably, the oxide ion activity and the free available O^{2-} ions are minimum at this condition and they give the lowest level of water solubility.

In table 5.13, the water analyses done by VEW(Austria) are compared with the presently developed isotope tracer technique at UBC. The VEW method analyzed water as H_2O as opposed to equivalent D_2 in the present method. In binary slags the agreement is better than that of CaF_2 based silicate slags. Also, the higher values of water solubility in the VEW technique can be accounted for in binary slags by considering the greater possibility of adsorbing moisture from the atmosphere in the solid slag samples before it has been encapsulated in an evacuated tube.

In the isotope tracer technique, "water" analyzed in the slag is D_2O. By considering the thermodynamic data on H_2O and D_2O and assuming the same degree of difference for the thermodynamic data on $Ca(OH)_2$ and $Ca(OD)_2$, it is possible to estimate the free energy of formation of $Ca(OD)_2$. At 1673K this difference due to isotopic variation is only 223 calories. Thus for all practical purposes, the measured D_2O solubility can be regarded

Table 5.11 **Water Solubility in Ternary (Fl-C-S) Slags at 1400°C**

Slag No.	(H_2O), ppm	
	p_{H_2O} = 31.8 torr	p_{H_2O} = 92.5 torr
SL-9	4300 ± 200	6200 ±300
SL-10	3000	4200
SL-11	4700	6800
SL-12	2000	2500
SL-13	1900	3800
SL-14	1000	1800
SL-15	1500	2000
SL-16	1900	2800

Table 5.12 Chemical Analysis Ternary (Fl-C-S) Slags

Slag No.	% CaF_2	% CaO	% SiO_2	N_{CaO}	N_{CaO}/N_{SiO_2}
SL-9	79.0	17	4	0.22	4.6
SL-10	64.4	26.8	8.8	0.33	3.3
SL-11	48.1	38.8	13.1	0.45	3.2
SL-12	41.8	39.4	18.8	0.45	2.2
SL-13	81.3	12.9	5.8	0.17	2.4
SL-14	62.1	25.5	12.4	0.31	2.2
SL-15	45.1	36.2	18.7	0.42	2.1
SL-16	35	42.7	22.3	0.48	2.1

Table 5.13 Comparison of the Present Analysis with the VEW-Analysis

Slag	Present Work (H_2O), ppm	VEW, Austria (H_2O), ppm
SL - 4a	5400	5500
SL - 4b	8700	9100
SL - 16a	1900	1000
SL - 16b	2800	1200

Note: a: For p_{H_2O} = 31.8 torr

b: For p_{H_2O} = 92.5 torr

as the H_2O solubility in the slag.

In light of the above comparison, the main reason for the differences of water solubility data in the literature and the values obtained in this work can be attributed to the sampling method employed. The normal method of using a metal rod for freezing out some liquid slag may result in substantial loss of moisture during its cooling period for water-saturated slags. In the present sampling technique, this possibility does not exist and consequently it is considered to be a better sampling technique for slags.

5.2.3 WATER SOLUBILITY AND WATER VAPOUR PRESSURE IN ESR

Even though the solubility data are higher by an order of magnitude, the straight line relationship with the square root of water vapour pressure is obtained (figure 5.8). This Sievert's law relationship also shows the fact that the binary slags have the highest water solubility and the CaF_2 - CaO -SiO_2 slags have the least. Walsh et al.[9] suggested that this type of relationship exists because of either of the following reactions:

$$\{H_2O\} + (O^{2-}) = 2(OH^-) \qquad 5.12$$

$$\{H_2O\} = 2(H^+) + (O^{2-}) \qquad 5.13$$

However, the second reaction can be ruled out in this case because of the finding that the solubility increases with the increase of oxide ion activity. Both these relationships can only be satisfied with the former equilibrium reaction which would control the water solubility level in the slag.

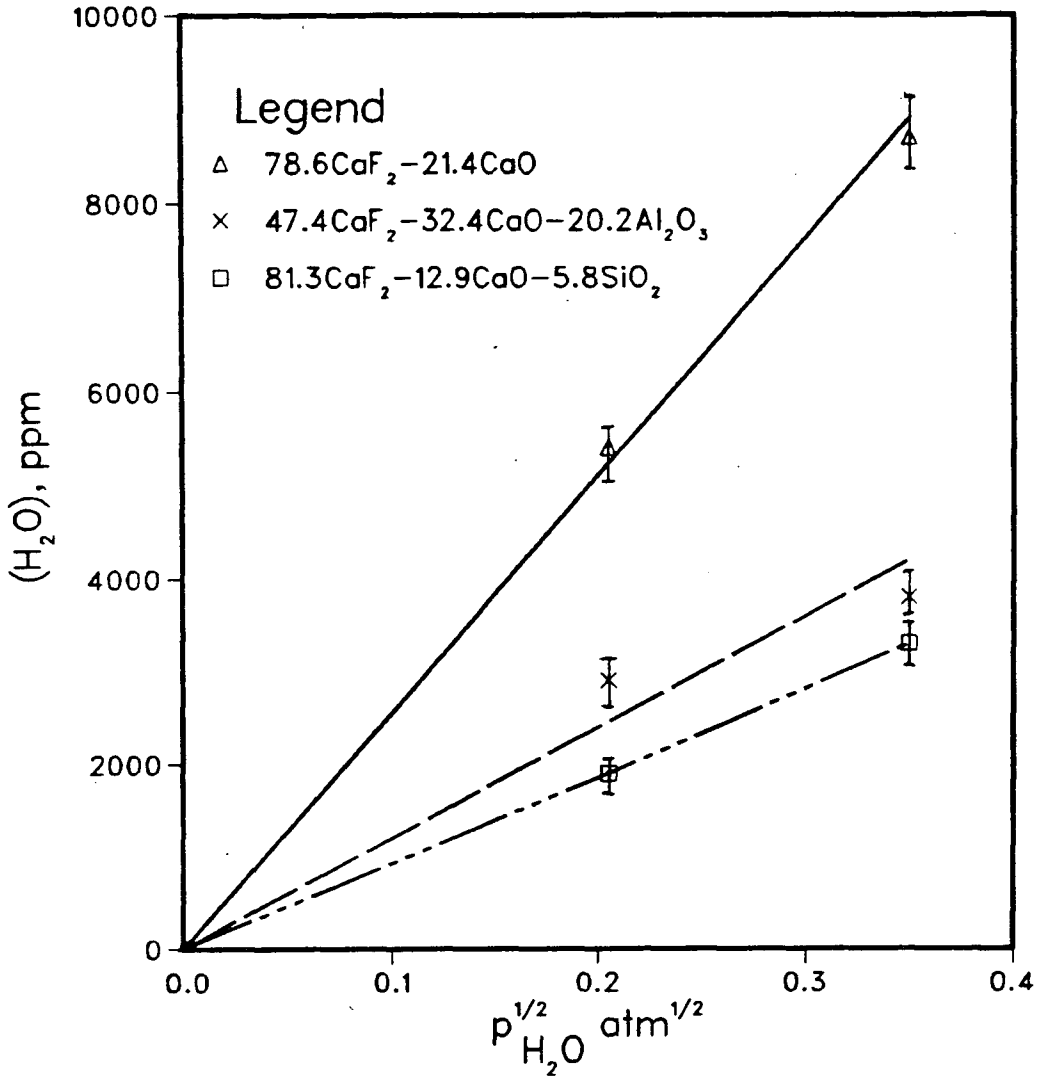

Fig. 5.8 Solubility of water in Fluoride-based slags as a function of water vapour pressure

The water vapour pressure considered here is the equilibrium water vapour pressure generated by saturating the gas stream at different water-bath temperatures. However, this gas is further heated up before reacting with the slag at 1400°C. The error due to corresponding dissociation of water vapour at high temperature can be checked by considering the equilibrium dissociation reaction:

$$H_2O = H_2 + 1/2\ O_2 \qquad 5.14$$

At 1400°C, since the equilibrium constant is only 1.6×10^{-5} $atm^{1/2}$, the maximum pressure of $p_{H_2} \cdot p_{O_2}^{0.5}$ is 7×10^{-7} when p_{H_2O} is equal to 0.04 atm. Consequently, the error involved in assuming that the equilibrium water vapour pressure of the constant temperature bath remains unchanged on top of the slag, is negligible. However, the values would have been different for a situation where a molybdenum or graphite crucible is used to hold the slag. In this case, the oxygen potential is governed by the oxidation potential of the crucible, resulting in a substantial dissociation of water vapour.

5.2.4 THERMODYNAMIC ANALYSIS OF THE WATER SOLUBILITY DATA

In highly basic slags, oxygen is present as free O^{2-} ions. The water vapour slag reaction in this type of slag can thus be represented by equation(5.12). The corresponding equilibrium constant, K_{hyd} is:

$$K_{hyd} = \frac{a^2_{OH^-}}{p_{H_2O} \cdot a_{O^{2-}}} \qquad 5.15$$

$$= \frac{\gamma^2_{OH^-} \cdot N^2_{OH^-}}{p_{H_2O} \cdot a_{O^{2-}}}$$

The free energy change for the above reaction involving only Ca^{2+} cation is given by[54]:

$$\Delta G^0_{hyd} = -27868 + 75.6T - 6.14T\ln T \quad cal/mole \qquad 5.16$$

Thus, at a particular temperature the equilibrium constant, K_{hyd}, can be calculated by the relationship:

$$K_{hyd} = e^{-\Delta G_{hyd}/RT} \qquad 5.17$$

At a particular water vapour pressure, p_{H_2O}, and known $a_{O^{2-}}$, as determined by carbonate equilibrium, the water solubility data can be used to estimate γ_{OH^-}, the activity coefficient of OH^- ion. In binary slags it is calculated to be in the range of 0.2-0.3, whereas in ternary slags it is found to vary from 0.07-0.09 (table 5.14). Unfortunately, there are no data available in the literature to compare with these findings.

In the literature, the ion-oxygen attraction, I, is considered to be an important parameter in controlling water solubility in different oxide slags. A more generalized term would be the cation-anion attraction, A, which could be defined in the same fashion i.e $A=Z_1Z_2/a^2$, where Z_1 is the anion valency, Z_2 is the cation valency and 'a' is the interionic distance. In table 5.15 this parameter A has been calculated for different salts which are of importance in ESR slag systems. The addition of Al_2O_3 in CaO - CaF_2 , which results in a lower water solubility, can be explained by this parameter, A, which influences the solubility in an inverse relationship. On this basis, salts containing silicon show the maximum values of A and thus this parameter conforms with the observation that the silicate slags exhibit minimum water solubility.

Table 5.14 Activity Coefficient of Hydroxyl ion, γ_{OH^-} at 1673K in Fluoride Slags obtained from experimental data of Oxide ion Activity and Water Solubility

Slag No.	N_{CaO}	N_{CaO}/N_{SiO_2} (or $N_{Al_2O_3}$)	N_{OH^-}	$a_{O^{2-}}$	γ_{OH^-}
SL - 1	0.16	Binary	4.85×10^{-3}	0.280	0.200
SL - 3	0.24	Binary	6.28×10^{-3}	1.000	0.280
SL - 6	0.21	5.1 (Al_2O_3)	7.82×10^{-3}	0.100	0.073
SL - 8	0.42	2.9 (Al_2O_3)	5.80×10^{-3}	0.070	0.080
SL - 9	0.22	4.6 (SiO_2)	8.52×10^{-3}	0.200	0.093
SL - 11	0.45	3.2 (SiO_2)	8.37×10^{-3}	0.180	0.090
SL - 12	0.45	2.2 (SiO_2)	3.49×10^{-3}	0.019	0.070

Table 5.15 Cation - Anion Attraction in Various Salts

Salt	Cation - Anion Attraction A
CaF_2	0.36
AlF_3	0.87
SiF_4	1.28
$Ca(OH)_2$	0.32
$Al(OH)_3$	0.73
CaO	0.70
Al_2O_3	1.66
SiO_2	2.44

Considering the water solubility reaction(5.12) again, the equilibrium constant, K_{hyd} can be written as in equation 5.15. Taking logarithms on both sides and rearranging:

$$\log a_{O^{2-}} = 2\log(N_{OH^-}/p^{0.5}_{H_2O}) + \log (\gamma^2_{OH^-}/K_{hyd}) \qquad 5.18$$

Similar to carbonate capacity, the hydroxyl ion capacity, C_{hyd}, can be defined as $N_{OH^-}/p^{0.5}_{H_2O}$. Also for a particular system, γ_{OH^-}/K would be constant, say,

$$B = \log (\gamma^2_{OH^-}/K) \qquad 5.19$$

Thus, the oxide ion can be expressed as:

$$\log a_{O^{2-}} = 2\log C_{hyd} + B \qquad 5.20$$

Therefore, the logarithmic plot of oxide ion activity and hydroxyl ion capacity would be a straight line. Unfortunately, the oxide ion activity as determined by the carbonate equilibrium does not correspond for all the slags for which the hydroxyl ion capacities have been determined. However, some literature data and some extrapolation of the present data assist in making the plot for different $\log C_{hyd}$ in fluoride based slags (figure 5.9). The uncertainities in oxide activity data make the plot more tentative (or qualitative!). However, some important features can be pointed out very clearly. All the highly basic slags such as CaO - CaF_2 , CaO - CaF_2 -SiO_2 with $N_{CaO}/N_{SiO_2} \geq 3$ and CaO - CaF_2 - Al_2O_3 show different straight lines but of similar slope, suggesting the operation of the same equilibrium reaction with water vapour and slag. In a less basic slag such as CaO - CaF_2 -SiO_2 where $N_{CaO}/N_{SiO_2} \simeq 2$, the operating reaction might deviate as the slope of the line changes. Also, γ_{OH^-} for a specific slag can be considered to be a constant, but it is a different value for different slag

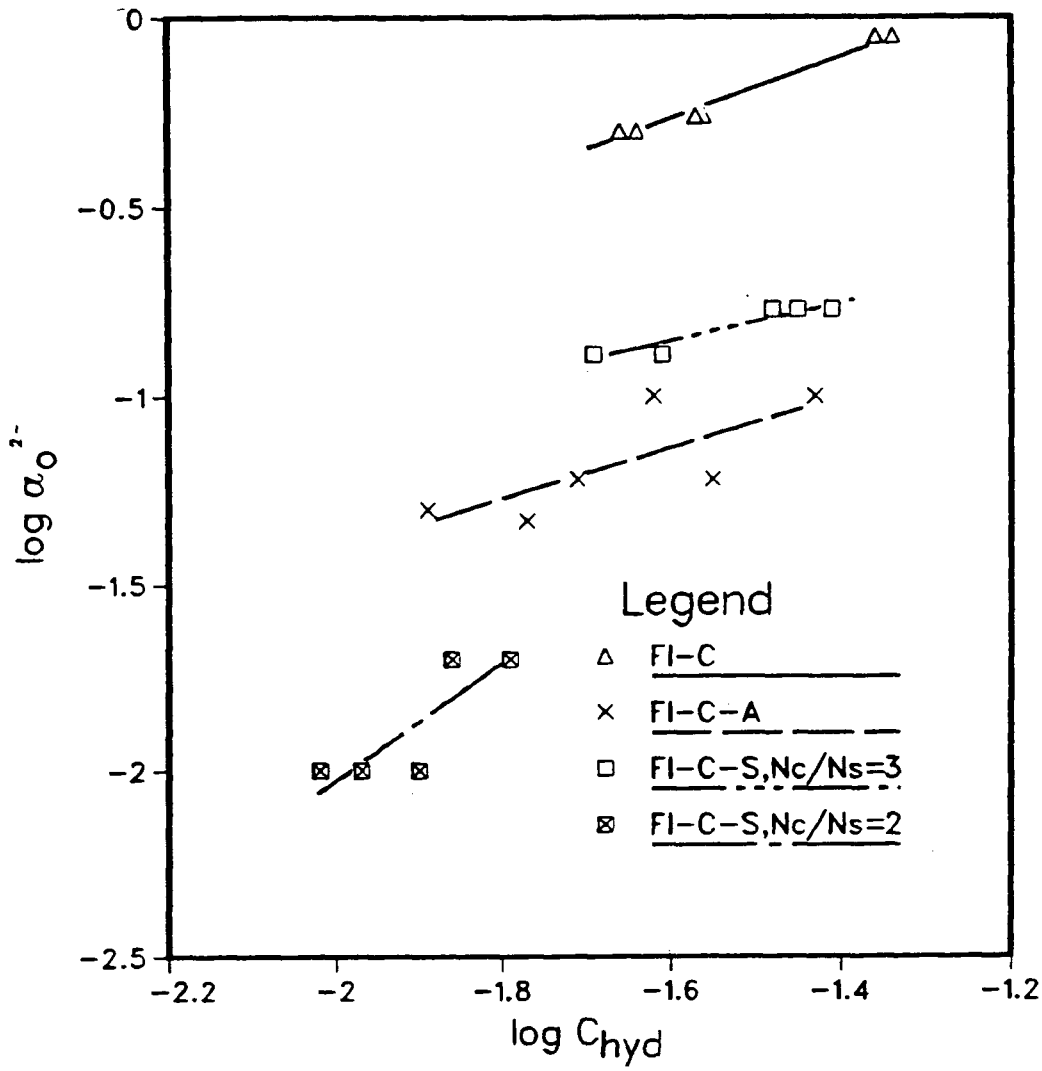

Fig. 5.9 Relationship between hydroxyl capacity and oxide ion activity in various fluoride slags

systems as shown earlier.

The above discussion reveals two important facts. The oxide ion activity and the activity coefficient of hydroxyl ion, γ_{OH^-}, are two critical parameters for characterizing slags with respect to water solubility in ESR slags. This investigation resulted in some useful data for both oxide ion activity and γ_{OH^-} in some fluoride-based slags used in ESR. A more complete and comprehensive study of these two parameters would help us to estimate water solubility accurately in all ESR slags.

5.2.5 PREDICTION OF HYDROGEN LEVEL IN ESR INGOTS

So far, the discussion has been mainly directed toward the determination and estimation of the hydrogen level in the slag. However, the final aim of the ESR process is to produce an ingot with a predictable and tolerable hydrogen content. As mentioned before, the hydrogen content in the ingot reaches a steady state value after about 30 minutes from starting the process. The ratio of hydrogen between the slag and the metal (L_H) also attains a constant value around the same length of time. Thus the water solubility data can help to predict the final hydrogen content in the ingot, depending on the temperature of operation, gaseous atmosphere on top of the slag and the slag composition. The previous studies[1-3] indicate that L_H changes from 2 to 10 depending on the slag basicity. However, in the present investigation, owing to the higher solubilities of water in fluoride slags, this ratio is higher by an order of magnitude. In that respect, the solubility data in CaF_2 - CaO - Al_2O_3 slag can be used to modify figure 2.23, assuming that the hydrogen in the ingot is the same. The resulting figure (figure 5.10) shows that the L_H varies from about 20 to 45, as expected earlier. Thus, the exact values of L_H and the available

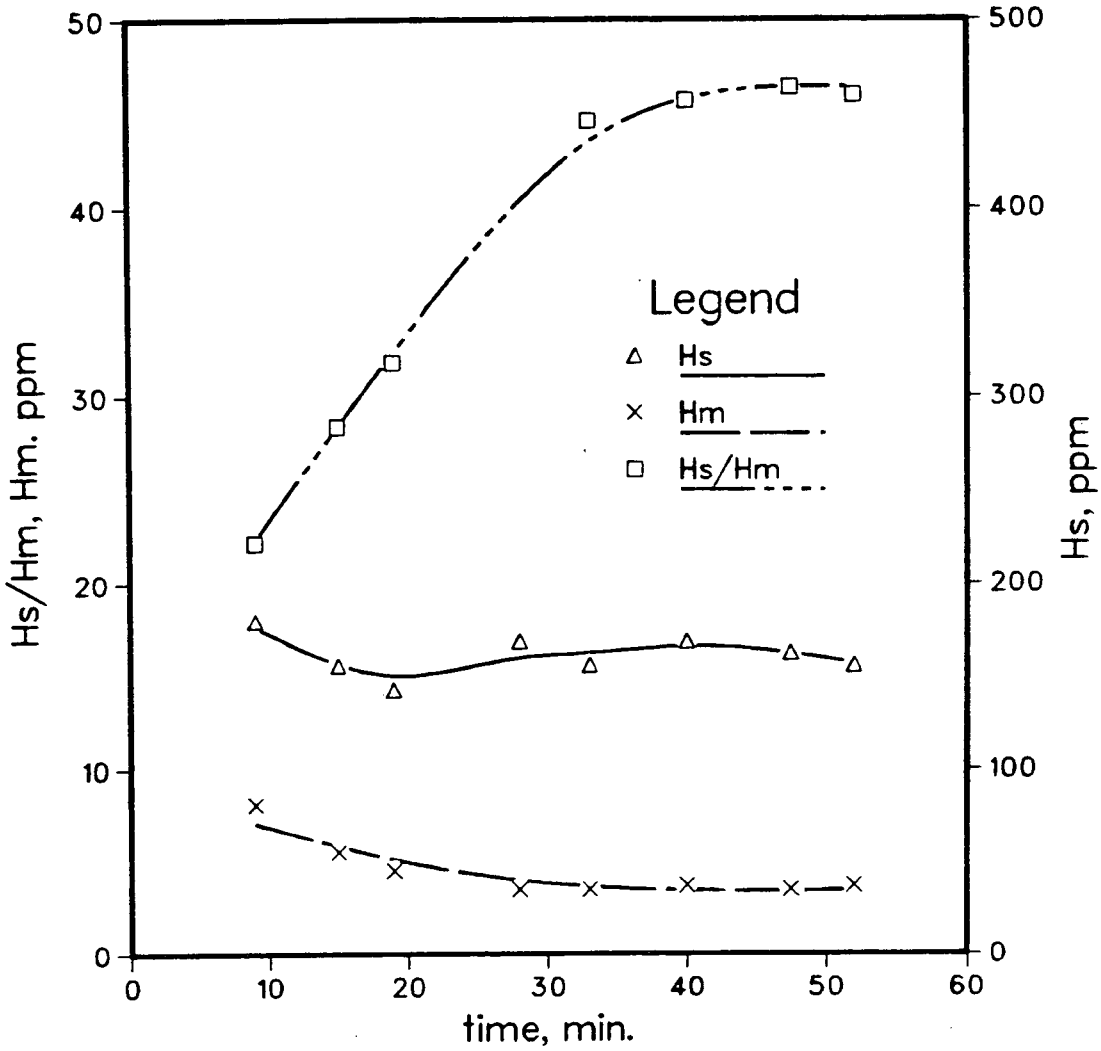

Fig. 5.10 The modified hydrogen equilibrium between slag and metal, based on the present work

data on water solubility in ESR slag would enable us to predict the final level of hydrogen in an ESR ingot.

At this stage, the constraints of the present water analysis technique and the unreliability of the conventional sampling and analytical methods do not permit us to establish an on-line hydrogen monitoring system in an ESR operation. However, the experimental data obtained during this study can be utilized to estimate the limiting partial pressure of moisture in the gas phase. For instance, the production of a 25ton ESR ingot containing a maximum of 2ppm hydrogen would tolerate a maximum partial pressure of moisture of 8.6×10^{-3} atm, which is equivalent to a dew point of approximately 5°C. This assumes that 1 ton of 50 CaF_2 -25 CaO -25 Al_2O_3 slag is employed during the process and that an equilibrium between the metal and the atmosphere is maintained at 1600°C, for which L_H is taken as 45. The corresponding values for γ_{OH^-} and $a_{O^{2-}}$ are considered to be 0.08 and 0.05 respectively.

Again, considering the above case, operating with some protective atmosphere, the starting slag should not contain more than 810ppm water. Unfortunately, the problem of hydrogen is most severe at the initial period of operation, where the L_H value is also substantially low. Taking, for example, the figure 5.10, L_H during the starting period is around 20 and thus the maximum allowable moisture level in the starting slag is only 360ppm. The commercial slag, such as S2022 (product of Wacker-Chemie), reported to contain 500ppm of H_2O, is unsuitable for the production of low hydrogen ESR ingot. This water level also corresponds to the analysis done at 650°C and is thus definitely not the absolute level of water in that slag.

Thus the present study not only looks into the fundamentals of hydrogen transfer during ESR operation but also serves the function of estimating the limiting parameters to produce an acceptable ESR ingot.

CHAPTER 6

SUMMARY

6.1. CONCLUSIONS

The conclusions that can be drawn from the present work are summarized below.

The oxide ion activity in the fluoride based binary and ternary slags has been determined and compared with the available literature data. The carbonate equilibrium is carried out by equilibrating the slag with CO_2. It is not only an independent and reliable technique but is also helpful in calculating the carbonate capacity of different slags.

In basic ESR slags, carbonate capacity exhibits a similar relationship with the slag composition, as previously reported, with respect to sulfide capacity. However, there is no clear relationship established between the carbonate capacity and the optical basicity. The latter parameter seems to be less sensitive in fluoride-based slags, most probably due to the inherent limitations of the optical basicity in characterizing non-oxide slags.

The water vapour-slag equilibrium is studied in similar slags at 1400°C at two different partial pressures of moisture. The saturated D_2O vapour in the stream of pure helium is used for the equilibration. All slags are sampled by a new technique, sampling in a quartz tube, which retains the equilibrium water level in the slag.

A new technique, employing a simple mass spectrometer, has been developed to analyze water in the slag. This method is better and more reliable than those reported in the literature, but is more complex. It has been verified by analysing standard non-fluoride slags and comparing the results of simultaneous analyses of fluoride slags performed both in our laboratory and at VEW, Austria, where a different, independent method is used.

The water solubility, determined by this new isotope tracer technique, shows values an order of magnitude higher than those reported in the literature. The major reasons for these differences are the better sampling technique and the reliable isotope tracer analysis employed. However, the solubility data show the square root relationship with water vapour pressure, reflecting the type of mechanism operating in a basic slag.

These data can be used together with literature information to generate a modified equilibrium ratio of hydrogen between ESR slag and an ingot. Finally, these results can be successfully employed to estimate the limiting controlling parameters for the production of an ESR ingot with an acceptable level of hydrogen.

6.2. SUGGESTIONS FOR FUTURE WORK

In light of the present findings, further studies in the following directions are indicated.

1. The partial heat of solution of the carbonate ion in different ESR slags should be determined. There are no data on the temperature dependence of the equilibrium in fluoride slags. Thus experiments on CO_2-slag equilibrium at different temperatures will lead to

better understanding of carbonate solution thermodynamics.

2. The CO_2-slag equilibrium experiments should also be extended to other slags containing MgO and rare-earth oxides. The direct determination of carbonate capacity would help to better characterize different ESR slags and these data can further be translated to compute their desulfurizing potentials.

3. The data on solution thermodynamics of water in fluoride slags are sparse. Thus the water vapour-slag equilibrium experiments at different temperatures would be highly desirable not only for a better definition of hydrogen thermodynamics of ESR slag but also to determine an optimum temperature of operation of the ESR process.

4. The present water analysis technique is not yet suitable for on-line monitoring of hydrogen during an ESR process. Hence, the method has to be modified to meet the final goal— the on-line control of hydrogen during the ESR process.

The high background level of hydrogen in the vacuum apparatus makes the direct analysis of water as hydrogen impractical. The analysis of water as H_2O or the isotope dilution method using deuterium are the two viable alternatives to be explored for direct monitoring of water in the slag.

REFERENCES

1. Schürmann, E. et al.: Arch. Eisenhüttenwes, Vol. 52, August 1981, pp 303-310.

2. Latash, Yu.V. et al.: Proc. 7th International Conference on Vacuum Metallurgy, November 1982, Tokyo, Japan, pp1237-1243.

3. Nakamura, Y and Harashima, K.: Tetsu-to-Hagane, Vol. 63, August 1977, pp 1235-1243.

4. Jaegar, H. et al.: "Investigations regarding the control of Hydrogen and Aluminium content in ESR-ingots', Boehler Bros. & Co. Ltd (Austria).

5. Masui, A.: Proc. 5th International Symp. on ESR, Part 1, 1974, Pittsburgh, pp 284-305.

6. Holzgruber, W. et al.: Special Electrometallurgy, 1976, pp 161-174.

7. Pocklington, D.N.: J. of Iron and Steel Institute, Vol. 211, June 1973, pp 419-425.

8. Chuiko, N.M. et al.: Metallurgy, July 1977, pp 21-22.

9. Walsh, J.H., Chipman, J., King, T.B. and Grant N.J.: Trans. AIME, Vol. 206, 1956, pp 1568-1576.

10. Kobayashi, M. et al.: Springer Series in Chemical Physics, Vol. 19 (SIMS3), 1982, pp 361-364.

11. Forno, A.E.J. et al.: J. of Iron and Steel Institute, Vol. 209, Dec. 1971, pp 966-968.

12. Medovar, B.I. et al.: Special Electrometallurgy, 1976, pp 101-117.

13. Bektursunov, Sh. Sh. et al.: Translation from Izvest. VUZ-Chern. Met., Sept. 1961, pp 44-53.

14. Schwerdtfeger, K and Schubert, G.: Met. Trans. B, Vol. 8B, Dec. 1977,

pp 689-691.

15. Vatolin, A.N. et al.: Fiz.-Khim. Issled. Metallurg. Protsessov, Sverdlovsk, Vol. 10, 1982, pp 144-152.

16. Jaroslav, S. et al.: Zvaranie, Vol. 26, May 1977, pp 149-152.

17. T. El Gammal and Waladan, M.: Second International Symp. on Metallurgical Slags and Fluxes, Nov. 1984, Lake Tahoe, Nevada, pp 453-465.

18. Zuliani, D.J. et al.: ISS Transactions, Vol. 1, 1982, pp 61-67.

19. Nikol'skii, V.S. et al.: Steel in the USSR, Dec. 1979, pp 619-622.

20. Saenko, V. Ya. et al.: Probl. Spets. Electrometall., Vol. 17, 1982, pp 32-33.

21. Rebrov, L.B. et al.: Probl. Spets. Electrometall., Vol. 11, 1979, pp 8-13.

22. Iguchi, Y. et al.: Trans. Iron and Steel Institute of Japan, Vol. 9, 1969, pp 189-195.

23. Hitachi, Ltd., Jpn. Tokkyo Koho JP 82 32, 698 (Cl. C22B9/18), 13 July 1982.

24. Latash, Yu. V. et al.: Izv. Akad. Nauk SSSR, No. 3, 1979, pp. 40-44.

25. Masui, A. et al.: Tetsu-to-Hagane, Vol. 63, 1977, pp 2181-2190.

26. Nicholls, J.: Short Course in application of Thermodynamics of Petrology and Ore deposits, April 1977, Vancouver, pp. 160-184.

27. Klöhne, C. and Nowack, N.: Arch. Eisenhüttenwes, Vol. 52, July 1981, pp. 271-273.

28. Russel, L.E.: J. Soc. Glass Tech., Vol. 41, 1957, pp. 304-317T.

29. Tomlinson, J.W.: J. Soc. Glass Tech., Vol. 40, 1956, pp 25-31T.

30. Kurkjian, C.R. and Russel, L.E.: J. Soc. Glass Tech., Vol. 42, 1958, pp 130-144.

31. Uys, J.M. and King, T.B.: Trans. AIME, Vol. 227, April 1963, pp 492-500.

32. Scholze, H. et al.: Advances in Glass Technology, 6th International Conf. Glass Technology, Washington, 1962, pp 230-245.

33. Fukushima, T. et al.: Trans. I.S.I.J., Vol. 6, 1966, pp 19-26.

34. Iguchi, y. et al.: Symp. on Chemical Metallurgy of Iron and Steel, ISI, BSC Corporate Lab, U. of Sheffield, 1971, pp 28-30.

35. Fincham, C.J.B. and Richardson, F.D.: Proc. Roy. Soc., A223, 1954, pp 40-62.

36. Sachdev, P.L. et al.: Met. Trans., Vol. 3, 1972, pp 1537-1543.

37. Coutures, J.P. et al.: C.R. Seances Acad. Sci., Ser. 2, Vol. 293, 1981, pp 1049-1052.

38. Wahlster, V.M. and Reichel, H.H.: Arch. Eisenhüttenwes, Vol. 40, Jan. 1969, pp. 19-25.

39. Schwerdtfeger, K. and Schubert, H.G.: Met. Trans. B, Vol. 9B, March 1978, pp 143-144.

40. Coutures, J.P. et al.: Rev. Int. Heutes Temper. Refract. Fr., Vol. 17, 1980, pp. 351-361.

41. Davies, M.W. and Spassov, A.: J. of Iron and Steel Institute, Oct. 1967, pp 1031-1033.

42. Imai, M. et al.: Studies in Metallurgy, 1969, pp 66-75.

43. Iguchi, Y. and Fuwa, T.: Trans I.S.I.J., Vol. 10, 1970, pp 29-35.

44. Sosinsky, D.J. et al.: Met. Trans. B, Vol. 16B, 1985, pp 61-66.

45. Wahlster, V.M. and Hilper, A.: Stahl und Eisen, Vol. 89, 1969, pp 710-716.

46. Novokhatskiy, I.A. et al.: Akademiia Nauk. SSSR, Izvestia., Metally, No. 5, 1968, pp 22-27.

47. Gibala, R. and DeMiglio, D.S.: Proc. of Third International Conf. on Effect of Hydrogen on Behaviour of Materials, Moran, Wyoming, August, 1980, pp 113-122.

48. Bagshaw, T.: Proc on Third International Symp. on ESR, Pennsylvania, Mellon Institute, 1971, pp 183-211.

49. Coutures, J.P. and Peraudeau, G.: Rev. Int. Hautes Temp. Refract., Vol. 18, 1981, pp 321-346.

50. Bloom, H.: The Chemistry of Molten Salts, W.A. Benjamin Inc., 1967, p 23.

51. Schmidt, J.: Arch. Eisenhüttenwes, Vol. 46, 1975, pp. 711-713.

52. Lloyd, M.H. and Shanahan, C.E.A.: J. of Iron and Steel Institute, Sept. 1973, pp 615-621.

53. Kalinyuk, N.N.: Industrial Lab., Vol. 44, June 1977, pp 740-742.

54. Handbook of Chemistry and Physics: CRC Press. Inc., Florida, 63rd Ed., 1982-1983.

55. Kor, G.J.W. and Richardson, F.D.: Trans. Met. Soc. AIME, Vol. 245, Feb. 1969, pp 319-327.

56. Mills, K.C. and Keene, B.J.: International Met. Rev., No. 1, 1981, pp 21-69.

57. Mitchell, A.: Canadian Met. Quart., Vol. 20, 1981, pp 101-112.

58. Nafziger, R.H.: High Temp. Science, No. 5, 1973, pp 414-422.

59. Salt, D.J.: Proc. 1st International Symp. on Electroslag consumable Electrode Remelting and Casting Tech., Vol. 1, Carnegie Mellon U.,

Pittsburg, 1967, pp 1-29.

60. Mitchell, A. et al.: J. Iron and Steel Institute, April, 1970, p 407.

61. Mukherjee, J.: J. Amer. Ceramic Soc., Vol. 48, 1965, pp 210-213.

62. Baak, T.: Acta Chem. Scand., Vol. 8, 1954, p 1727.

63. Kojima, H. and Masson, C.R.: Can. J. Chem., Vol. 47, 1969, pp 4221-4228.

64. Ries, R. and Schwerdtfeger, K.: Arch. Eisenhüttenwes, Vol. 51, April 1980, pp. 123-129.

65. Kuo, C.K. et al.: Acta Chim. Sinica, Vol. 30, 1964, pp 381-385.

66. Budnikov, P.P. and Tresvyatsii: Dokl. Akad. Nauk. SSSR, Vol. 89, 1953, p 479.

67. Edmunds, D.M. and Taylor, J.: J. of Iron and Steel Institute, Vol. 210, 1972, pp 280-283.

68. Mitchell, A. and Cameron, J.: Met. Trans., Vol. 2, Dec. 1971, pp 3361-3366.

69. Evseev, P.P.: Autom. Weld. (USSR), Vol. 20, 1967, p 42.

70. Baak, T. and Olander, A.: Acta Chem. Scand., Vol. 9, 1955, pp 1350-1354.

71. Shinmei, M. et al.: Canad. Met. Quart., Vol. 22, 1983, pp 53-59.

72. Sommerville, I.D. and Kay, D.A.R.: Met. Trans. Vol. 2, June 1971, pp 1727-1732.

73. Suito, H. and Gaskell, D.R.: Met. Trans. B, Vol. 7B, Dec. 1976, pp 567-575.

74. Sommerville, I.D. and Sosinsky, D.J.: 2nd International Conf. on Metallurgical Slags and Fluxes, Lake Tahoe, Nevada, Nov. 1984,

TMS-AIME, pp 1015-1025.

75. Nagata, K. and Goto K.S.: Trans. Iron and Steel Inst. of Japan, Vol. 25, 1985, pp 204-211.

76. Wagner, C.: Met. Trans. B, Vol. 6B, Sept. 1975, pp 405-409.

77. Sosinsky et al.: Presentation at the 24th CIM Conf., Vancouver, August 1985.

78. Muratov, A.M.: UDC 669, 891'787'546.16.669, 0.46, 584, 1973, pp 55-56.

79. Mehrotra, G.M. et al.: Arch. Eisenhüttenwes, Vol. 47, Dec. 1976, pp. 719-723.

80. Hawkins, R.J. et al.: J. of Iron and Steel Institute, Vol. 209, Aug. 1971, pp 646-657.

81. Zhdanovski, A.A.: Prob. Spets. Electromet., No. 9, 1977, pp 114-119.

82. Allibert, M. and Chatillion, C.: Canad. Met. Quart., Vol. 18, 1979, pp 349-354.

83. Raschev, Z. et al.: Arch. Eisenhüttenwes, Vol. 53, Jan. 1982, pp. 1-4.

84. Blander, M.: Molten Salt Chemistry, Interscience, New York, 1964, pp 127-237.

85. Kubaschewski, O. and Alcock, C.B.: Metallurgical Thermochemistry, 5th ed., Pergamon Press, 1979, p379.

86. Mitchell, A.: Trans. Met. Soc. of AIME, Vol. 242, Dec. 1968, pp 2507-2511.

87. Hara, S. and Ogino, K.: Canad. Met. Quart., Vol. 20, Jan. 1981, pp 113-116.

88. Morinaga, K. et al.: TMS paper selection, A79-18, The Met. Soc. of AIME, pp 1-13.

89. Hara, S. et al.: Proc. of first International Symp. on Molten Salt Chemistry and Technology, Kyoto, Japan, April 1983, pp 257-260.

90. Richardson, F.D.: Physical Chemistry of Melts in Metallurgy, Academic Press, New York, 1974, Vol. 2, pp 291-304.

91. Frohberg, M.G. et al.: Arch. Eisenhüttenwes, Vol. 44, Aug. 1973, pp. 585-588.

92. Goto, K.S. et al.: Second International Symp. of Met. Slags and Fluxes, Lake Tahoe, Nevada, Nov. 1984, pp 467-481.

93. Maeda, M. et al.: Met. Trans. B, Vol. 16B, Sept. 1985, pp 561-566.

94. Turkdogan, E.T.: Physical Chemistry at High Temperature Technology, Academic Press, N.Y., 1980, pp 131-133.

95. Fraser, M.E. and Mitchell, A.: Metal-Slag-Gas Reaction Processes, Ed. by: Foroulis, Z.A. and Smeltzer, W.W., Electrochem. Soc. Inc., Princeton, N.J., 1975, pp 199-209.

APPENDIX I

I.1. CHEMICAL ANALYSIS OF SLAG

I.1.1 FLUORIDE ANALYSIS

100 mg of a dried and powdered sample is weighed in a platinum crucible. Also 500mg Na_2CO_3 and 100mg ZnO are weighed in it and mixed thoroughly with the sample. The mixture is then fused at 900°C for 30 minutes. The time and temperature are to be kept constant as they are critical to obtain proper fusion and to keep fluorine loss to a minimum. The fused product is dissolved in a plastic beaker containing 50ml distilled water and 4ml conc. HCl. The solution is filtered and made up to 100ml in a volumetric flask.

This stock solution is diluted 10 times in water. 10ml of this solution along with the equal volume of buffer is taken in a plastic beaker. The solution is stirred slowly by a magnetic stirrer and the potential through the fluoride ion electrode is recorded to the nearest 0.1mV. All potential measurements are done after 3 minutes of immersion of the electrode to obtain consistently stablized EMF data. The same method is applied to measure potentials of the standards. Both the temperature and the stirring rate are maintained constant for all measurements.

The standard potentials are plotted on a semilog graph paper, keeping the concentration in the log-scale. The straight line so obtained

can be used to determine fluoride concentration in an unknown sample. The slope of the line should be close to 56mV for each decade change of concentrations.

Buffer: (1.0M sodium citrate - 0.2M potasium nitrate) 294 gm of sodium citrate and 20 gm of potasium nitrate are dissolved and diluted to make 1 liter solution in water.

Stock Fluoride: 2.22 gm of dry, reagent grade NaF dissolved and diluted to 1 liter with water.

Working Standards: The stock fluoride is diluted to make standards containing 4, 16, 20 and 40 mg/L Fluorine. Appropriate amounts of Na_2CO_3, ZnO, Al stock solution (if needed) and Si stock solution (if needed) are added to maintain the same levels as in the samples.

I.1.2 ANALYSIS FOR CALCIUM, SILICON AND ALUMINUM

Fresh graphite crucibles (spec-grade graphite) are pre-ignited at 1000°C for 30 minutes. 50 mg powdered sample and 300mg reagent grade lithium metaborate are weighed and mixed thoroughly in a graphite crucible. The mixture is fused at 1000°C for 15 minutes. The melt is swirled to coalesce and immediately poured into a beaker containing 25ml 8% HNO_3. The solution is stirred to dissolve completely and diluted to 50 ml with water in a volumetric flask. Similar steps are followed to make a blank containing 300mg $LiBO_2$.

I.1.3 ATOMIC ABSORPTION METHODS

Silicon: Silicon is analyzed first since it is most sensitive to losses. Standards containing 5, 10, 20, and 50 mg/L Si are made up. They also contain 100 mg/L Ca, 4%HNO_3 and 0.6%$LiBO_2$. The sample solutions are run

in an Atomic Absorption Spectrophotometer 'as is' in a nitrous oxide-acetylene flame with the filament current at 40 mA and burner angle 0°. The standards are run at the beginning and at the end to check the stability of calibration. The blank and a reference solution containing known amounts of all the element are also analyzed.

Calcium: Calcium standards of 5, 10, 15, and 20 mg/L Ca are made by diluting one silicon standards. The samples are diluted 1/50 and run in a flame of nitrous oxide-acetylene with the filament current at 10mA and burner angle of 0°. The blank and a reference solution are also tested during the run.

Aluminum: Aluminum standards of 20, 60, 80 and 100 mg/L Al are made and these also contain 100 mg/L Ca, 4% HNO_3, 0.6% $LiBO_2$ and 1% La. Samples are diluted 1/2 to 1/5 to contain 1% La and run in nitrous oxide-acetylene flame with the filament current at 18mA and burner angle at 0°.

APPENDIX II

II.1. DEFINITION OF OPTICAL BASICITY

The concept of Lewis basicity is related to the electron donor power of the oxygen present in a system. However, there is no numerical scale to define this parameter quantitatively. An optical scale has been proposed to measure the Lewis basicity of various oxide glass systems and some molten salts[1]. This optical scale of basicity is termed as optical basicity.

When a trace quantity of probe ions, such as Tl^{+}, Pb^{2+} or Bi^{3+}, are introduced in a system, frequency shifts, depending on the basicity are recorded in their ultraviolet s-p spectra. The greater the degree of red shift, greater is the basicity of the system. The red shift can also be viewed as a result of the expansion of the outer s and p orbitals of the probe ion.

The optical basicity of various low temperature oxide glasses (for example, $Na_2O-B_2O_3$ and $Li_2O-B_2O_3$) and sulfate-chloride glasses is measured[1,2]. However, in some glass systems and metallurgical slags, experimental measurements are difficult and sometimes not feasible due to opaqueness in the ultraviolet region. In these cases, the theoretical calculations of optical basicity proved to be a good alternative[3,4]. The next section shows how to do these theoretical calculations on the basis of electronegativity of different cations, normally present in metallurgical slags.

II.2. CALCULATION OF OPTICAL BASICITY

The optical basicity, OB, of a slag can be calculated by the following expression:

$$(OB)_{slag} = X_A.(OB)_A + X_B.(OB)_B \qquad II.1$$

where $(OB)_A$ and $(OB)_B$ are the optical basicities of different oxide components in the slag, X is the equivalent cation fraction which can be calculated from the mole fraction of components, such as in A-B slag:

$$X_A = \frac{\text{mole fraction of comp. A x no. of oxygen atoms in A}}{\sum_{i=a,b} \text{mole fraction of comp. i x no. of oxygen in i}} \qquad II.2$$

In CaF_2 based slags, the contribution from CaF_2 is ignored, and thus only the oxide components are considered. For example, in a CaF_2-CaO-SiO_2 melt:

$$X_{SiO_2} = \frac{2N_{SiO_2}}{N_{CaO} + 2N_{SiO_2}} \qquad II.3$$

The optical basicity of a pure oxide component is related to the Pauling electronegativity, x, of the cation by the following expression:

$$OB = \frac{0.74}{(x-0.26)} \qquad II.4$$

For example, for CaO, the x of Ca is 1.0 therefore:

$$(OB)_{CaO} = 1.0$$

Similarly, considering the x of Si and Al as 1.8 and 1.5 respectively, the optical basicities of SiO_2 and Al_2O_3 are calculated to be 0.48 and 0.61 in

that order.

REFERENCES

1. Duffy, J.A. and Ingram, M.D.: J. Amer. Chem. Soc., Vol.93, Dec.1971, pp.6448-6454.

2. Duffy, J.A. and Ingram, M.D.: Phys. Chem. Glasses, Vol.16, Dec.1975, pp.119-123.

3. Duffy, J.A. and Ingram, M.D.: J. Inorg. Nucl. Chem., Vol.37, 1975, pp.1203-1206.

4. Duffy, J.A. et al: J. Chem. Soc. Faraday Trans. I, Vol.74, 1978, pp.1410-1419.